Dissertation zu Erlangung des Doktorgrades

der Fakultät für Chemie und Pharmazie

der Ludwig-Maximilians-Universität München

Mechanism of cancer evading metronomic chemotherapy and

action of Archazolid as an anti-metastatic drug

Rebekka Kubisch
aus Frankfurt am Main
eingereicht am 10.05.2013

meinen Eltern

Table of Contents

1   Introduction

"*Cancer is the uncontrolled growth of abnormal cells in the body*" (A.D.A.M. Medical Encyclopedia). In 2010 cancer was one of the major causes of death in the European Union (166.9 deaths per 100 000 inhabitants). The history of neoplastic diseases is long: a first case of breast cancer was already described in the Edwin Smith Papyrus written approximately 3000 BC [1].

In the past tumor tissue was seen as an insular mass of proliferating cells, but as cancer research progressed in the past years, nowadays neoplastic tissue is understood as a complex aggregate of multiple cell types that participate in heterotypic interactions with each other. The recent research was compiled in a review of Hanahan and Weinberg in 2000 [2]. Lately, in a follow up review in 2012 additionally the immune system was stressed as a major key player in cancer progression [3].

Neoplastic diseases display a remarkable diversity, thus treatment strategies are numerous. Besides resection and radiation, chemotherapy plays an important role in the treatment of solid tumors. Although potent chemotherapeutics have been developed one major hurdle is emerging. In many cases resistance to the applied therapy occurs. Two main resistances categories are known: 1) acquired or 2) intrinsic chemoresistance. Acquired chemoresistance means that a tumor which has been chemosensitive develops resistances against a certain kind of therapy. In contrast, intrinsic chemoresistance implies that a neoplastic disease is resistant already before a therapy is applied. Fast proliferating malignant cells form the bulk tumor. These cells are targeted by chemotherapeutics. However, slow proliferating cells often remain after therapy. The diversity of the tumor cells allows the transition of epithelial tumor cells to mesenchymal cells (EMT). Mesenchymal cells carry an elevated migratory potential. Thus, they are able to evade the tumor and invade other tissues to form metastases. A treatment can therefore even facilitate this effect, by killing only a part of the tumor and forcing surviving cells to a molecular evolution to increased aggressiveness and chemoresistance.

1.1 Resistance formation upon metronomic cyclophosphamide therapy

To overcome acquired resistance to chemotherapeutic treatment is one of the major issues of clinical cancer research nowadays. Up to now a variety of molecular mechanisms leading to chemoresistance of cancer cells have been investigated and led to the development of new treatment strategies. Besides targeted therapy and combinatorial treatments, anti-angiogenic therapy is a promising option to circumvent resistance formation [4, 5]. For example, in prostate cancer the prognosis for patients with hormone resistant prostate carcinoma (HRPC) is poor, because of frequent occurrence of chemoresistance often followed by relapse and further tumor progression [6, 7]. One suggested follow up therapy for taxane-resistant HRPC is the metronomic treatment (frequent administration of low dose) with cyclophosphamide (CPA), reviewed by Emmenegger *et al.,* 2010 [8].

The alkylating agent CPA, if given in normal dose, preferably targets tumor cells. However, metronomic therapy acts as an anti-angiogenic drug [9-11].

The pivotal targets of anti-angiogenic therapy are not cancer cells but blood vessels, supplying the tumor with nutrients and oxygen. Thus, one advantage of anti-angiogenic therapy is that it targets endothelial cells, not carrying a malignant phenotype. These cells are, unlike cancer cells, not able to develop resistance to the treatment due to their comparably stable genetics. Studying the mechanisms leading to resistance to anti-angiogenic therapy is of great interest, as they may differ from resistance to classical chemotherapy. In general, resistance to anti-angiogenic therapy can be classified into four major groups: 1) *evasive resistance*, 2) *vascular cooption*, 3*) reduced vascular dependence* and 4) *vascular remodeling* [12].

In 2011 Emmenegger *et al.* pointed out that the applied CPA dose (maximum dose or a metronomic dosing) directly changes the mechanisms of resistance formation. After treatment of PC3 xenografts with maximum dose, tumor cells acquired resistance both *in vivo* and *in vitro* [12]. However after metronomic application of CPA the resistant phenotype became manifested only *in vivo*. Furthermore, Thoenes *et al.* showed that prostate cancer xenografts, treated metronomically with CPA, acquire chemoresistance. After a response phase of around 50 days cells develop resistance and tumors size increases (Figure 1-1 A). Resistant tumors were reisolated and cell lines were established

[13]. An overview of the distinct cell lines is shown in Figure 1-1 C. When analyzed *in vitro*, cells were chemosensitive to the metabolized, active form of CPA (4-HOO-CPA, Figure 1-1 B).

C.

PC3 wt	parental PC3 cell line (ATCC# CRL1435)
PC3 A3	*in vivo* passaged control cell line
PC3 D3	*in vivo* resistant cell line
PC3 D4	*in vivo* resistant cell line
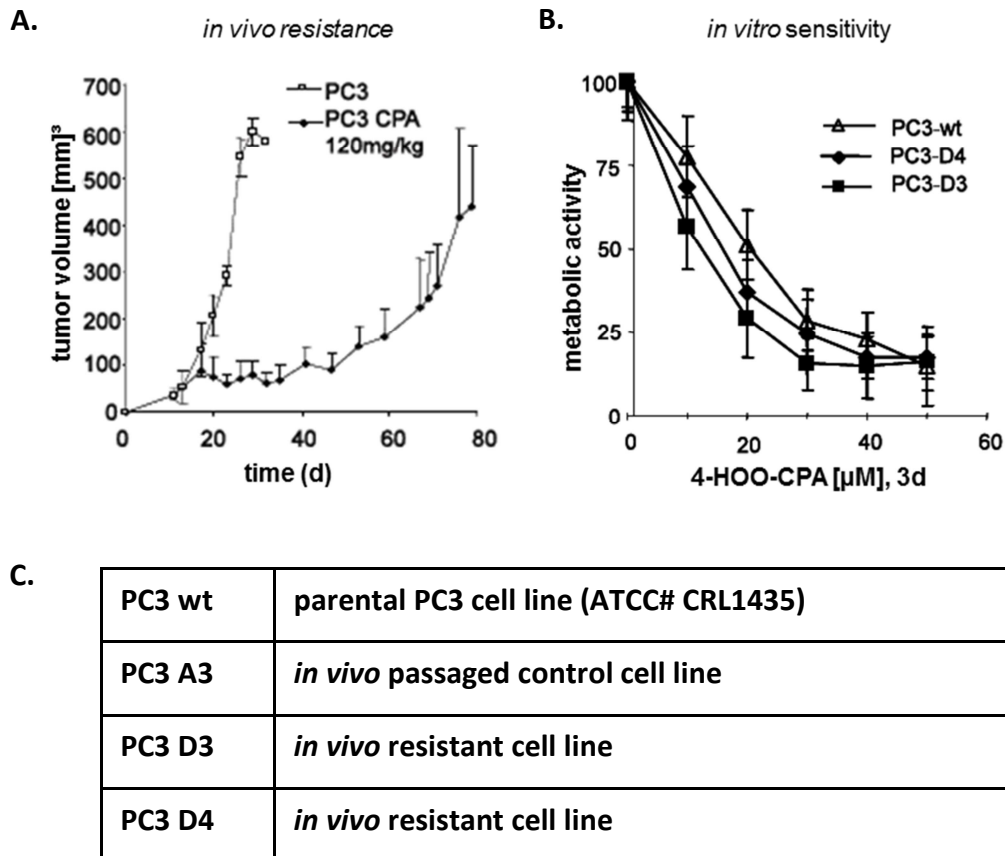
Figure 1-1 Resistance formation upon metronomic cyclophosphamide therapy, from Thoenes *et al.* [13]
A. Growth curve of *s.c.* PC3 wt tumors in SCID mice during metronomic CPA therapy **B.** *in vitro* 4-HOO-CPA (active form of CPA) treated PC3 clones **C.** list of cell lines

As summarized in Figure 1-2 CPA has an anti-angiogenic effect in this model, which is still present in the resistant state. Tumor vessels are destroyed and blood supply is reduced during the treatment. Tumors developed a resistance to the therapy regimen without restoring tumor vessels or vascular mimicry (Figure 1-2 A). Moreover resistant cells did neither acquire a multidrug resistance nor detoxified CPA by alcohol dehydrogenase ADH or aldehyde dehydrogenase ALDH (Figure 1-2 B, C). Taken together the underling mechanism can be proposed as a member of the major group of *reduced vascular dependence*.
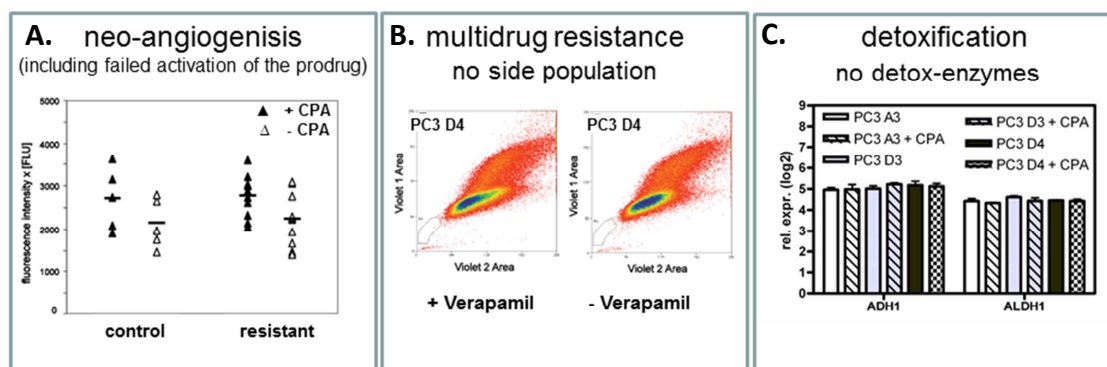
Figure 1-2 Overview of potential resistance mechanisms (A. and B. originate from Thoenes *et al*. [13])

Isolated tumor cell lines from resistant tumors revealed their resistant phenotype upon reimplantation *in vivo* [13]. A comparative proteome analysis of chemoresistant *versus* parental PC3 cells was performed, suggesting the involvement of Annexin A3 [13]. To further analyze the gene expression of chemoresistant tumor tissue *in vivo*, a genome wide microarray of xenografted PC3 tumor cell lines was performed. Four PC3 sublines PC3 wt (standard PC3 cells), PC3 A3 (*in vivo* passaged control cells) and PC3 D3, PC3 D4 (*in vivo* resistant cells) were injected subcutaneously into SCID mice (overview of cell lines Figure 1-1 C). After tumor formation, one group of each PC3 subline was treated with CPA, whereas the other group was kept untreated. Microarray analysis of four individual tumors per group was performed. In order to detect distances and similarities between different samples, RMA (robust multichip analysis) normalized data were subjected to hierarchical clustering. Here a distinct clustering of the different cell lines was observed. In contrast, acute CPA treatment of the different tumors did not induce additional clusters (Figure 1-3). This indicates only a minor effect of CPA on the gene expression profile. The resistant tumor sublines PC3 D3 and PC3 D4 showed a close relation of their gene expression profile, suggesting a similar resistance genotype. Furthermore, *in vivo* passaging strongly influenced the gene expression pattern, demonstrating the influence of the tumor environment [14].

Further analyses were focused on the inherent differences between samples of resistant cell lines PC3 D3 and PC3 D4 *versus in vivo* passaged cell line PC3 A3 without the direct influence of CPA.
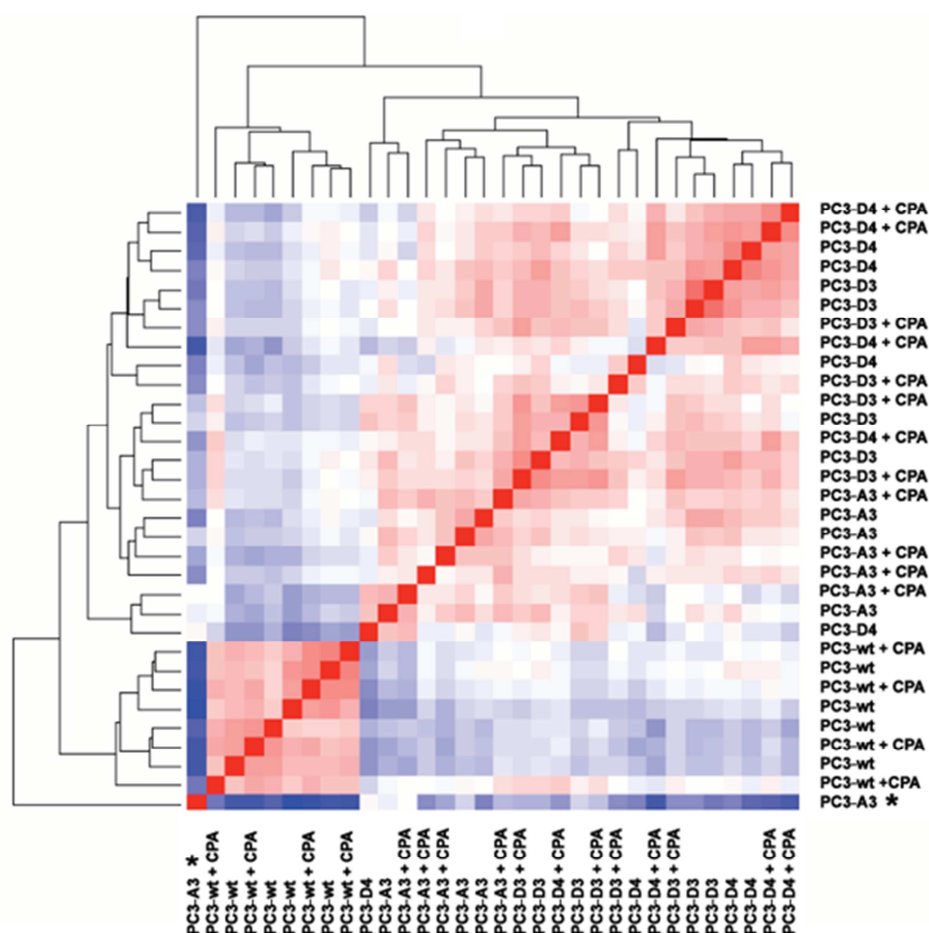
Figure 1-3 Robust multichip analysis (RMA) of parental PC3 wt, *in vivo* passaged PC3 A3, and resistant tumors PC3 D3 and PC3 D4
Hierarchical clustering on robust multichip analysis (RMA) normalized arrays. red = low distance, blue = high distance. Outliners, marked by * are excluded from further data analysis. Data originate from PhD thesis of Lilja Thoenes (LMU, 2009) and Kubisch et al. [14]

Analysis of PC3 D3 (resistant) *versus* PC3 A3 (control) and PC3 D4 (resistant) *versus* PC3 A3 (control) revealed 415 differentially expressed genes for PC3 D3 and 566 for PC3 D4. An intersecting set of 212 genes were differentially expressed in both resistant tumor lines (Figure 1-4). The expression of dehydrogenase/reductase member 2 (DHRS2), PAS domain containing protein 1 (PASD1) and special AT-rich sequence-binding protein-1 (SATB1) was increased in the resistant tumors compared to PC3 A3 tumors, whereas neurotensin (NTS) and bone morphogenetic protein receptor type I B (BMPR1B) expression was decreased in resistant tissue (Figure 1-4).
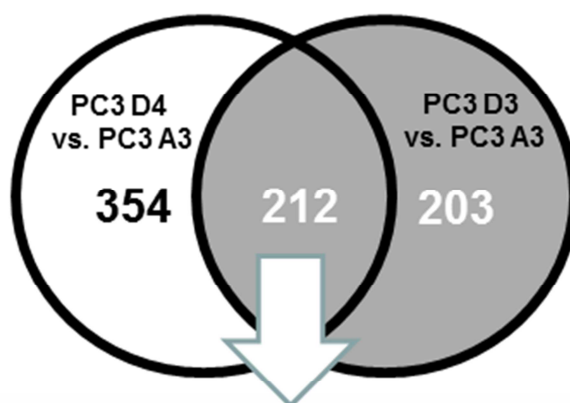
Transcript Cluster ID	Gene Symbol	Gene Title	fold expr. (log2)
7973433	**DHRS2**	dehydrogenase/reductase (SDR family) member 2	2,02
8170488	**PASD1**	PAS domain containing 1	1,98
7917875	F3	coagulation factor III (thromboplastin, tissue factor)	1,16
8169949	RP6-213H19.1	serine/threonine protein kinase MST4	1,10
8035795	ZNF626	zinc finger protein 626	1,09
8112053	CDC20B	cell division cycle 20 homolog B (S. cerevisiae)	1,02
8147351	ESRP1	epithelial splicing regulatory protein 1	1,00
8025992	ZNF788	zinc finger family member 788	0,96
8085716	**SATB1**	SATB homeobox 1	0,96
7997504	CDH13	cadherin 13, H-cadherin (heart)	0,95
Transcript Cluster ID	**Gene Symbol**	**Gene Title**	**fold expr. (log2)**
7957458	**NTS**	neurotensin	-2,34
7948444	TCN1	transcobalamin I (vitamin B12 binding protein, R binder family)	-1,38
8174598	IL13RA2	interleukin 13 receptor, alpha 2	-1,22
8175562	MAGEC2	melanoma antigen family C, 2	-1,19
8089911	HCLS1	hematopoietic cell-specific Lyn substrate 1	-1,12
8166593	IL1RAPL1	interleukin 1 receptor accessory protein-like 1	-1,03
8056376	SCN3A	sodium channel, voltage-gated, type III, alpha subunit	-0,93
8096511	**BMPR1B**	bone morphogenetic protein receptor, type IB	-0,92
8021623	SERPINB7	serpin peptidase inhibitor, clade B (ovalbumin), member 7	-0,91
7898057	PDPN	podoplanin	-0,86

Figure 1-4 Microarray analysis (from Kubisch *et al*. [14])
Venn diagram of PC3 D4 versus A3 (566 genes) and PC3 D3 *versus* PC3-A3 (415 genes) differentially expressed genes (+/- 0.4-fold change cutoff) and table including top 10 higher and lower fold expression (log2) score of genes differentially expressed by both PC3 D3 and PC3 D4. bold: qPCR validated genes

An altered exon expression was found for tissue factor (F3). As shown in Figure 1-5 only exon 3-6 displays an elevated expression in resistant tumors (PC3 D4). Further analysis of the underling mechanisms was to be performed based on these previous findings.
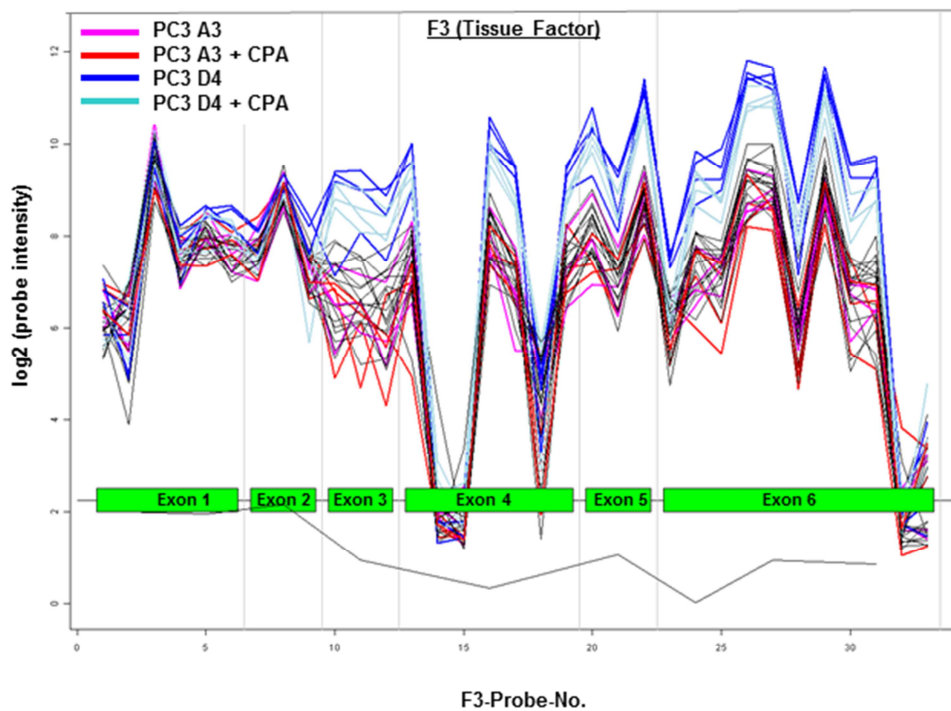
Figure 1-5 Microarray expression profile (probe intensity) of F3 (tissue factor) (from Kubisch *et al.* [14])

In summary, metronomically administered CPA acts anti-angiogenic by destroying tumor vessels. Xenografted PC3 tumors in SCID mice develop a resistance against this therapy after around 50 days. Isolated cells do not display a resistant phenotype *in vitro* but are resistant after reimplementation *in vivo*. Neoangiogenesis, vascular mimicry, enzymatic detoxification as well as multidrug resistance (MDR) transporter activity could be ruled out as a cause for resistance. Moreover, cells develop a *reduced vascular dependence* leading to resistance to the anti-angiogenic therapy.

1.2   Myxobacterial compounds in cancer treatment

A further approach to overcome resistance or even circumvent resistance formation is development of novel anti-cancer drugs. Here, myxobacteria are of great pharmaceutical interest as they are producing a variety of secondary metabolites with different biological activities. Up to now more than 7,500 myxobacteria have been isolated. Many of them were chemically analyzed and about 100 different core structures (plus 500 derivatives) are published [15]. The most prominent myxobacterial compound, the paclitaxel mimic epothilone is in clinical trials for the treatment of breast cancer [16]. Besides tubulin stabilizer epothilone, other myxobacterial compounds like the microtubule destabilizer tubulysin and disorazol are known [17, 18]. Furthermore, compounds rhizopodin and the chondramides which interfere with the actin filaments of eukaryotes are important members of myxobacterial compounds [19-21]. Recently three classes of myxobacterial compounds have come into focus: 1) tubulin inhibitor tubulysin and its derivatives, 2) the chondramides (F-actin binding) and 3) archazolid A and B which are potent V-ATPase inhibitors [22, 23]. A schematic overview of their proposed action in the cell is shown in Figure 1-6.
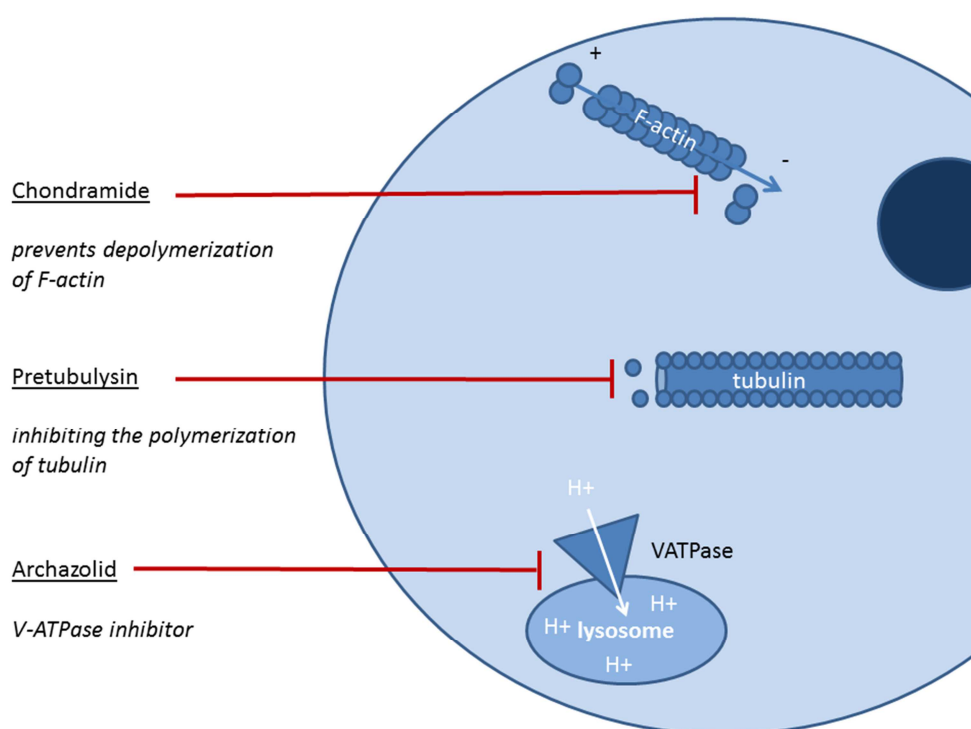
Figure 1-6 Myxobacterial compounds in cancer treatment

The tubulysin derivative pretubulysin has been shown to have anti-angiogenic properties and thus potently reduced tumor growth of hepatocellular xenografts *in vivo* [24]. Chondramides strongly prevent polymerization of F-actin and thus exhibit a cytostatic effect *in vitro* [21]. Furthermore, both pretubulysin and chondramid B hamper lung colonization of 4T1*luc* breast cancer cells in BALB/c mice (PhD thesis Laura Schreiner, LMU 2013).

1.2.1 Archazolid a novel V-ATPase inhibitor

Archazolid A and B (Figure 1-7) are macrolactone structures with V-ATPase Inhibitor function [22, 23, 25-28]. Both show similar bioactivity [29]. Archazolid induces apoptosis in cancer cells in a nanomolar range [30]. Moreover, it was previously shown that it inhibits migration of highly metastatic cancer cells *in vitro* and reduces the lung colonization of breast cancer cells *in vivo* [29]. Notably, other targets are proposed despite V-ATPase but not yet proven.
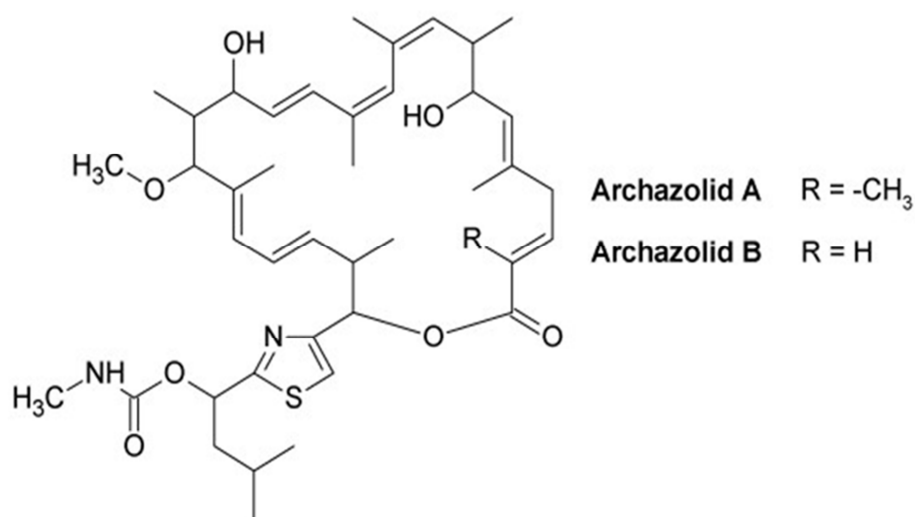
Figure 1-7 Chemical structure of archazolid A and B from Huss *et al.* [25]

1.3 V-ATPase

The main target of archazolid is the V-ATPase. Vacuolar (H+)-ATPases are found on various membranes, including lysosomes, endosomes, vesicles and the plasma membrane. As V-ATPases are ATP dependent proton pumps they are crucial for maintaining the pH of these compartments. Thus, they play a vital role in various cellular processes like, intracellular targeting of lysosomal enzymes, protein processing and degradation as well as receptor-mediated endocytosis [31, 32].

In cancer a combination of increased metabolism and reduced oxygen and nutrient supply leads to an acidic tumor environment (reviewed by Vaupel *et al.* [33]). Thus, tumors have to control their intracellular pH strictly. V-ATPases are reported to play a crucial role in tumor pH homeostasis of cancer cells either by pumping protons out of the cell or into acidic lysosomes [34, 35]. Therefore, compounds inhibiting V-ATPase are proposed as novel drugs for cancer therapy (reviewed by Fais *et al.* [36]).

V-ATPases are composed of two major domains: 1) peripheral domain V_1 and 2) integral domain V_0. Each domain is composed of different subunits: V_1 A-H and V_0 a-e (Figure 1-8). Subunit V_1 is responsible for ATP hydrolysis and V_0 for proton translocation-through the membrane.

Bafilomycin A1 and concanamycin A as well as archazolid are natural compounds efficiently inhibiting the V_0c subunit of V-ATPases [23, 37-41]. In contrast to archazolid, which inhibits V-ATPase function by binding between the membrane and subunit c, concanamycin A and bafilomycin A1 are binding between the different subunits c [23].

V-ATPase inhibitors display a novel group of anti-cancer compounds, as their unique mode of action strongly differs from common anti-cancer drugs.
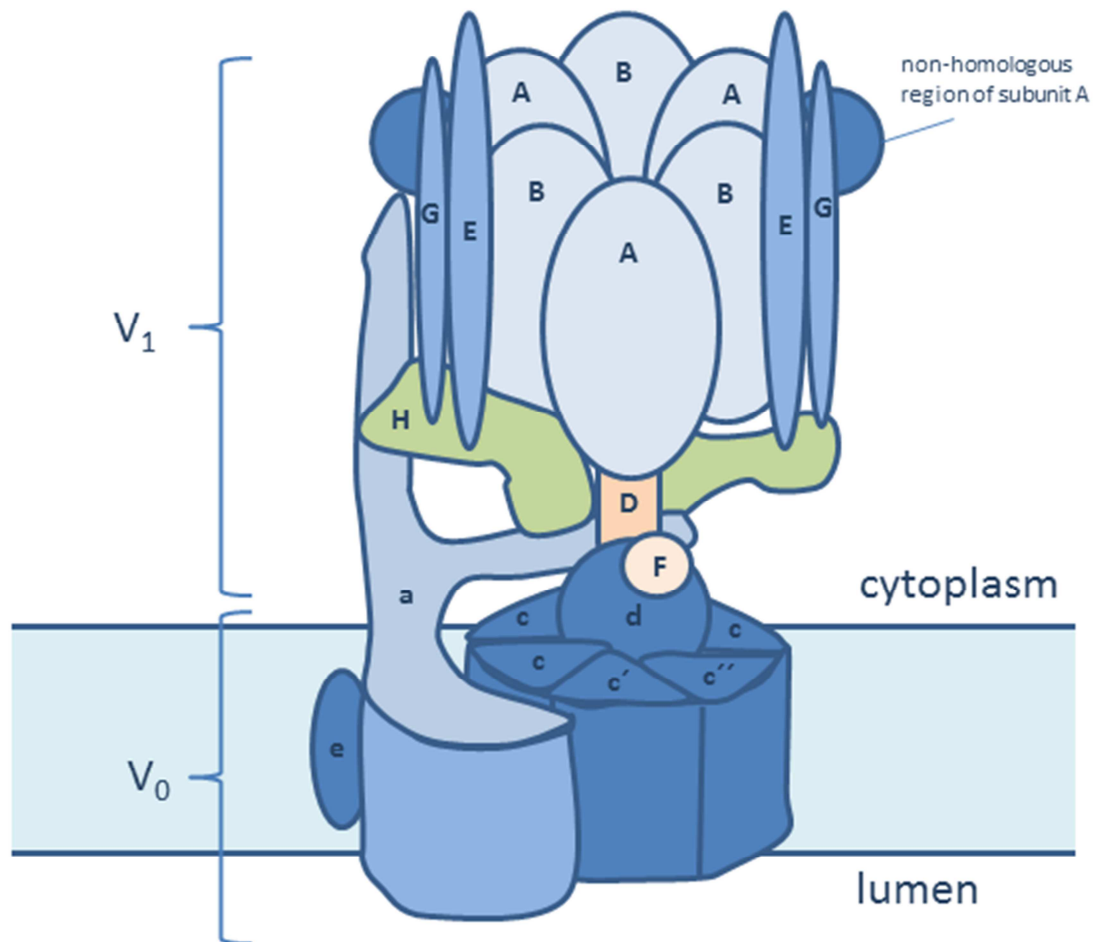
Figure 1-8 Schematic overview of the vacuolar V‑ATPase complex (drawn after Forgac *et al.* [32])
The V-ATPase complex is composed of a peripheral domain (V_1), responsible for ATP hydrolysis, and an integral domain (V_0), involved in proton translocation across the membrane. Here Archazolid binds to the proteolipid subunits c and thus blocks H^+ transfer.

1.4 Cathepsin B

In cancer research lysosomal proteases like the cathepsins became more and more important as tumor markers. In particular, cathepsin B is upregulated in many types of cancer [42-45]. Nevertheless, its distinct role in tumor progression is not fully understood and controversially discussed. During metastasis tumor cells are invading the surrounding tissue and migrate to distant sites. One of the crucial steps for this process is the degradation of extracellular matrix by extracellular proteases (for review see [46-48]). Some authors state that extracellular cathepsins directly contribute to matrix degradation [49-53]. In contrast, others show that intracellular cathepsin B is in

an indirect way crucial for extracellular matrix degradation by other proteases like urokinase (uPA) or matrixmetalloproteinases [54, 55].

Cathepsin B is synthesized at the rough endoplasmic reticulum (ER) as preprocathepsin B (Figure 1-9). Signal peptides target cathepsin B into the ER lumen. Here it becomes cleaved co-translationally to procathepsin B. Thereafter, procathepsin B is transported through the ER to the Golgi apparatus. Here it is substituted with two asparagine-linked mannose-containing oligosaccharides. These residues are then phosphorylated. After phosphorylation procathepsin B is bound to membrane associated mannose-6-phosphate receptor (M6PR) in the trans-Golgi network (TGN). M6PR-procathepsin B containing vesicles are leaving the TGN and direct to prelysosomal compartments (PLC). Importantly, the dissociation of the M6PR-procathepsin B complex is pH dependent. If the pH in the compartment is neutral, the complexes will not dissociate. Consequently, during the lysosome maturation process the pH of these PLC is decreasing which leads to the release of cathepsin B from the M6PR and recycling of the receptor to the TGN (for review see [56-58].
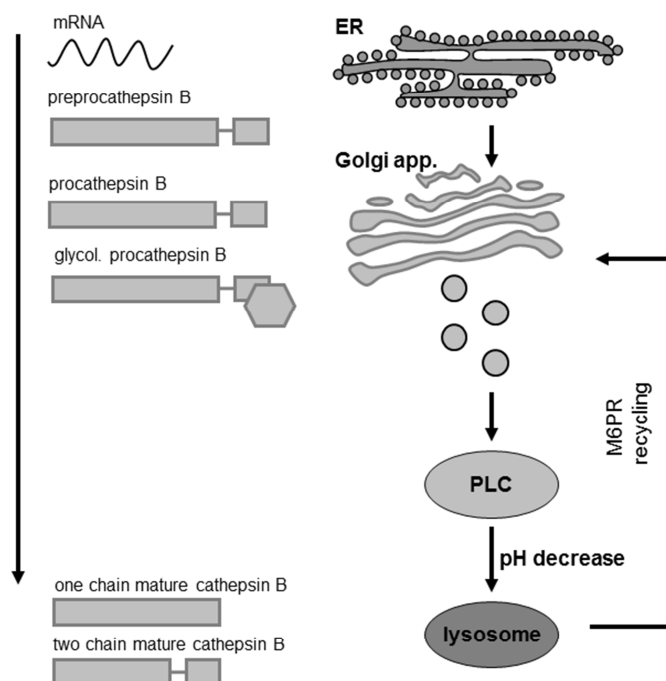
Figure 1-9 Cathepsin B maturation process; a schematic overview
ER = endoplasmic reticulum, Golgi app. = Golgi apparatus, PLC = prelysosomal compartment, M6PR = mannose-6-phosphate receptor

1.5   Aim of the thesis

In this thesis the mechanisms leading to acquired chemoresistance as well as new treatment strategies implying the prevention of tumor cell evasion and metastases formation will be addressed.

As chemoresistance is one of the major hurdles in cancer treatment, the elucidation of underlying molecular mechanisms is of great interest. Therefore, one aim of this thesis is the analysis of the molecular changes after resistance formation upon metronomic cyclophosphamide therapy in a prostate cancer model. The analysis is based on a microarray gene expression experiment. In particular the clarification of mechanisms leading to the survival of tumor cells during maintained, anti-angiogenic, metronomic cyclophosphamide therapy is in focus using state of the art bioinformatics and expression analysis methods.

Moreover, new treatment strategies using novel myxobacterial compounds will be elucidated, with special regard to the anti-metastatic action of archazolid, a potent V-ATPase inhibitor. V-ATPase inhibitors are known to alter endo- and exocytotic events. In the current thesis, secreted proteins of archazolid treated, highly migratory urinary bladder carcinoma cells should be identified using a proteomic approach. Furthermore, the molecular consequences of V-ATPase inhibition on cellular trafficking should be elucidated *in vitro* using different biochemical, molecular biological and imaging techniques. Finally, *in vitro* results should be confirmed *in vivo* using a syngenic mouse model. This model enables the monitoring of archazolid action on cancer cells by the *in vivo* application of mouse mammary gland tumor cells (4T1*luc*) stably expressing the transgene luciferase as a reporter. In the following, the influence of archazolid on tumor growth and metastasis then can be analyzed using the *in vivo* measurement of luciferase activity. Moreover, it facilitates to evaluate also other biochemical parameter *ex vivo* after a certain treatment regimen.

2 Material and Methods

2.1 Material

2.1.1 Cell culture reagents and media

DMEM 4,5 g/l Glucose	Invitrogen (Karlsruhe, Germany)
RPMI	Invitrogen (Karlsruhe, Germany)
McCoy's 5A modified medium	Biochrom (Berlin, Germany)
fetal bovine serum (heat inactivated)	Invitrogen (Karlsruhe, Germany)
L-alanyl-L-glutamine	Biochrom (Berlin, Germany)
trypsin EDTA solution	Biochrom (Berlin, Germany)
Opti-MEM	Invitrogen (Karlsruhe, Germany)

2.1.2 Cells

PC3 wt (# CRL1435)	ATCC, USA
PC3 A3	[13]
PC3 D3	[13]
PC3 D4	[13]
T-24	Barbara Mayer LMU (Germany)
4T1*luc*	Caliper (Alamenda, CA, USA)
MCF-7	Cell line Services (Germany)

2.1.3 Plastic- and glassware

well-plates (6,12,24,48 and 98)	TPP (Switzerland))
tissue culture flask (25,75 and 100 cm^2)	TPP (Switzerland))
cell culture dish 10 cm	NUNC, USA
Coverslips and slides	Gerhard Menzel GmbH (Germany)
Amicon Ultra-4 Centrifugal Filter Units (3 and 10 kDa cut off)	Merck Millipore (USA)

2.1.4 Instruments

Phase contrast microscope Carl Zeiss Axiovert 200	Carl Zeiss (Germany)
Fluorescence microscope Carl Zeiss Axiovert 200	Carl Zeiss (Germany)
Laser scanning microscope Carl Zeiss Laser Scanning Microscope LSM 510 Meta	Carl Zeiss (Germany)
CyAnTM ADP	Dako cytomations (Germany)
LightCycler 480 system	Roche (Germany)
Luminometer Lumat LB9507 instrument	Berthold (Germany)
FastPrep-24 tissue/ cell homogenizer MP	Biomedicals GmbH (Germany)
Hybaid PCR thermal cycler	Thermo Fisher Scientific (USA)
Tecan spectra fluor plate reader	Tecan (Switzerland)
SDS-Page Running system	Biorad (Germany)
Wet-Blot-System	Biorad (Germany)
Olympus BX41 microscope	Olympus (Japan)

2.1.5 Kits

CellTiterGlo	Promega (USA)
Transcriptor High Fidelity cDNA Synthesis	Roche (Germany)
NucleoSpin RNA II	Macherey and Nagel (Germany)
BCA-Assay	Thermo Fisher Scientific (USA)
iTRAQ® Reagent 4plex	AB Sciex (USA)

2.1.6 Antibodies

antigen	art.-no.	source	company	WB	IF
alpha-Tubulin	T9026	mouse	sigma-aldrich (USA)	1:10,000	
ANXA3	PA5-12438	rabbit	Thermo Scientific (USA)	1:1000	1:200
Cathepsin B	IM27L	mouse	Calbiochem (Germany)	1:500	1:200
Cathepsin B	#3383	rabbit	CST (USA)	1:1000	
Cathepsin D	#2284	rabbit	CST (USA)	1:1000	
F3	sc-23596	goat	SantaCruzBiotech. (USA)	1:1000	
GAPDH	#2118	rabbit	CST (USA)	1:5000	
M6PR (IGF-IIR)	sc-25462	rabbit	SantaCruzBiotech. (USA)		1:50
SATB1	ab49061	rabbit	Abcam (USA)	1:1000	1:200

2.1.7 Primer

<u>Primer human</u>

ATP6V0C		UPL Probe #76	left: ttcgtttttcgccgtcat,
			right ccactgggatgatggacttc
ACTIN BETA		UPL Probe #64	left: ccaaccgcgagaagatga,
			right ccagaggcgtacagggatag
ANXA3		UPL Probe #29	left: tccggaaagctctgttgact,
			right: atcttgtttggccagatgct
B2M		UPL Probe #42	left: ttctggcctggaggctatc,
			right: tcaggaaatttgactttccattc
BMPR1B		UPL Probe #21	left: tttcatgccttgttgataaaggt,
			right: gcttgtttaactttttgtttcctctc
CATHEPSIN B		UPL Probe #26	left: ttcggacttcctgctctacaa
			right: tagggtgtgccattctccac
CATHEPSIN D		UPL Probe #37	left: ggtacctgagccaggacact
			right: acctgcctctccactttgac
DHRS2		UPL Probe #4	left: tgagactatcacctatcgccaag,
			right: cagcatagtggttggtgtctg

16

F3 Exon 1-2	UPL Probe #15	left: cgccaactggtagacatgg,
		right: gctgccacagtatttgtagtgc
F3 Exon 5-6	UPL Probe #2	left: cagacagcccggtagagtgt,
		right: ccacagctccaatgatgtagaa
GAPDH	UPL Probe #60	left: ctctgctcctcctgttcgac,
		right: gcccaatacgaccaaatcc
NTS	UPL Probe #17	left: cagcttgtatgcatgctactcc,
		right: aatgctttcatttcctcttctga
PASD1	UPL Probe #20	left: caacccacctaccatcaggt,
		right: ctgctccgcagat ctcatc
PLAT	UPL Probe #59	left: cgggtggaatattgctggt,
		right: cttggctcgctgcaactt
PROS1	UPL Probe #46	left: acatacctgggtggccttc,
		right: tccagatccaactgtacaccat
SATB1	UPL Probe #44	left: aatggcattgctgtctctagg,
		right: actttccaacctggattagcc
SERPINA1	UPL Probe #73	left: gcttaaatacggacgaggaca,
		right: acgagacagaagacggcatt
SERPIND1	UPL Probe #29	left: tggtggagagatggcaaaa,
		right:gattgtagttcttctccagcttgaat
SERPINB7	UPL Probe #8	left: gattgtagttcttctccagcttgaat,
		right: caaattgaacttccgttcctg

Primer mouse

ACTIN BETA	UPL mouse ACTB Gene Assay, Roche (Germany)	
CATHEPSIN B	UPL Probe #47	left: gtgtctgctgaagacctgctt
		right: gggatagccaccattacagc
CATHEPSIN D	UPL Probe #79	left: gcgtcttgctgctcattct
		right: acttgcgcagagggattct
GAPDH	UPL mouse GAPDH Gene Assay, Roche (Germany)	

17

2.1.8 Chemicals and Solutions

Hoechst 33342	Sigma Aldrich (Germany)
Paraformaldehyde	Sigma Aldrich (Germany)
Triton X 100	Sigma Aldrich (Germany)
Gelatin solution	Sigma Aldrich (Germany)
FlourSave mounting reagent	Merck KGaA (Germany)
Bafilomycin A1	Sigma Aldrich (Germany)
Concanamycin A	Sigma Aldrich (Germany)
Tunicamycin	Sigma Aldrich (Germany)
Brefeldin	Sigma Aldrich (Germany)
Cyclophosphamide	Sigma Aldrich (Germany)
Complete®	Roche (Germany)
Cell lysis buffer	Promega (USA)
Lumi-Light Western Blotting Substrate	Roche (Germany)
X-ray films	Fisher Scientific
DAPI	Sigma Aldrich (Germany)
CA-074 ME (cathepsin B inhibitor)	Enzo Life Sciences (USA)
Z-Arg-Arg-7-amino-4-methylcoumarin hydochlorid (cathepsin B substrate)	Sigma Aldrich (Germany)

Archazolid A was purified and isolated as described previously [22], archazolid B was chemically synthesized by Roethle *et al.* [28]. Both compounds were dissolved in dimethyl sulfoxide (DMSO) and show similar bioactivity (supplementary information of Wiedmann *et al.* [29]). For all *in vitro* experiments archazolid B was used. For all *in vivo* experiments archazolid A was used.

2.2 Methods

2.2.1 Cathepsin B activity assay

Cathepsin B activity assay was performed in a modified version of the protocol published by Barrett, 1980 [59]. The assay buffer was titrated from 2 buffers to get a distinct pH: buffer 1: 0.1 M NaH_2PO_4, 0.4 M NaCl, 10 mM EDTA and buffer 2: 0.1 M Na_2HPO_4, 0.4 M NaCl, 10 mM EDTA. In a first experiment different pH values were tested (Figure 2-1). All other experiments were carried out using an assay buffer of pH 6.5. pH 6.5 was the pH were the cathepsin B activity was in a medium range. By choosing this pH is should be avoided to activate procathepsin B by mature cathepsin B. Assay procedure was carried out as follows: First assay buffer was placed into a reaction tube. 2 mM cysteine and 30 µg total protein sample was added. For background subtraction in one of two samples a specific cathepsin B inhibitor (CA-074 ME, 50 µM) was added. To start the reaction 50 µM Z-Arg-Arg-7-amino-4-methylcoumarin hydrochloride a fluorogenic cathepsin B substrate was supplemented. After an incubation time of 30 min at 40 °C the reaction was stopped by adding 2 M Tris (pH is raised to 10). Fluorescence of the cleaved substrate was quantified using a tecan reader (em 360 nm, ex 450 nm). To determine the specific cathepsin B activity values were calculated blank (without sample) and inhibitor corrected.
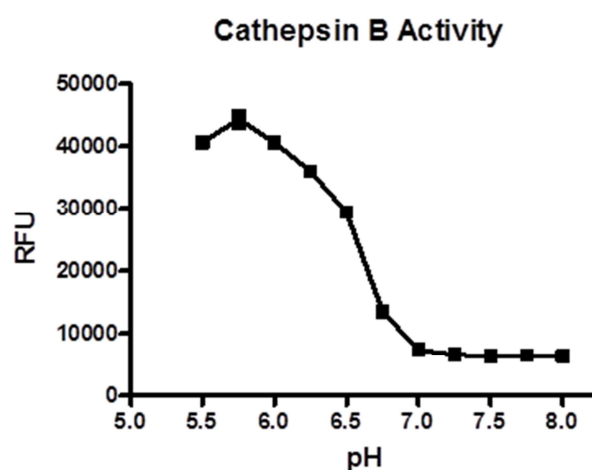

Figure 2-1 pH dependent cathepsin B activity of recombinant cathepsin B

2.2.2 Cell culture

PC3 human prostate carcinoma cells (PC3 wt, ATCC # CRL1435) and reisolated clones PC3 A3, PC3 D3 and PC3 D4 as well as 4T1*luc* breast cancer cells were cultured in RPMI 1640 medium supplemented with 10% FBS. T-24 cells were cultured in McCoy´s modified 5A media supplemented with 10% FBS. Cells were grown at 37°C in 5% CO_2 in a humidified atmosphere. Generation of PC3 subclones was previously described by Thoenes *et al.* [13]. Briefly standard PC3 cells (PC3 wt) had been injected into male SCID mice and treated with a metronomic regimen of CPA (120 mg/kg every 6 days). After a response phase, tumors restarted growing. Cells of two different resistant tumors were isolated (PC3 D3 and PC3 D4). Additionally, a cell lines of untreated tumors was established (PC3 A3), representing an *in vivo* passaged control cell line ([13] and Figure 1-1 C).

2.2.1.2 Freezing and thawing of cells

For cell storage in liquid nitrogen, freezing medium (90% culture medium and 10% DMSO) was added to the cell pellet. For a slowly freezing of the cells, vials were put into an isopropanol containing container and stored at -80°C for at least 24 hours. Thereafter vials were transferred into liquid nitrogen. For reculturing of the cells, the cell suspension was thawed at 37°C. To remove DMSO residues a media change was carried out 24 hours later.

2.2.3 Isolation of primary human monocytes

All experiments including human primary monocytes and macrophages were done in cooperation with Professor Dr. Oliver Werz, Chair of Pharmaceutical / Medicinal Chemistry, University of Jena. For isolation of PBMC (peripheral blood mononuclear cells) human buffy coats (fraction of an anti-coagulated blood sample containing blood cells and platelets following density gradient centrifugation) were diluted 1:1 with PBS. To remove erythrocytes 1:5 dextran was added and samples were incubated for 30-45 min at RT until dextran bound erythrocytes were sedimented. Supernatants were collected and slowly put onto density gradient centrifugation media (LSM 1077 lymphocyte separation media (PAA, GE Healthcare, UK).
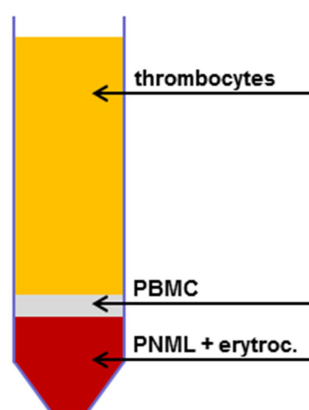
Figure 2-2 Schematic overview of the different phases after density gradient centrifugation

After centrifugation at 2000 rpm for 10 min (without break) PBMC can be found in the in a grey phase indicated in Figure 2-2. PBMC fraction was washed two times with ice cold PBS (1200 rpm, 4 °C) counted and 400 x 10^6 vital cells were seeded per 100 cm^2 flask in 10% FCS containing RPMI media. After 1 - 1.5 hours floating cells were removed. After two washing steps with PBS cells were detached by using a cell scraper. For the secretome analysis 5 x 10^6 vital cells were seeded per 25 cm^2 flask in 10% FCS RPMI. After 1 hour monocytes were attached and treatment was performed after two washing steps in FCS free RPMI media.

For macrophage differentiation 15 x 10^6 vital monocytes were seeded per 100 cm^2 flask in 5% FCS containing RPMI + 25 ng/ml hM-CSF (human macrophage-colony stimulating factor). Differentiation was carried out for 6 days. Subsequently, 5 x 10^6 vital macrophages were seeded per 25 cm^2 flask. After 1 hour cells were attached and treatment was performed in FCS free RPMI media after 2 washing steps.

2.2.4   Cell viability assay (CellTiterGlo)

To analyze the cell viability the CellTiterGlo assay was applied. This assay detects the ATP content of a given sample, thus indicating the relative amount of metabolizing, living cells in an ATP dependent luciferase reaction.

CellTiterGlo assay was performed according to the manufacturer's instructions. Shortly cells were seeded in 96-well plates. 24 hours after seeding cells were treated with the respective compound in FCS free media. After compound incubation half of the volume of each well was replaced by the reaction buffer containing cell lysis buffer, ATP depended luciferase and

a luciferase substrate. The luminescence was recorded using a Luminometer Lumat LB9507 instrument.

2.2.5 Data-analysis (Microarray)

Functional analysis of regulated genes was performed using DAVID bioinformatics [60]. Description by [60] specifies the stated p-value as the threshold of EASE Score, a modified Fisher Exact P-Value, for gene-enrichment analysis. It ranges from 0 to 1. Fisher Exact P-value = 0 represents perfect enrichment. Usually P-values equal or smaller than 0.05 are considered strongly enriched in the annotation categories.

2.2.6 *In vivo* experiments

Mice were housed in individually ventilated cages, under specific pathogen free conditions, with a 12 hours day/night cycle and food and water *ad libitum*. All animal procedures were approved and controlled by the local ethics committee and carried out according to the guidelines of the German law of protection of animal life

2.2.6.1 *Warfarin and CPA combinatorial therapy of PC3 A3 tumors*

For tumor formation 1 x 10^6 PC3 A3 cells in 100 µl PBS were injected subcutaneously with a 25 G needle into the flank of SCID mice (CB17/lcr-PrkdcSCID/Crl) (8–10 weeks) with 5-7 animals per group. Two of in total four groups were treated with CPA (120 mg/kg every 6. day, i.p.) starting at day 12 after tumor inoculation. The other two groups served as control. One of the CPA groups and one of the control groups were treated additionally with warfarin, starting at day 11 after tumor inoculation. Until day 18, warfarin was administered over the drinking water (7.5 mg/l).

Warfarin was solved in ethanol. Accordingly the water of the control groups was supplemented with the corresponding amount of ethanol (max. 750 µl in 1 l). Although acceptance of the ethanol and warfarin supplemented drinking water was tested in a pretrial (data not shown), mice stopped drinking around day 16. The treatment regimen was changed to warfarin 5 mg/kg i.p. every third day. Mice of the non CPA treated groups were euthanized, if the tumor volume was higher than 1000 mm³. On day 57 the experiment had

to be stopped due to severe weight loss. For analysis mice of the CPA treatment groups which had to be euthanized before day 57 were excluded.

2.2.6.2 *4T1luc tumors*

In a first experiment 2 x 10^6 4T1*luc* cells were injected into the flanks of BALB/c mice. At day 3, mice were treated 3 times per week *i.v.* with 3 mg/kg archazolid (n=7), 0.1 mg/kg pretubulysin (n=8), 0.5 mg/kg chondramid B (n=8) or vehicle control (5% DMSO in PBS). Tumors were measured every two to three days with a caliper, using the formula *a x b2/2* (*a* as the largest side of the tumor and *b* the largest side vertical to *a*). On day 18 mice were euthanized. During the experiment 3 archazolid treated mice had to be euthanized due to tail inflammation caused by subcutaneous archazolid. In the following special effort was applied to directly inject *i.v.*. Analysis was done with archazolid n=4.

In a second experiment 2 x 10^6 4T1*luc* cells were injected subcutaneously into the flank of BALB/c mice (10 per group). One group was treated with 3 mg/kg archazolid A in 5% DMSO/PBS or equal amounts of 5% DMSO/PBS in a second control group. Treatment was performed on day 2, 3, 4, 5, 6, 9, 13 and 17 after tumor inoculation. The average tumor volumes of the two groups were compared over time. On day 18, mice were sacrificed through cervical dislocation. Tumor, lung, liver, kidney and heart of each animal were harvested.

2.2.7 *Ex vivo* luciferase imaging

To detect distant metastases of 4T1*luc* cells in the lung, whole lungs were homogenized using a FastPrep-24 tissue/cell homogenizer MP. After homogenization samples were centrifuged 13,000 rpm for 10 min at 4°C. Luciferase activity of each sample was determined using a Luminometer Lumat LB9507 instrument.

2.2.8 H&E staining

Tumors were fixed in formalin and embedded into paraffin. Subsequently paraffin embedded tumors were cut with a microtome into 4.5 µm slices and stained with hematoxylin (2 min) and eosin (5 min). Results were documented, using an Olympus BX41 microscope.

2.2.9   Proteomics

2.2.9.1   *In-gel-digestion*

After electrophoresis, gels were scanned and each lane was cut into similar pieces. Each piece was transferred into a reaction tube and covered with 45 mM DTT in 50 mM NH_4HCO_3. After an incubation of 30 min at 55 °C gel-pieces were covered with 100 mM iodoacetamide in 50 mM NH_4HCO_3 for 15 min at RT in the dark. This step was repeated. Subsequently, gel-pieces were washed two time using 50 mM NH_4HCO_3. For tryptic digestion pieces were chopped using a pipet tip and covered with 50 mM NH_4HCO_3 containing trypsin in a ratio of 1 µg trypsin to 50 µg of protein. Incubation was carried out at 37 °C overnight. After the digestion supernatants were collected and pieces covered with 70 % acetonitrile for 10 min. Supernatants were combined afterwards. After freeze-drying peptide samples were stored at -80 °C until LC-MS/MS measurement.

2.2.9.2   *LC-MS/MS analysis*

All LC-MS/MS measurements were done in cooperation with Dr. Thomas Froehlich and Dr. Georg J. Arnold (Genzentrum, LMU, Munich, Germany).

Nano-LC separation was done with a nano-liquid chromatography system (Ettan MDLC, GE Healthcare, USA). Peptide samples were loaded on a trap column (10 µl per min, loading buffer: 0.1% formic acid; trap column: C18 PepMap 100, 5 µm bead size, 300 µm i.d., 5 mm length, LC Packings, USA) and separated with an analytical reversed phase column (Reprosil-Pur C18 AQ, 3 µm; 150 mm x 75 µm, Dr. Maisch, Germany) using a 30 min gradient from 0 % B to 60% B (solvent A: 0.1 % formic acid; solvent B: 84% CH_3CN/0.1 % formic acid), at a flow rate of 280 nl/min. For electrospray ionization a distal coated SilicaTips (FS-360-20-10-D-20, New Objective, USA) and a needle voltage of 1.7 kV was used. Tandem mass spectrometry was performed with an Orbitrap XL mass spectrometer (Thermo Scientific, USA). MS and MS/MS spectra were acquired using cycles of one MS scan (mass range m/z 300-2000) and five subsequent data dependent CID MS/MS scans ("dynamic exclusionTM activated"; collision energy: 35%). RAW data were processed using MASCOT Daemon and MASCOT Server (V2.3, Matrix Science, Boston, USA) with the human subset of the SwissProt Database (Release 2012_11) and the following parameters: a) "Fixed modifications": Carbamidomethyl

(C) b) Variable modifications: Oxidation (M); c) Decoy database: checked, d) Peptide charge: 1+, 2+ and 3+; e) Peptide tol. ±: 2 Da; f) MS/MS tol. ±: 0.8 Da.

To generate a high quality dataset of secreted proteins and in order to minimize the number of false positive identifications the results were evaluated with the Scaffold software using the Peptide Prophet and Protein Prophet algorithms [61]. The probability threshold for identified proteins was set to ≥ 99% and exclusively IDs with at least 2 individual peptides were accepted. The reliability of the data was further evaluated by counting false positive MASCOT hits from the Decoy database [62].

2.2.10 Gene expression profiling

2.2.10.1 RNA isolation

Cell culture samples were lysed after treatment using cell lysis buffer of the *nucleo spin* RNA Isolation Kit (Macherey-Nagel). For isolation of RNA from tumor samples 30 mg of each tumor was lysed in 350 µl of cell lysis buffer additionally using FastPrep-24 tissue / cell homogenizer for tissue disruption. RNA isolation was performed according to the manufacturer's instructions.

2.2.10.2 Reverse transcription

1 µg of isolated RNA was transcribed with the Transcriptor High Fidelity cDNA Synthesis Kit (Roche) according to manufacturer's protocols using oligo-dT-primer.

2.2.10.3 Quantitative real-time PCR (qPCR)

Quantitative real-time PCR was performed using UPL Probes (Roche) and Probes Master (Roche) on a LightCycler 480 system (Roche) using GAPDH, Actin B and B2M as controls. Experiments were done in triplicates and the obtained average CT values of target genes were normalized to control as ΔCT. Changes in expression levels were shown as fold expression ($2^{-\Delta\Delta CT}$), calculated by the ΔΔCT method [62].

2.2.11 Protein analysis

2.2.11.1 Collection of cell culture supernatants

1×10^6 T-24 or MCF-7 cells were seeded per 10 cm dish or 1.5×10^6 cells per 75 cm² flask. 24 hours after seeding cells were washed 3 times (for proteomic analysis) or 1 time (western blot) with FCS free media. After treatment of the cells in 10 ml of FCS free media, supernatants were harvested, followed by centrifugation of 5 min at 1000 rpm to remove cells and cell debris. Supernatants were concentrated to a total volume of 50 µl using Amicon Ultra-4 Centrifugal Filter Units (cut off 3 kDa for proteomics and 10 kDa for western blot).

2.2.12 Preparation of whole cell lysates

After treatment cells were washed with cold PBS and lysed using 0.5 x cell lysis buffer from Promega. Cells were lysed on ice for 10 min and centrifuged at 13,000 rpm for 20 min to remove cell debris.

2.2.12.1 Protein quantification

Protein concentration was determined using the BCA (bicinchoninic acid) Protein Assay Kit from Thermo Scientific. The assay principle is that distinct protein side chains are reducing in an alkaline medium Cu^{2+} to $Cu^{1+.}$ Bicinchoninic acid selectively detects generated Cu^{1+} by a colorimetric reaction. BCA assay was performed in 96-well format according to the manufacturer's instructions. Shortly, 5 µl of sample or standard solution were incubated with 200 µl of reaction reagent for 30 min at 36 °C. Absorption was quantified at 590 nm with background correction at 630 nm using a tecan plate reader.

2.2.12.2 SDS-PAGE

The SDS-PAGE was performed according to Laemmli *et al.* [63]. 15-50 µg of total protein lysate or 30 µl concentrated supernatant were supplemented with Laemmli buffer and boiled for 5 min at 95 °C for protein denaturation. Samples were loaded on 10% or 12.5% SDS-PA-gels. Protein separation was performed at 0.03 mA per gel for approximately two hours.

2.2.12.3 Western Blot

After separation proteins were transferred to a nitrocellulose membrane by wet-blotting using the Mini Trans-Blot system from Biorad, Germany.

For each gel a sandwich was prepared where the gel and a nitrocellulose membrane are enclosed by two filter papers. The sandwiches were placed in the apparatus with the gel facing the cathode and the membrane facing the anode, to allow the negatively charged proteins (negative charge of associated SDS) to migrate from the gel onto the membrane. Blotting was performed in transfer buffer at 100 V for 35 min.

After blotting membranes were incubated with NET-gelatin buffer to block free protein binding sides of the membrane for 45 min. Incubation of the primary antibody was performed in NET-gelatin buffer at 4 °C overnight. Subsequently, primary antibody was removed and membranes were washed three times for 10 min with NET-gelatin buffer. Incubation of secondary antibodies coupled to peroxidase was done for 1 hour at room temperature, followed by a second washing step (3 x 10 min).

For developing the specific protein signals membranes were incubated with peroxidase substrate (Lumi-Light Western Blotting Substrate, Roche) for 5 min and chemiluminescence was detected by exposing the membranes to X-ray films for a distinct time period.

2.2.13 siRNA transfection

Cells were seeded in 10 cm dishes or 6-well plates. 24 hours after seeding and at a confluence of approximately 70% cells were transfected using lipofectamine 2000 reagent from Invitrogen. If put together Lipofectamine 2000 reagent forms liposomes with siRNA leading to an enhanced uptake into the cell. Lipoplexes were formed prior to transfection by adding siRNA in Opti-MEM to Lipofectamine 2000 in Opti-MEM. In a 10 cm dish 600 pmol siRNA (control or target siRNA) in 1.5 ml Opti-MEM and 60 µl Lipofectamine 2000 in 1.5 ml were used and were later added to 10 ml of cell culture media. In a 6-well 100 pmol siRNA (control or target siRNA) in 250 µl Opti-MEM and 10 µl Lipofectamine 2000 in 250 µl Opti-MEM were used and were later added to 2 ml of cell culture media. Lipoplexes were formed for 20 min at RT ad subsequently added to the cells. 4 hours later to transfection media was changed. Analysis was performed 24 and 48 hours post transfection. Control siRNA sequence:

5'-AUGUAUUGGCCUGUAUUAG-3' (sense) V-ATPase subunit V_0c: SMARTpool: ON-TARGETplus ATP6V0C siRNA, Thermo Fisher Scientific (USA).

2.2.14 Lysotracker staining

Cells were seeded in chamber slides. 24 hours after seeding archazolid treatment was performed. For lysosome staining 75 nM LysoTracker (Invitrogen) was added to the culture medium and incubated for 30 minutes. To stain the nuclei, Hoechst was added in a final concentration of 1 µg/ml and incubated for 5 minutes.

2.2.15 Confocal microscopy

2×10^4 cells were seeded on coverslips in 6-well plates. After treatment they were fixed with 4% PFA for 15 min. For intracellular staining samples were permeabilized with 0.2% triton X 100 in PBS for 10 min followed by blocking with 10% FCS + 0.05% Triton X 100 in PBS for 45 minutes. Incubation with indicated primary antibodies (1:100-1:200) was performed for one hour at RT or overnight at 4 °C, followed by incubation with respective secondary antibodies (1:400) for 1 hour and Hoechst or DAPI (1 µg/ml) for 10-15 min. Coverslips were mounted using FlourSave (Calbiochem) mounting medium. Images were captured using 63 X 1.4 Oil DIC objective of Laser Scanning Microscope LSM 510 Meta and analyzed using Zeiss image browser version 3.2.0.115.

2.2.16 Statistical analysis

For statistical significance unpaired Students t-test was performed using GraphPadPrismTM. P-values < 0.05 were considered as significant. Furthermore in the *ex vivo* luciferase experiment significant outlier were removed using Grubbs' test (alpha = 0.05).

3 Results

3.1 Gene expression analysis of resistance formation upon metronomic CPA therapy

To analyze the changes in gene expression after resistance formation upon metronomic cyclophosphamide therapy a microarray was performed previously as described in the dissertation of Lilja Thoenes (2009, LMU) and in the introduction part (1.1).

In the following the validation and a detailed evaluation of the microarray results is presented. Analysis was focused on the differences between tumors of the *in vivo* passaged control cell line PC3 A3 and tumors of the two resistant cell lines PC3 D3 and PC3 D4. The most differentially regulated genes dehydrogenase/reductase member 2 (DHRS2), PAS domain containing protein 1 (PASD1) and neurotensin (NTS) as well as resistance related genes special AT-rich sequence-binding protein-1 (SATB1) and morphogenetic protein receptor type I B (BMPR1B) were chosen for microarray validation. Moreover, the involvement of two distinct genes 1) SATB1 and 2) ANXA3 was further evaluated. Furthermore, a KEGG-Pathway analysis revealed 3 potentially resistance associated pathways.

3.1.1 Validation of regulated genes

To validate the microarray results (Figure 1-4) five genes were chosen for qPCR analysis. Confirming the microarray results, expression of DHRS2, PASD1 and SATB1 was increased in resistant tumors compared to PC3 A3 control tumors. NTS and BMPR1B expression was decreased in resistant tissue (Figure 3-1).

In general, gene regulations were stronger in PC3 D4 than in PC3 D3. For example DHRS2 expression was increased 11-fold in PC3 D4 and 7-fold in PC3 D3. BMPR1B was reduced significantly in PC3 D4, whereas in PC3 D3 BMPR1B was only marginally reduced. Furthermore, expression of PASD1 was induced 11.7-fold in PC3 D3 and 9.1-fold in PC3 D4 compared to PC3 A3 control tumors. Also SATB1 expression was induced in resistant tissue (2.4-fold in PC3 D3 and 2.3-fold in PC3 D4). In contrast, expression of NTS was clearly reduced in resistant sublines (5-fold in PC3 D3 and PC3 D4) (Figure 3-1).
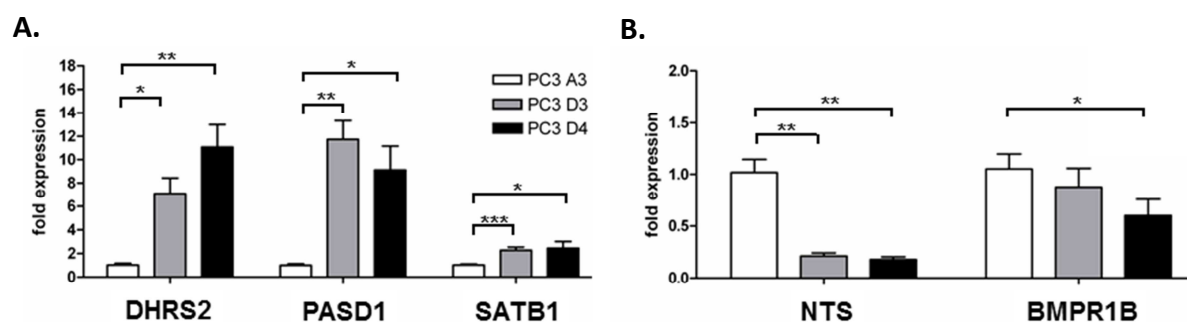
Figure 3-1 Target gene expression
Validation of differentially expressed genes by qPCR: **A.** dehydrogenase/reductase member 2 (DHRS2), PAS domain containing protein 1 (PASD1), special AT-rich sequence-binding protein-1 (SATB1), **B.** neurotensin (NTS) and bone morphogenetic protein receptor, type I B (BMPR1B) $*p < 0.05$, $**p < 0.005$, $***p < 0.0005$ (t-test)

As resistant cell lines displayed their resistance only upon reimplantation *in vivo* and were sensitive to the activated form of CPA (4-HOO-CPA) *in vitro* (Figure 1-1 B), the expression of these five genes in the sublines under cell culture conditions was analyzed. As shown in Figure 3-2, *in vitro* expression of these genes clearly differed from *in vivo* expression. Whereas, DHRS1, PASD1 and SATB1 were less but still differentially expressed in resistant cell lines PC3 D3 and PCR D4, NTS and BMPR1B were not significantly reduced *in vitro*.
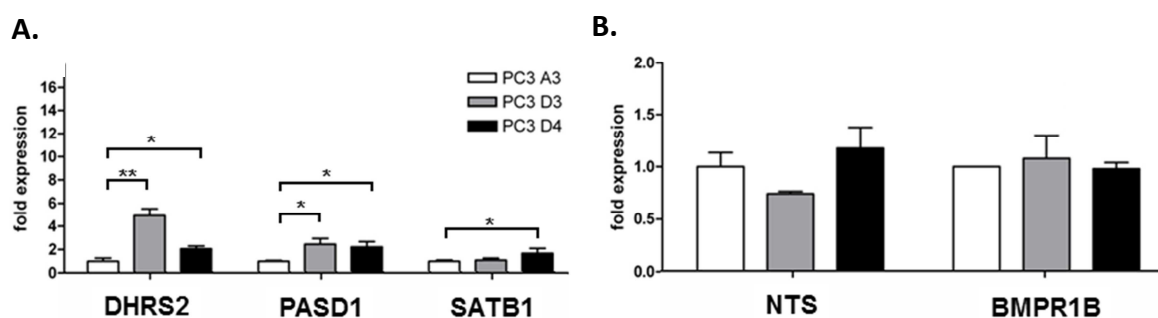

Figure 3-2 Target gene expression *in vitro*
Target gene expression in cell culture was analyzed by qPCR: **A.** dehydrogenase/reductase member 2 (DHRS2), PAS domain containing protein 1 (PASD1), special AT-rich sequence-binding protein-1 (SATB1), **B.** neurotensin (NTS) and bone morphogenetic protein receptor, type I B (BMPR1B) $*p < 0.05$, $**p < 0.005$, $***p < 0.0005$ (t-test)

3.1.2 Generation and analysis of ANXA3 and SATB1 over expressing PC3 clones

As the microarray results were approved by qPCR, the particular involvement in chemoresistance of two distinct genes was checked. 1) SATB1, a transcription factor, which

was reported to play a role in resistance upon cisplatin resistance in hepatocellular carcinoma [64] and 2) ANXA3, a protein previously found in a proteomic study to be more abundant in resistant PC3 clones on protein level [13]. In cooperation with Mark Laible, Stephanie Blaich and Melanie Hudler (DKFZ, Heidelberg) PC3 clones were stably transfected with SATB1 (PC3 SATB1), ANXA3 (PC3 ANXA3) or an empty vector construct (PC3 ev). The target genes are expressed under the regulation of a doxycycline dependent promoter. To ensure a stable over-expression a system which uses homologous recombination was applied (see dissertation of Stephanie Blaich, Ruprecht - Karls – Universität Heidelberg, 2007 for details). To control the correct expression of the target genes mRNA and protein expression was determined by qPCR and western blot analysis. PC3 SATB1 and PC3 ev (control) were seeded. 24 hours later the expression was induced with 50 nM doxycycline for another 24 hours. Induction of the target gene expression was analyzed by qPCR. Results are shown in Figure 3-3 A. SATB1 expression was strongly induced by doxycycline in PC3 SATB1 but not in the empty vector control. Notably, PC3 SATB1 already expressed minor amounts of SATB1 mRNA without induction of doxycycline. In a next step the correct translation of the protein was analyzed by western blot. As shown in Figure 3-3 B detectable amounts of SATB1 were only expressed by induced PC3 SATB1 cells.
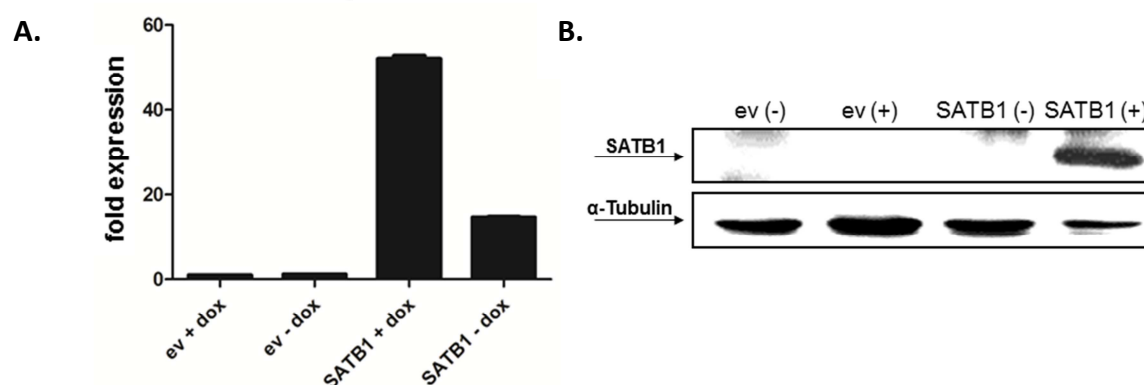
Figure 3-3 Validation of PC3-SATB1 by qPCR and western blot
A. qPCR of RNA **B.** western blot of protein lysates isolated from induced (24 hours, 50 nM doxycycline (+dox)) and not induced (-dox) PC3 SATB1 cells and PC3 ev (control).

To evaluate the correct localization of SATB1 inside the cell, immuno-fluorescence imaging was performed. As shown in Figure 3-4 SATB1 protein was localized in the nucleus of doxycycline induced PC3 SATB1 cells.
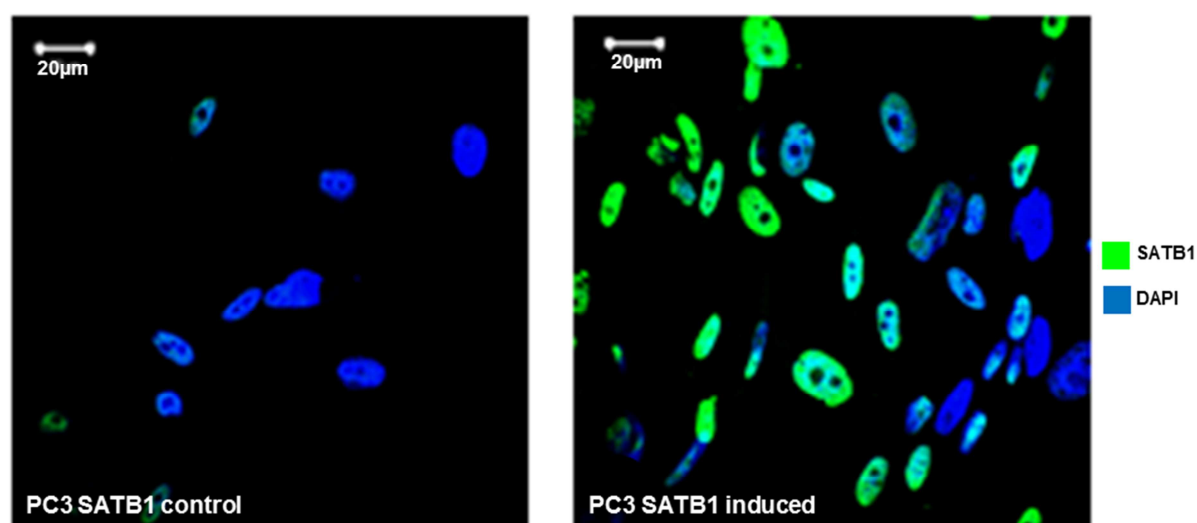
Figure 3-4 Immuno-fluorescence imaging of PC3-SATB1
PC3-SATB1 cells were cultivated on coverslips in 6-well plates and **A.** not induced (control) or **B.** induced using 50 nM doxycycline for 24 hours; blue = nuclei (Hoechst) green = SATB1 (alexa 488)

Subsequent to validation of the correct inducible over-expression of SATB1 in PC3 SATB1 cells its influence on the chemo-sensitivity *in vitro* was evaluated. CPA is a prodrug which is only active in its metabolized form (4-HOO-CPA). After activation in the liver 4-HOO-CPA is a strong alkylating drug, targeting proliferating cancer cells (reviewed by Fenselau [65]). In the *in vitro* experiments CPA was substituted by melphalan another alkylating drug which does not have to be metabolically activated. Additionally, cell death induction by cisplatin was analyzed, as SATB1 earlier had been shown to induce cisplatin resistance in hepatocellular carcinoma [64]. Cells were seeded in 96-well plates and expression of SATB1 was induced by 50 nM doxycycline for 24 hours. Subsequently melphalan or cisplatin treatment was carried out. As shown in Figure 3-5 A SATB1 overexpression had no influence on the chemo-sensitivity to melphalan *in vitro*. Cell death was provoked under induced and not induced conditions at the same level. In contrast, SATB1 overexpression altered the chemo-sensitivity against cisplatin. As shown in Figure 3-5 B SATB1 overexpressing cells were less sensitive to the cisplatin treatment than not induced cells.
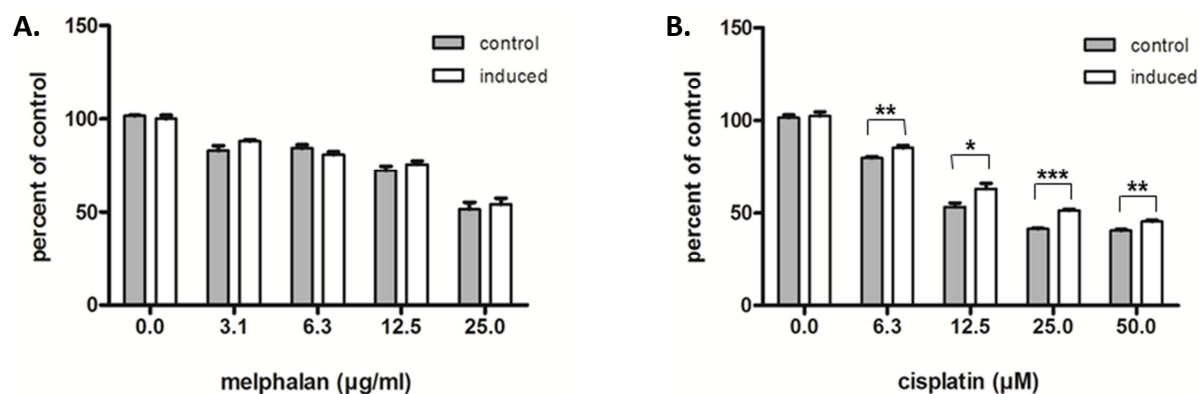
Figure 3-5 Functional analysis of SATB1 overexpression PC3 SATB1 cell line
Cells were seeded in 96-well plates. One day after seeding STAB1 expression was induced by 50 nM doxycycline for 24 hours. Subsequently chemotherapy, melphalan **A.** or cisplatin **B.,** was applied for 72 hours. Cytotoxicity was determined by CellTiterGlo assay. Data is presented as percent of untreated control cells. *p < 0.05, **p< 0.005, ***p<0.0005 (t-test)

Similar experiments were performed using the PC3 ANXA3 cell line. Again the empty vector cell line (PC3 ev = empty vector) served as control.

As shown in Figure 3-6 A the endogenous expression of ANXA3 mRNA and protein was already high. The induction by doxycycline increased the mRNA expression about 1.75-fold. In concordance, the expression on protein level was only increased marginally (Figure 3-6 B). Immuno-fluorescence imaging showed that ANXA3 was located in the cytoplasm of both ANXA3 induced and not induced cells (Figure 3-6 C).

The functional analysis showed no alteration in chemo-sensitivity to neither melphalan nor cisplatin of ANXA3 overexpressing cells compared to not induced control cells (Figure 3-6 D and E).
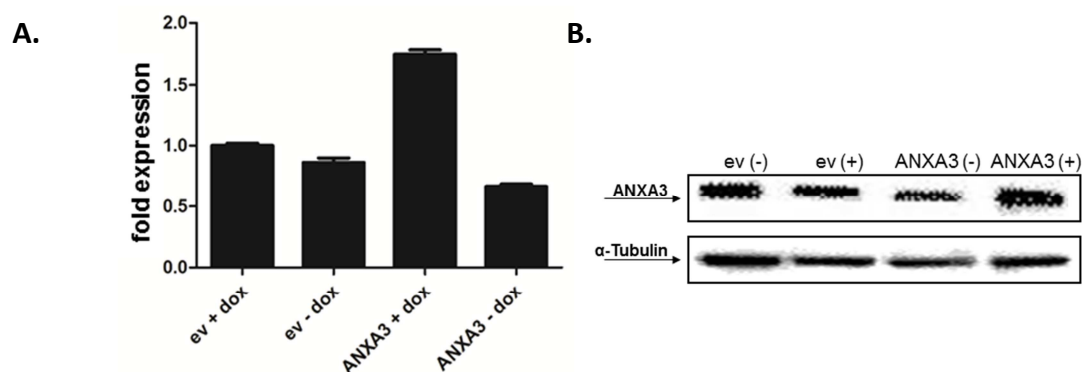

Figure 3-6 continued
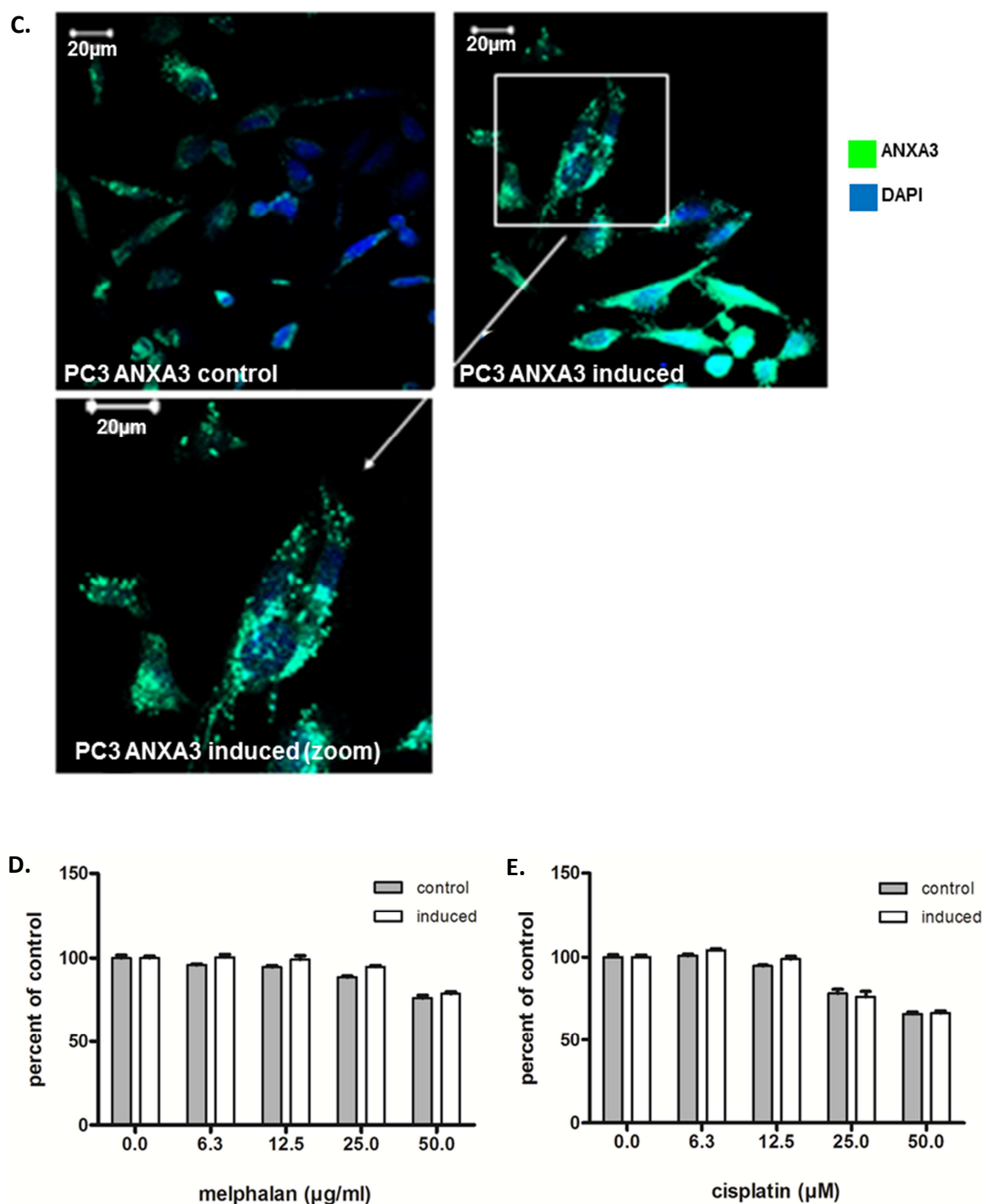
Figure 3-6 Analysis of ANXA3 overexpression PC3 ANXA3 cell line
A. qPCR of RNA **B.** western blot of protein lysates isolated from induced (24 hours, 50 nM doxycycline (+dox))
and not induced (control (-dox)) PC3 ANXA3 cells and PC3 ev (control) **C.** ANXA3 expression was induced using
50 nM doxycycline and not induced (control) for 24 hours; blue = nuclei (Hoechst) green = ANXA3 (alexa 488).
D. + E. ANXA3 expression was induced by 50 nM doxycycline for 24 hours. Thereafter, chemotherapy,
melphalan or cisplatin, was applied for 72 hours. Cytotoxicity was determined by CellTiterGlo assay. Data is
presented as percent of untreated control cells.

Taken together neither ANXA3 nor SATB1 alone were able to induce an *in vitro* resistance to the alkylating drug melphalan. Notably, a potential influence of ANXA3 or SATB1 overexpression *in vivo* was not evaluated within the framework of this thesis.

Further analysis was no longer focused on one special gene but more on the involvement of whole pathways and microenvironmental factors.

3.1.3 Analysis of pathways involved in chemoresistance

For further analysis different points were taken into account: 1) Resistant cell lines showed no *in vitro* resistance [13]. 2) The expression of *in vivo* regulated genes differed a lot from *in vitro* (Figure 3-1 and Figure 3-2). 3) No correlations of single target genes to resistance could be made *in vitro* (3.1.2). All these points lead to the hypothesis that the mechanism leading to chemoresistance to anti-angiogenic therapy are very complex, including the alteration of whole signaling pathways.

To evaluate which pathways might be involved in resistance formation, a KEGG-pathway analysis was performed, including all genes with an expression change of 0.4 fold (up- and downregulated). This analysis revealed a potential involvement of three pathways: 1) *axon guidance*, 2) *steroid biosynthesis* and 3) *complement and coagulation cascades* (Figure 3-7). As blood flow might play a crucial role during resistance formation to anti-angiogenic therapy, further analysis was focused on the genes grouped in *complement and coagulation cascades*. In *complement and coagulation cascades* grouped genes included: tissue factor (F3), plasminogen activator tissue (PLAT), protein S (PROS), serine peptidase inhibitors A1 and D1. After the analysis two differentially expressed coagulation genes annexin A3 (ANXA3) and serine peptidase inhibitor clade B 7 (SERPINB7) were added to this group from the list of differentially expressed genes, as they are also reported to be correlated with coagulation. ANXA3 was shown to inhibit coagulation *in vitro* and SERPINB7 is a member of the serpins, a coagulation related protein-family [66, 67].

The expression pattern of the grouped genes was as follows: In resistant tissue the expression of coagulation related genes tissue factor (F3), plasminogen activator tissue (PLAT) and annexin A3 (ANXA3) was increased in resistant tumors, whereas the expression of protein S (PROS1), and serine proteinase inhibitors: SERPIND1, SERPINA1 and SERPINB7 was decreased (Table 3-1).
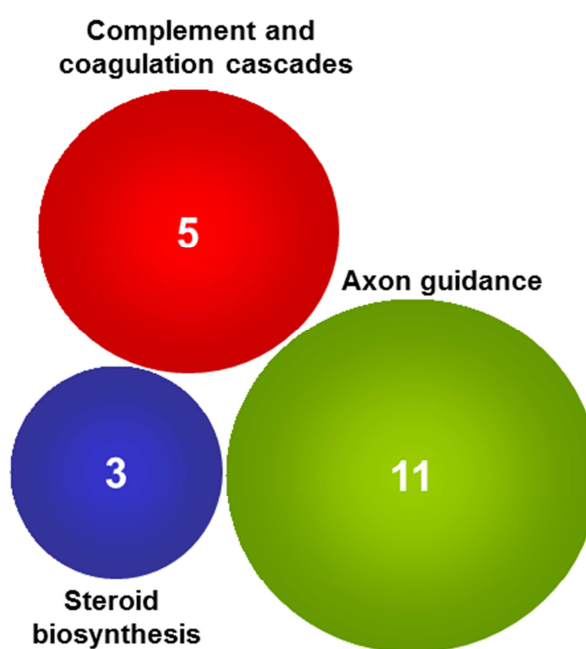
term	count	%	p-value
Axon guidance	11	3.4	0.00019
Steroid biosynthesis	3	0.9	0.04298
Complement and coagulation cascades	5	1.5	0.04605

**Figure 3-7 KEGG-Pathway analysis of regulated genes**
KEGG-Pathway analysis of differentially expressed genes (377 genes +/- 0.4 rel. expr. change)

Table 3-1 Expression of *complement and coagulation cascades* associated genes

transcript cluster ID	gene symbol	gene title	fold expression	p-value (ANOVA)
7917875	F3	coagulation factor III (thromboplastin, tissue factor)	1.16	0.053523
8150509	PLAT	plasminogen activator, tissue	0.77	0.000282
8095986	ANXA3	annexin A3	0.44	0.023838
8089015	PROS1	protein S (alpha)	-0.46	0.002819
8071420	SERPIND1	serpin peptidase inhibitor, clade D (heparin cofactor), member 1	-0.55	0.002667
7981068	SERPINA1	serpin peptidase inhibitor, clade A (alpha-1 antiproteinase, antitrypsin), member 1	-0.72	0.000050
8021623	SERPINB7	serpin peptidase inhibitor, clade B (ovalbumin), member 7	-0.91	0.026533

3.1.3.1 Gene expression of coagulation in resistant tumors

To confirm the in the microarray predicted differential expression of coagulation related genes qPCR analysis was performed. Results are shown in Figure 3-8 as fold expression of control tumors (PC3 A3). The expression level of tissue factor was slightly increased. In PC3 D3 tumor tissue and in PC3 D4 tumor tissue F3 was highly expressed.
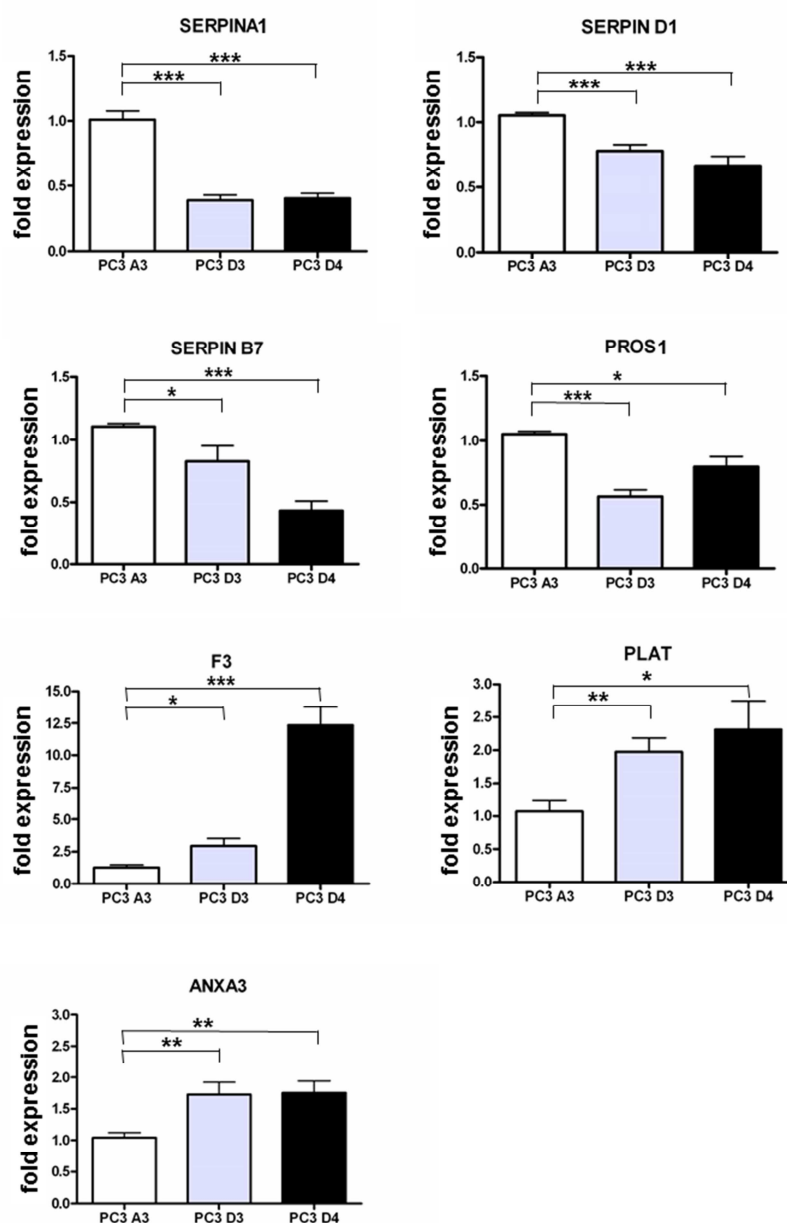

Figure 3-8 Expression of coagulation related genes
Validation of coagulation related gene expression by qPCR, SERPINA1 = serpin peptidase inhibitor clade A member 1, SERPIND1 = serpin peptidase inhibitor clade D member 1, SERPINB7 = serpin peptidase inhibitor clade B member 7, PROS1 = protein S (alpha), F3 = tissue factor, PLAT= plasminogen activator tissue and ANXA3 = annexin A3 *p < 0.05 (t-test)

In contrast, SERPINA1 expression was reduced in resistant tumor tissue. In accordance, two potentially coagulation promoting genes SERPIND1 and SERPINB7 were downregulated in resistant tumors. Moreover, mRNA expression of proteins hampering coagulation PLAT and ANXA3 was increased in PC3 D3 and PC3 D4 tumor tissue compared to PC3 A3 control tissue (Figure 3-8).

When analyzing the gene expression from *in vitro* cultured cell lines again a different pattern was observed: F3, PLAT, ANXA3 showed no altered gene expression in PC3 D3 and PC3 D4 *versus* PC3 A3 (Figure 3-9), whereas the expression profile of SERPINA1, SERPIND1, SERPINB7 and PROS1 were similar to that *in vivo*.

In summary PLAT and ANXA3 that encode anti-coagulation proteins were upregulated and the SERPINs which are potentially promoting coagulation were downregulated in resistant tumor tissue, compared to *in vivo* passaged control tumors. These effects were not present *in vitro*. Interestingly, in contrast to the SERPINS the expression of pro-coagulation F3 gene was upregulated.
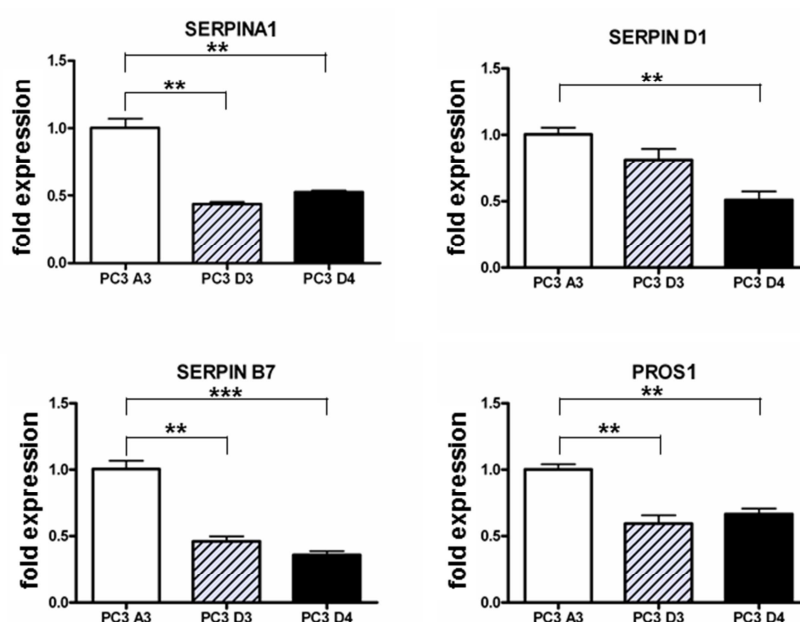

Figure 3-9 continued
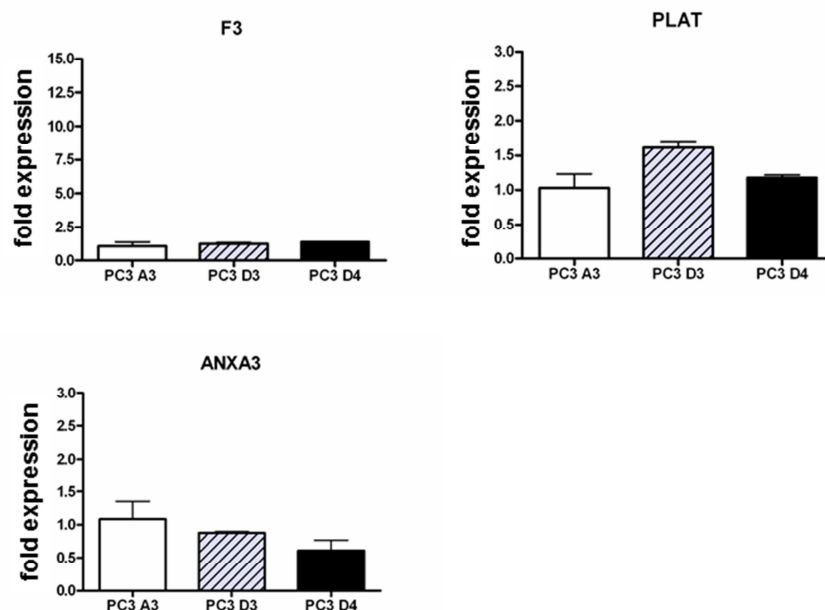
Figure 3-9 expression of coagulation related genes i*n vitro*
Expression of coagulation related genes in cell culture samples: SERPINA1 = serpin peptidase inhibitor clade A member 1, SERPIND1 = serpin peptidase inhibitor clade D member 1, SERPINB7 = serpin peptidase inhibitor clade B member 7, PROS1 = protein S (alpha), F3 = tissue factor, PLAT= plasminogen activator tissue and ANXA3 = annexin A3 *p < 0.05 (t-test)

3.1.3.2   F3 exon structure is altered in resistant PC3 D4 tumors

F3 is a candidate which does not fit into the structure of an anti-coagulative status. F3 is highly upregulated in resistant tumors, but is a coagulation promoting gene. As shown in the introduction part (Figure 1-5), the exon structure of F3 was irregular. The microarray probe setup allows the expression of a single exon in detail. Comparing resistant PC3 D4 to *in vivo* passaged control PC3 A3 tissue, the exon expression profile of F3 shows an altered signal intensity between exon 3 and 6, whereas no differences were detected in exon 1 and 2 (Figure 1-5). This indicates an expression of different F3 isoforms. Sequencing of the F3 gene transcript revealed no mutations in the coding sequence (data not shown). Thus it was hypothesized that two diverse transcripts of the F3 gene are present, one being prominently expressed in PC3 D4 tumors. To prove this finding, the expression levels of exon 1-2 and exon 5-6 were analyzed by qPCR respectively. In PC3 D4 a higher relative expression of exon 5-6 compared to exon 1-2, providing evidence for the presence of two different F3 transcripts (Figure 3-10 A) was observed. Western blot analysis of the F3 protein expressed

by PC3 D4 cell line when cultured *in vitro* compared to samples from tumor tissue directly reflects the qPCR results (Figure 3-10 B). *In vitro* PC3 D4 cells expressed low levels of F3 protein, with a molecular weight of 47 kDa. On the contrary, in PC3 D4 tumor samples two types of F3 protein were observed, one with 47 kDa and another one with a lower molecular weight. The smaller F3 form is more abundant than the 47 kDa form (Figure 3-10 B).
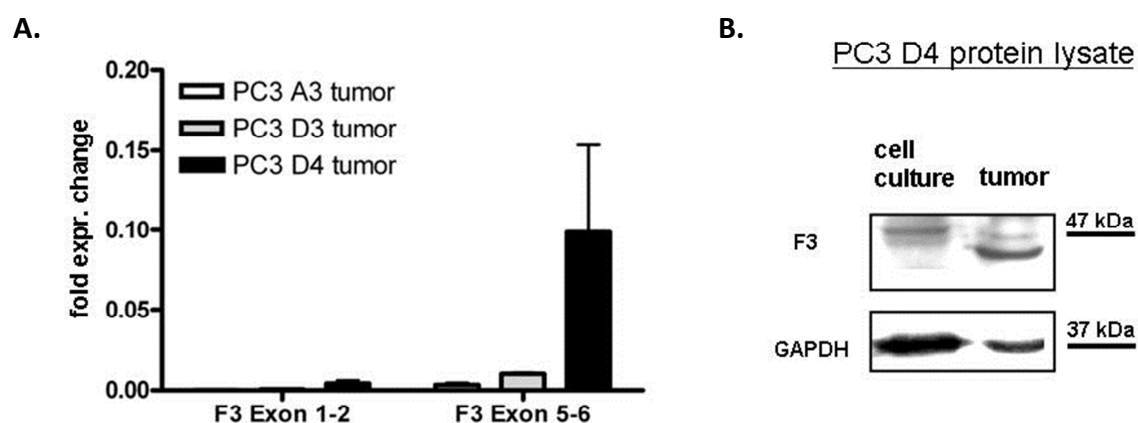

Figure 3-10 Analysis of F3 exon expression
A. qPCR of exon 1-2 and exon 5-6 of F3 **B.** western blot analysis of F3 in resistant cell line PC3 D4 from *in vitro* cell culture samples and *in vivo* tumor samples

Overall, it can be hypothesized that the additional short form of F3 missing exon 1 and 2 in resistant tumors is present *in vivo*. This shortening might lead to a loss of function, helping to maintain the anti-coagulative status.

Taken together microarray analysis revealed a potential involvement of anti-coagulation in resistances formation upon metronomic CPA therapy.

3.1.4   Anti-coagulation *in vivo*

It could be shown that coagulation might be one of the pathways involved in resistance to metronomic CPA therapy. Anti-coagulation genes were upregulated and pro-coagulation genes were downregulated. To analyze if an anti-coagulative status contributes to resistance formation upon metronomic CPA treatment, the effect of warfarin was tested. Warfarin is an anti-coagulative drug.

PC3 A3 cells were injected subcutaneously into the flanks of male SCID mice (5-7 per group). Two of in total four groups were treated with CPA (120 mg/kg every sixth day, *i.p.*) starting

at day 12 after tumor inoculation. The other two groups served as control. One of the CPA groups and one of the control groups were treated additionally with warfarin, starting at day 11 after tumor inoculation. Until day 18, warfarin was applied over the drinking water. As mice stopped drinking around day 16 the treatment regimen was change to warfarin 5 mg/kg *i.p.* every third day. Mice carrying tumors bigger than 1000 mm³ were euthanized. On day 57 the experiment had to be stopped due to severe weight loss. Analysis was carried out including only those 3 mice per group which lived until day 57, mice of the CPA treatment groups which had to be euthanized before day 57 were excluded. As shown in Figure 3-11 CPA treatment significantly reduced tumor growth. Approximately at day 40 PC3 A3 tumors restarted growing. Warfarin had no significant effect on resistance formation. Comparing tumor sizes relative to day 11 warfarin and CPA treated tumors are growing slightly but not significantly faster than CPA treated tumors without warfarin administration (Figure 3-11).
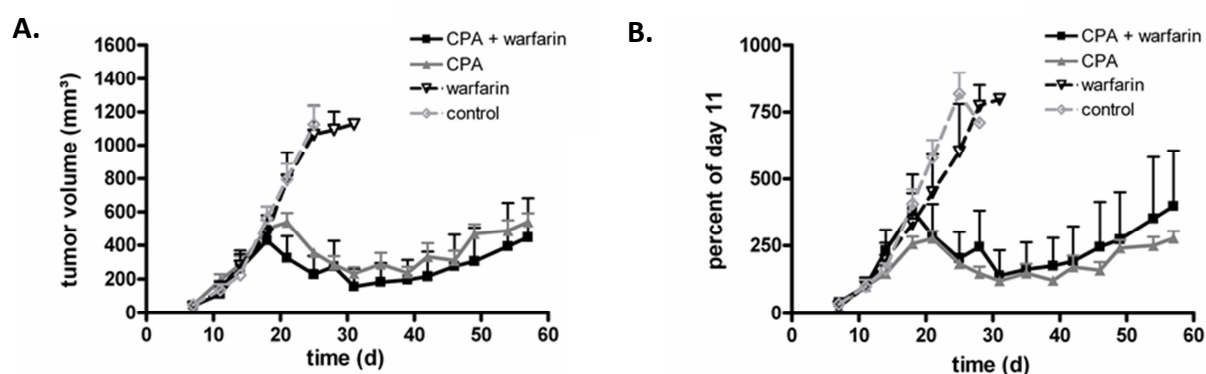

Figure 3-11 PC3 A3 tumor growth *in vivo*
Growth of PC3 A3 *s.c.* tumors over time. **A.** tumor volume **B.** percent of tumor volume on day 11

In summary, it could be shown that resistance to metronomic therapy is a complex mechanism. Neither overexpression of ANXA3 nor SATB1 (both genes were upregulated in resistant tissue) were able to provoke an *in vitro* resistance. Moreover, the involvement of whole pathways and signaling cascades in resistance formation was shown. In particular, the pathway of *complement and coagulation cascades* was shown to be altered in resistant tissue. Up to now this involvement could not been proved *in vivo,* as warfarin, an inhibitor of coagulation did not accelerate resistance to metronomic CPA therapy in a first *in vivo* experiment.

3.2   Characterization of archazolid action on the secretion profile of eukaryotic cells

In cancer the V-ATPase plays a pivotal role. It can be located on the plasma membrane as well as on intracellular membranes like the lysosome membrane. The V-ATPase is an ATP dependent proton pump and pumps protons out of the cell or into lysosomes. Thus it maintains the intracellular pH and acidifies endosomes and prelysosomal compartments.

It is known from literature that V-ATPase inhibition strongly alters exo- and endocytotic events by interfering intracellular trafficking [68, 69]. As the microenvironment plays an important role in cancer progression the influence of archazolid, a novel V-ATPase inhibitor, on the secretion profile of eukaryotic cells was evaluated. Therefore, the protein abundance in supernatants of archazolid treated highly migratory [70] human urinary bladder carcinoma cells and primary human monocytes were analyzed by LC-MS/MS.

All LC-MS/MS measurements were performed in cooperation with Dr. Thomas Froehlich and Dr. Georg J. Arnold (Genzentrum, LMU Munich, Germany).

3.2.1   Secretome analysis of archazolid treated monocytes

As mentioned before the microenvironment plays a crucial role in cancer progression. Especially, the influence of the immune system is critical, as it can defeat and actively kill tumor cells as well as promote tumor growth. To get a first insight, which proteins are secreted from primary human monocytes a qualitative analysis was performed. Monocytes were treated with 10 nM archazolid for 24 hours in serum free media. To promote the secretion of pro-inflammatory cytokines, stimulation with lipopolysaccharides (LPS) was performed simultaneously. Supernatants were collected, concentrated and separated using SDS-PAGE (Figure 3-12 A). The coomassie stained gel shows a slightly stronger staining in lanes C and D compared to the control in lane A and B which leads to a first assumption that an increased amount of proteins was secreted during archazolid treatment. In contrast, an alteration of the secretion profile by LPS was not visible on the gel. Furthermore, one can estimate that the fetal calf serum (FCS) contamination was neglect able, as the serum albumin signal around 60 kDa was in the appropriate intensity. To identify the present proteins, lanes were cut into 10 pieces and analyzed using LC-MS/MS.

In total 152 proteins were identified. Further, an analysis of the cellular components of the identified genes using uniprot.org identified 17% as secreted proteins. The majority was identified as intracellular proteins (Figure 3-12 B). Notably, identification of secreted proteins is strongly depended on the algorithm applied by the used software. Thus, the assignment of the identified proteins to cellular compartments only served to get a first insight to the data (Figure 3-12 B). Furthermore a *KEGG-Pathway* analysis using DAVID bioinformatics indicated the involvement of different pathways. The five most enriched are: 1) *regulation of the actin cytoskeleton*, 2) *glycolysis and gluconeogenesis,* 3) *leukocyte transendothelial migration*, 4) *focal adhesion* and 5) *systemic lupus erythematosus* (Figure 3-12 C).

A.

B.

C.

	pathway	count	p-value
1	Regulation of actin cytoskeleton	19	2,80E-06
2	Glycolysis / Gluconeogenesis	14	3,70E-09
3	Leukocyte transendothelial migration	10	7,90E-03
4	Focal adhesion	10	1,10E-01
5	Systemic lupus erythematosus	9	9,30E-03
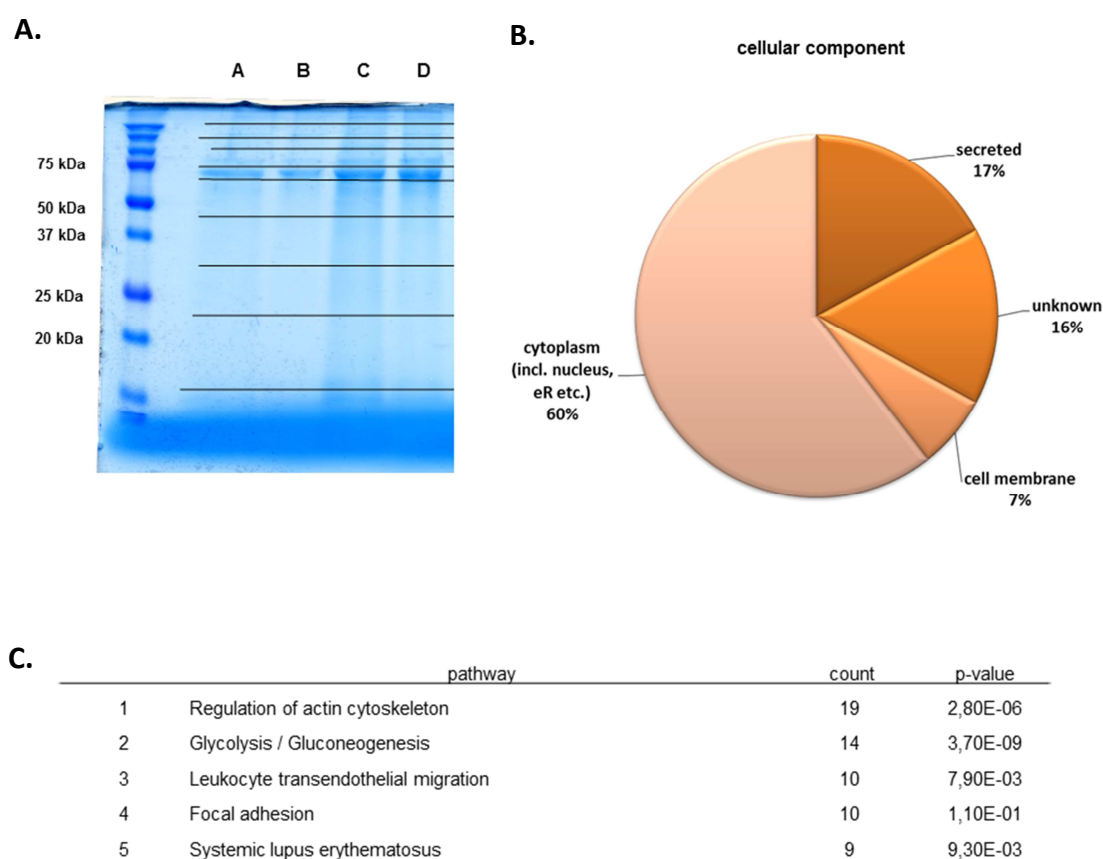
Figure 3-12 LC-MS/MS Analysis of secreted proteins
A. 5×10^6 human primary monocytes were seeded per 75 cm^2 cell culture flasks and treated with 10 nM archazolid (lanes C and D) or 0.01% DMSO as control (lanes A and B). LPS stimulation was done using 1 µg/ml (lanes A and C). Supernatants were collected after 24 hours, concentrated and SDS-PAGE was performed using a 12.5% gel. After electrophoresis each lane was cut into 10 similar pieces. A total number of 152 proteins were identified. Identified proteins were analyzed using uniprot.org and DAVID bioinformatics. **B.** Cellular component of identified proteins **C.** KEGG-Pathway analysis of identified proteins, p-values equal or smaller than 0.05 were considered as strongly enriched. 16 pathways were identified as strongly enriched. Shown are the 5 pathways with the highest count numbers.

In a second approach secreted proteins of human monocytes were quantified using the iTRAQ (**I**sobaric **t**ag for **r**elative and **a**bsolute **q**uantitation) method (Figure 3-13). Here, protein abundance in a given sample can be quantified using an isotope-coded covalent tags (reviewed by Zieske, 2006 [71].
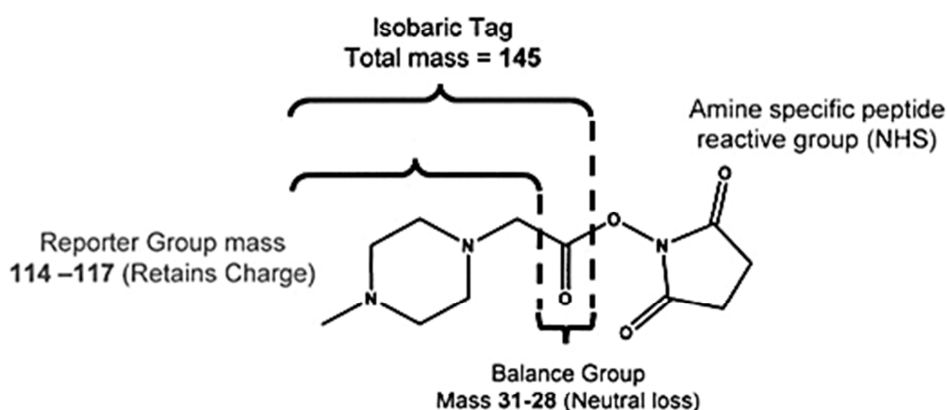

Figure 3-13 Chemical structure of the iTRAQ-label
The iTRAQ-label contains an isobaric tag consisting of a charged reporter group, a peptide reactive group, and a neutral balance portion to maintain an overall mass of 145 [71].

Human primary monocytes activated with LPS (lipopolysaccharides) were treated with 10 nM archazolid for 24 hours or not treated. Protein abundance in the respective supernatants was analyzed. Three LC-MS/MS measurements, comparing one treated sample with one control sample were performed. In Table 3-2 results of all three measurements are shown. A cut off of 0.4 relative differences in abundance was set. Although all samples were prepared simultaneously, differences in relative abundance appeared very diverse within the measurements.

To draw further conclusions western blot validation has to be performed in future experiments. Potential candidates for validation may be: 1) thrombospondin 1 (TSP1_HUMAN) as it is differentially abundant in all three samples, 2) interleukin 6 and 8) interleukin 8 as they are both cytokines involved in monocyte mediated signal transduction.

Table 3-2 Relative quantification (iTRAQ) of secreted proteins

withe background: less abundant, gray= more abundant

	Sample 7_5			Sample 7_6			Sample 7_7	
#	Accession Number	rel. a	#	Accession Number	rel. a	#	Accession Number	rel. a
1	ALBU_HUMAN	-1,3	1	VIME_HUMAN	-1,4	8	**TSP1_HUMAN**	-1,9
2	ACTB_HUMAN	-0,9	2	MOES_HUMAN	-1,2	98	ANXA6_HUMAN	-1,7
3	VIME_HUMAN	-0,6	3	PROF1_HUMAN	-1	40	IL6_HUMAN	-1,4
4	ENOA_HUMAN	-0,6	4	ACTB_HUMAN	-1	72	K2C1_HUMAN	-1,4
5	PROF1_HUMAN	-0,6	5	ENOA_HUMAN	-1	31	PAI2_HUMAN	-1
6	**TSP1_HUMAN**	-0,4	6	MYH9_HUMAN	-0,8	58	IL8_HUMAN	-1
7	TPIS_HUMAN	-0,4	7	PLSL_HUMAN	-0,7	45	S10A8_HUMAN	-0,8
			8	FLNA_HUMAN	-0,7	53	CLIC1_HUMAN	-0,7
			9	ALBU_HUMAN	-0,7	27	S10A9_HUMAN	-0,5
			10	**TSP1_HUMAN**	-0,6	28	CXCL7_HUMAN	-0,5
			11	K2C1_HUMAN	-0,6	41	TLN1_HUMAN	-0,5
			12	H4_HUMAN	-0,6	46	COF1_HUMAN	-0,5
			13	1433Z_HUMAN	-0,6	23	H2B1C_HUMAN	-0,4
			14	TKT_HUMAN	-0,6	71	H31T_HUMAN	-0,4
			15	ALDOA_HUMAN	-0,6			
			16	LYSC_HUMAN	-0,6			
			17	ACTN4_HUMAN	-0,5			
			18	G6PI_HUMAN	-0,5			
			19	H2B1C_HUMAN	-0,5			
			20	ANXA1_HUMAN	-0,4			
			21	COR1A_HUMAN	-0,4			
			22	K1C10_HUMAN	-0,4			
			23	S10AB_HUMAN	-0,4			
			24	HSP7C_HUMAN	-0,4			
			25	TALDO_HUMAN	-0,4			
27	ITAM_HUMAN	0,4	78	H12_HUMAN	0,4	17	1433Z_HUMAN	0,4
28	MYH9_HUMAN	0,4	79	HEXB_HUMAN	0,4	33	GDIR2_HUMAN	0,4
29	PRDX1_HUMAN	0,4	80	HNRH1_HUMAN	0,4	67	PPIB_HUMAN	0,4
30	SH3L3_HUMAN	0,5	81	KCD12_HUMAN	0,5	93	SH3L1_HUMAN	0,4
31	TPM3_HUMAN	0,6	82	LEG1_HUMAN	0,5	32	HSP71_HUMAN	0,5
32	TALDO_HUMAN	0,6	83	LKHA4_HUMAN	0,5	36	H14_HUMAN	0,5
33	ELNE_HUMAN	0,6	84	PPIB_HUMAN	0,9	65	PERM_HUMAN	0,5
34	DEF1_HUMAN	0,7	85	SHPS1_HUMAN	0,9	70	CATS_HUMAN	0,5
			86	STMN1_HUMAN	0,9	82	FETUA_HUMAN	0,5
			87	SUMO2_HUMAN	1	75	TAGL2_HUMAN	0,7
			88	THIO_HUMAN	1	88	NPC2_HUMAN	0,8
			89	ANXA2_HUMAN	1,1	84	G3P_HUMAN	0,9
			90	CATS_HUMAN	1,1	90	PLBL1_HUMAN	1,3
			91	NUCL_HUMAN	1,4	38	SAP_HUMAN	1,4
			92	PAI2_HUMAN	1,5			
			93	B2MG_HUMAN	1,7			
			94	CALR_HUMAN	6,2			

Additional to the proteomic analysis of monocytes supernatants, corresponding cell lysates were analyzed by western blot. Furthermore, human primary monocytes were differentiated into macrophages and treated with 10 nM archazolid for 4 hours. As it will be shown in the following chapters, abundance of the lysosomal protease and tumor marker cathepsin B is strongly altered by archazolid treatment. Thus, cathepsin B protein in cell lysates of macrophages and monocytes was analyzed by western blot. As shown in Figure 3-14 cathepsin B protein was not detectable in monocytes. In contrast in macrophages cathepsin B was strongly expressed. Here archazolid treatment significantly reduced the amount of mature cathepsin B.
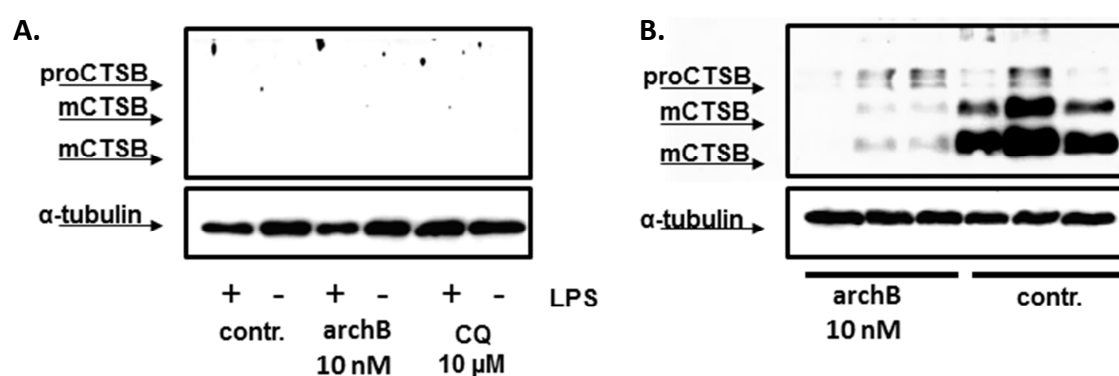
Figure 3-14 Cathepsin B secretion of primary human monocytes and macrophages
A. Human primary monocytes were treated with 10 nM archazolid = archB, lysosomotropic agent chloroquine = CQ (10 μM) or control treated with 0.01% DMSO. LPS stimulation was done using 1 μg/ml. Cells were lysed after 24 hours, concentrated and western blot analysis of cathepsin B was performed. **B.** Human primary macrophages were seeded in cell culture flasks and treated with 10 nM archazolid (n=3) or with 0.01% DMSO (n=3). Cells were lysed after 4 hours (macrophages), concentrated and western blot analysis of cathepsin B was performed. proCTSB = procathepsin B, mCTSB = mature cathepsin B

3.2.2 Secretome analysis of archazolid treated urinary bladder carcinoma cells

After analyzing the influence of archazolid on immune cells it was analyzed how V-ATPase inhibition by archazolid alters the secretion profile of migratory cancer cells. Thus, in a first experiment the secretion profile of archazolid treated T-24 (urinary bladder carcinoma cells), was determined. Therefore, supernatants of archazolid treated and control treated T-24 cells were collected and concentrated. A concentration of 1 nM archazolid was chosen as no cytotoxicity was detected for this concentration after 24 hours in FCS free media (Figure 3-15 B). Moreover, a staining of acidic compartments using the lysotracker reagent showed that starting with a concentration of 1 nM archazolid the size and distribution of acidic compartments is altered. At a concentration of 10 nM no lysotracker staining was detectable, indicating that lysosomes are no longer acidic (Figure 3-15 C). In concordance immunofluorescence staining of the lysosomal marker protein (lamp1) shows and altered lamp1 protein distribution already at 1 nM archazolid (Figure 3-19).
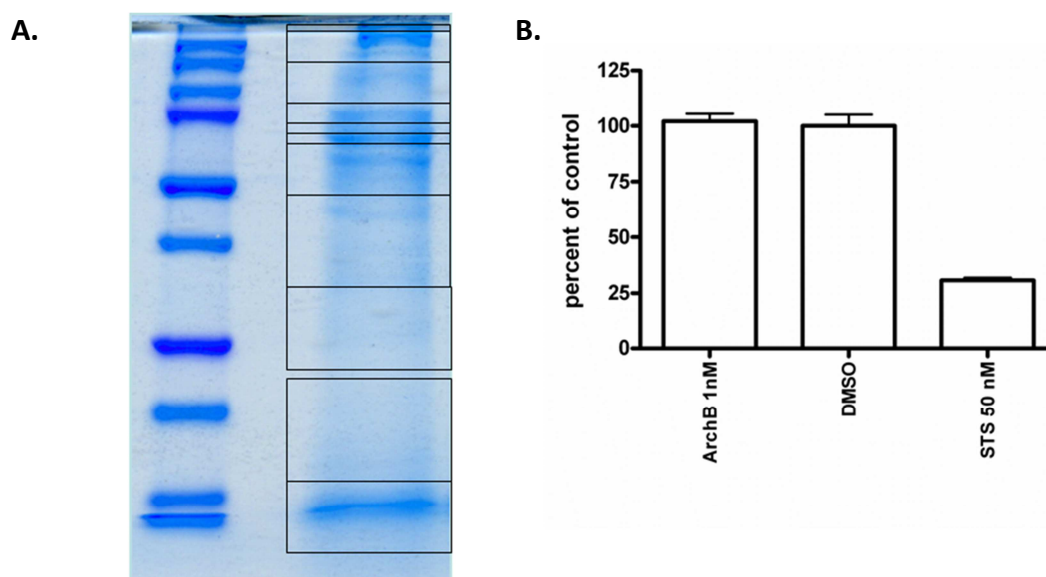
Figure 3-15 continued
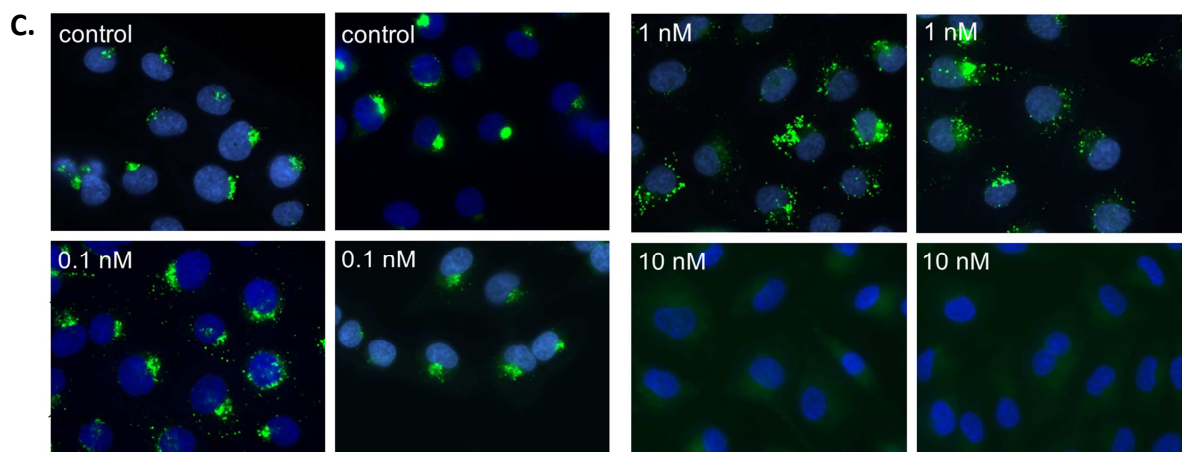
Figure 3-15 Analysis of archazolid treated T-24 cells

A. 1.5 x 10^6 T-24 cells were seeded in cell culture flasks and treated with 1 nM archazolid for 24 h. Supernatants were collected, concentrated and SDS-PAGE was performed using a 12.5% gel. After electrophoresis each lane was cut into 10 similar pieces. **B.** CellTiterGlo-Assay of T-24 cells after 24 hours of treatment, STS = staurosporine (positive control). **C.** lysotracker staining of archazolid treated (1 nM and 10 nM for 24 hours) T-24 cells.

Thus, T-24 cells were treated 24 hours with 1 nM archazolid for analysis of the secretion profile. Supernatants were collected and concentrated. In the following, proteins were separated using SDS-PAGE (12.5%) and each lane was cut into 10 pieces (Figure 3-15 A).Proteins were reduced, alkylated and digested with trypsin by in-gel-digestion (2.2.9.1), prior to LC-MS/MS analysis.

Identified proteins were analyzed using uniprot.org and DAVID bioinformatics. Analysis of cellular component showed that 26% of all identified proteins were mapped into the category of secreted cellular component (Figure 3-16 A). Furthermore, KEGG-Pathway analysis showed the enrichment of 16 pathways. The five carrying the highest count numbers are shown in Figure 3-16 B.

A.

B.
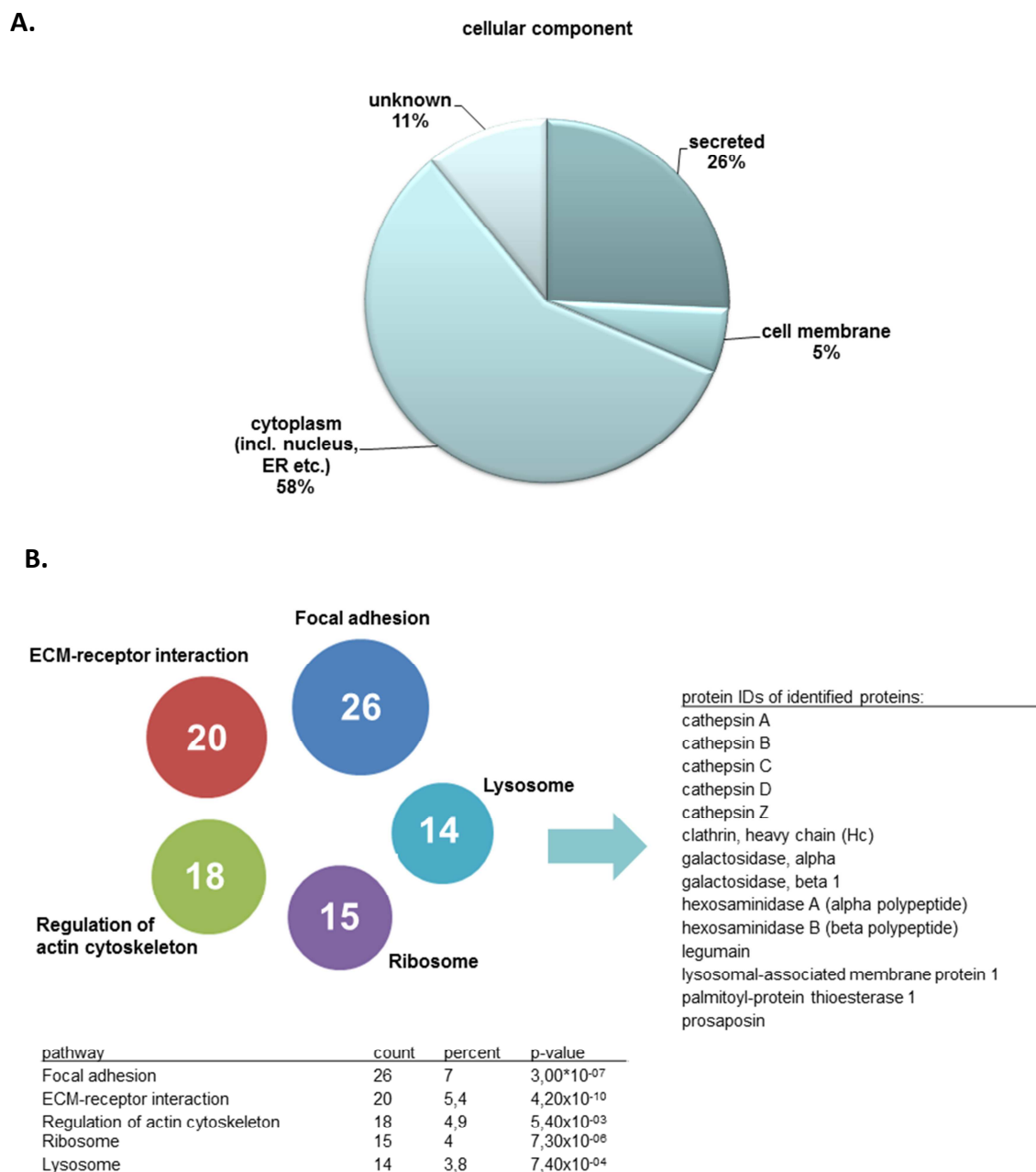
Figure 3-16 LC-MS/MS analysis of secreted proteins
A total number of 374 proteins were identified. Identified proteins were analyzed using uniprot.org and DAVID bioinformatics. **A.** Cellular component of identified proteins **B.** KEGG-Pathway analysis of identified proteins: 16 pathways were identified as strongly enriched. Shown are the 5 pathways including the highest count-numbers. p-values equal or smaller than 0.05 were considered. In the included table on the right identifiers of the pathway *lysosome* are listed.

Namely, the five most enriched pathways were 1) *focal adhesion*, 2) *ECM-receptor interaction*, 3) *Regulation of actin cytoskeleton*, 4) *Ribosome* and 5) *Lysosome*. As it is known from literature that V-ATPase inhibitor bafilomycin induces lysosomal enzyme secretion in macrophages and lysosomal proteases are correlated with enhanced invasion further analysis was focused on the lysosomal pathway. Identified proteins annotated in the

category *lysosome* are shown in Figure 3-16 B, right table. Especially members of the cathepsin family were prominent in the secretion profile. Therefore quantification by western blot was performed for cathepsin B and cathepsin D. Both proteins are tumor makers and potentially involved in metastatic processes [42, 45]. T-24 cells were treated with archazolid in FCS free media and supernatants were collected after 24 hours. Thereafter, samples were concentrated and western blot was performed. As shown in Figure 3-17 both proteins were significantly more abundant in supernatants of archazolid treated cells. Signals indicated that not the active enzymes (25 kDa cathepsin B and 28 kDa cathepsin D) but the inactive and larger preforms (41 and 46 kDa) were secreted.
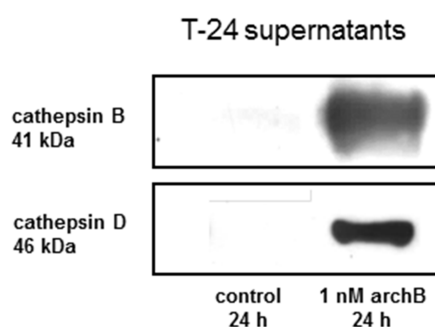
Figure 3-17 Western blot analysis of secreted cathepsin B and cathepsin D
Supernatants of archazolid treated T-24 cells (-FCS, 1 nM archazolid, 24 hours) and control supernatants (-FCS, DMSO, 24 hours) were collected. After SDS-Page gels were blotted on a nitrocellulose membrane and probed with either anti-cathepsin B or anti-cathepsin D specific antibodies.

To prove that the secretion of procathepsin B and not of mature cathepsin B was induced by archazolid, supernatants of treated T-24 cells were separated by SDS-PAGE. The part where the signals of the western blot appeared around 41 kDa was excised from the coomassie stained gel and proteins in this fraction analyzed by LC-MS/MS. As shown in Figure 3-18 a peptide was identified, which is part of the propeptide of cathepsin B proving that procathepsin B is the prominent secreted form during archazolid treatment.
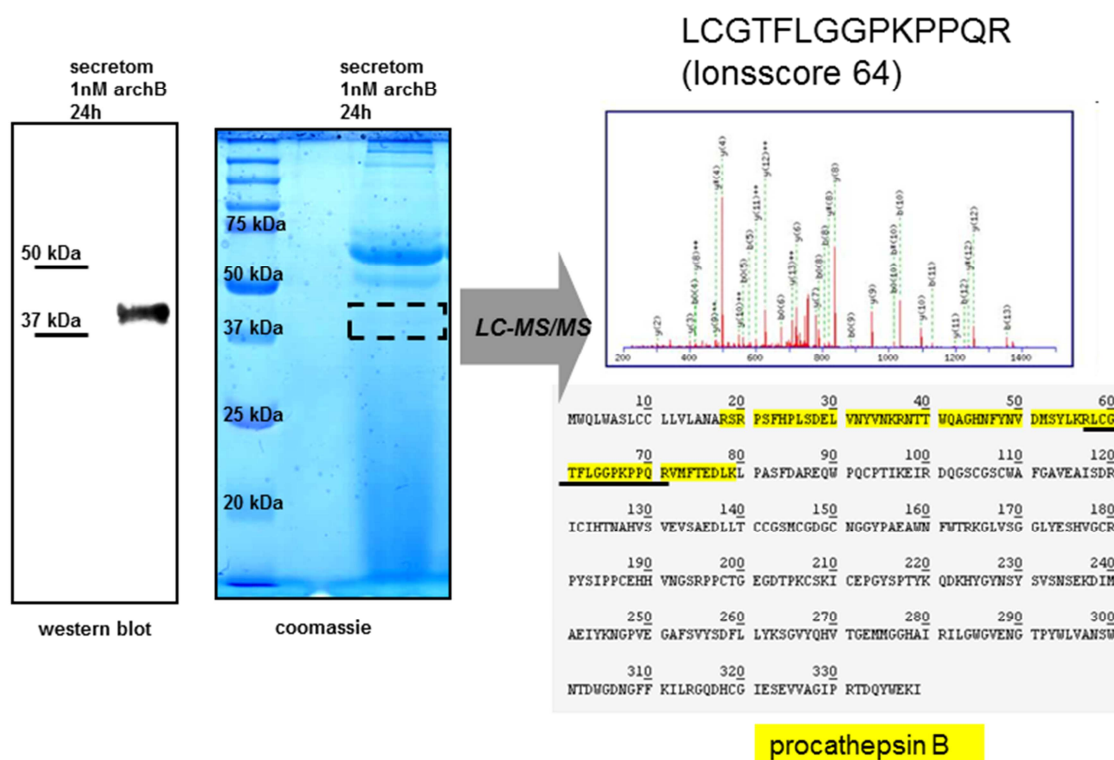
Figure 3-18 Identification of procathepsin B by qualitative LC-MS/MS
Supernatants of archazolid treated T-24 cells were separated by SDS-PAGE, a section of the coomassie stained cell around >37 kDa (where the signals of the western blot appear) was excised, digested and subjected to LC-MS/MS. Source of sequence data: uniprot.org

3.3 Lysosome inhibition by archazolid in cancer cells

Since the secretome analysis showed that archazolid strongly alters the fate of lysosomal proteins and induces the secretion of their proforms, in the following the influence of lysosome inactivation by archazolid on urinary bladder carcinoma cells was analyzed.

As previously shown, archazolid neutralizes lysosomes by V-ATPase inhibition similar to other V-ATPase inhibitors like bafilomycin or concanamycin [29, 30].

Furthermore, an immuno-fluorescence staining of lamp1 (Lysosomal-associated membrane protein 1) protein showed that the enlarged lamp1 containing structures, which were earlier described as a result of concanamycin and bafilomycin treatment [68] arise also after archazolid treatment (Figure 3-19). Lysosome marker lamp1 is located on relatively small vesicles in untreated T-24 cells. After 24 hours of 1 nM archazolid the lamp1 signals appear in bigger vesicular compartments, which are even larger when cells were treated with 10 nM archazolid.

Taken together archazolid induced inactivation of V-ATPase led to neutralization of the lysosomes (Figure 3-15 C) and to the formation of mega-lysosomal compartments (Figure 3-19).
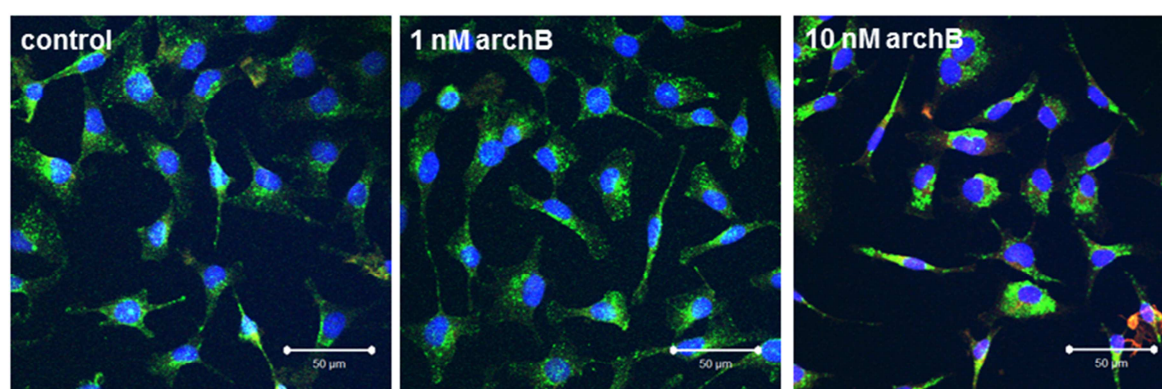
■ DAPI ■ lamp1

Figure 3-19 Immuno-fluorescence imaging of lamp1 protein
T-24 cells were seeded on cover slips in 6-well plates. Cells were treated for 24 hours with 1 nM and 10 nM archazolid, fixed and immuno-fluorescence imaging of lamp1 (green) was performed.

3.3.1 Concentration and time dependent secretion of procathepsin B

Archazolid induced the secretion of procathepsin B. Thus, in this chapter the archazolid induced secretion of procathepsin B was analyzed more in detail.

First T-24 cells (urinary bladder carcinoma) as well as a second cancer cell line MCF-7 (breast cancer) were treated with increasing concentrations of archazolid. Procathepsin B secretion was monitored by western blot analysis of cathepsin B in concentrated supernatants. After 24 hours procathepsin B secretion by T-24 cells was detected starting at a concentration of 0.5 nM archazolid (Figure 3-20 A, upper panel). MCF-7 cells secreted detectable amounts of procathepsin B at 1 nM of archazolid (Figure 3-20 A, lower panel).

To evaluate the secretion kinetics, T-24 and MCF-7 cells were treated for extended time periods with 1 nM archazolid. Both T-24 and MCF-7 cells secreted detectable amounts of procathepsin B after 5 hours of archazolid treatment. Procathepsin B accumulated in the supernatants over time (Figure 3-20 B).
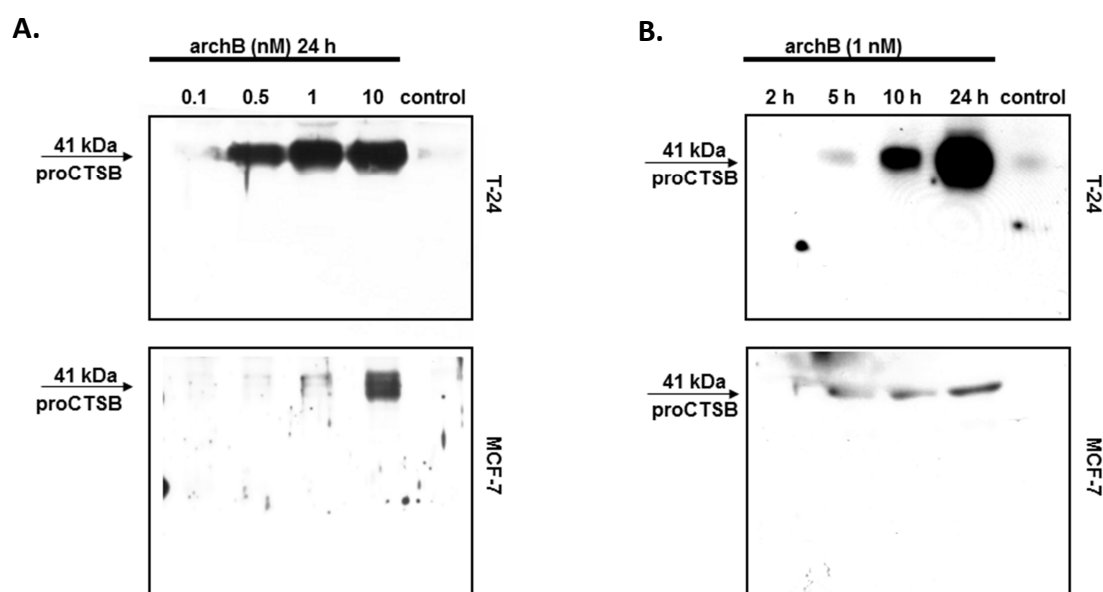
Figure 3-20 Western blot analysis of supernatants of archazolid treated cells
A. T-24 cells or MCF-7 cells were treated with 0.1 nM, 0.5 nM, 1 nM and 10 nM archazolid for 24 hours, supernatants were collected, concentrated and western blot was performed. **B.** T-24 cells or MCF-7 cells were treated with 1 nM archazolid; supernatants were collected after 2, 5, 10 and 24 hours, concentrated and western blot was performed. proCTSB = procathepsin B

Taken together, archazolid induced procathepsin B secretion was concentration and time dependent in both cell lines. In general, detected effects were stronger in T-24 cells than in MCF-7 cells.

3.3.2 Reduction of intracellular cathepsin B activity by archazolid

Previously it was shown that archazolid induces the secretion of lysosomal proenzymes procathepsin B and procathepsin D. To evaluate the intracellular fate of different cathepsin B forms during V-ATPase inhibition, T-24 cells were treated with increasing concentrations (0.1 – 10 nM) of archazolid for 24 hours and cell lysates were analyzed by western blot (Figure 3-21 A). As it is shown in Figure 3-21 A the abundance of procathepsin B (41 kDa) increased, whereas the amount of mature cathepsin B (heavy chain, 25 kDa) decreased with increasing archazolid concentrations. Also the amount of mature cathepsin D decreased while the proform of cathepsin D increased. Furthermore, the mRNA expression of cathepsin B and cathepsin D was evaluated. qPCR analysis showed that the mRNA of cathepsin B and cathepsin D was more than 3-fold increased in archazolid treated T-24 cells (Figure 3-21 B).
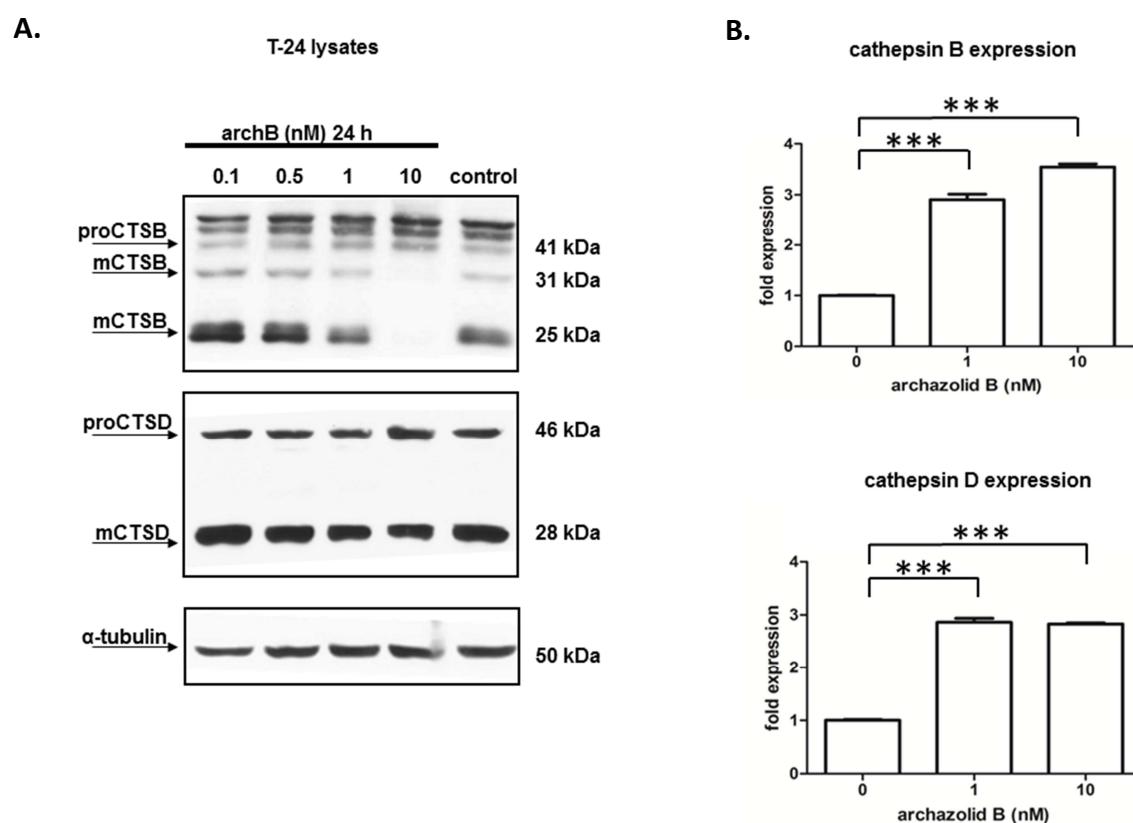
Figure 3-21 Cathepsin B expression
A. T-24 cells were treated with 0.1, 0.5, 1 and 10 nM archazolid or mock treated with DMSO (control). Cells were lysed after 24 hours of treatment proCTSB/D = procathepsin B/D, mCTSB/D = mature cathepsin B/D; **B.** T-24 cells were treated with 1 or 10 nM archazolid or mock treated for 24 hours. Cathepsin B and cathepsin D mRNA expression was determined using qPCR.

To investigate the cellular distribution of cathepsin B immunofluorescence imaging of intracellular cathepsin B (all cathepsin B forms) was performed. As shown in Figure 3-22 cathepsin B was primarily located in small vesicular compartments in control cells. These compartments appeared larger at a concentration of 1 nM archazolid. Even larger, cathepsin B positive vesicular compartment were detected after archazolid treatment of 10 nM.
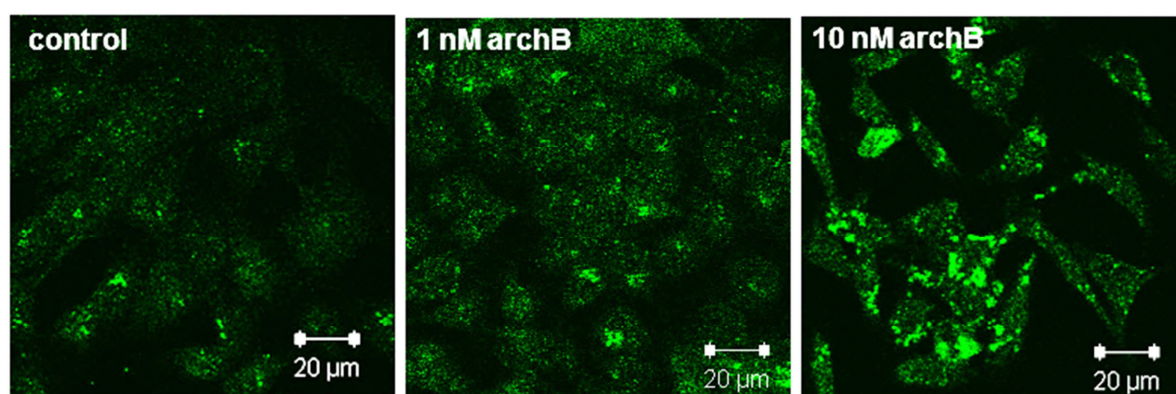
Figure 3-22 Immuno-fluorescence imaging of cathepsin B
T-24 cells were seeded on cover slips in 6-well plates. Cells were treated for 24 hours with 1 nM and 10 nM archazolid, fixed and immuno-fluorescence cathepsin B (green) was performed.

Since western blot analysis showed that archazolid induced a dramatic decrease of mature cathepsin B (Figure 3-21 A), the proteolytic activity of cathepsin B in archazolid treated cell lysates was evaluated by a cathepsin B activity assay (2.2.1). In Figure 3-23 it is shown that archazolid significantly reduced the cathepsin B activity down to less than 40% of the control.
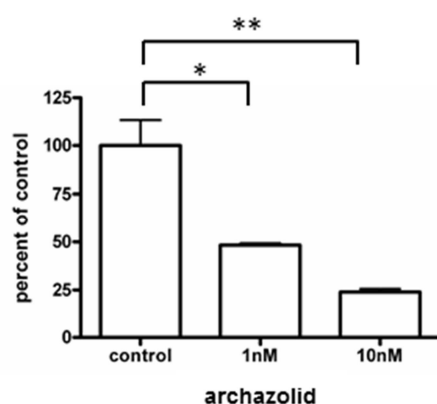
Figure 3-23 Cathepsin B activity in cell lysates
T-24 cells were treated with 1 or 10 nM archazolid or were mock treated with DMSO (control). After 24 hours cells were lysed. The relative cathepsin B activity in 30 µg (total protein) of each lysate was determined. *p < 0.05, **p< 0.005, (t-test)

In summary, archazolid treatment reduced the amount of intracellular mature cathepsin B, which resulted in a decreased cathepsin B proteolytic activity. Concomitantly, the mRNA level of cathepsin B increased during archazolid treatment.

3.3.3 Effects on cathepsin B by V-ATPase V_0c silencing

To estimate if the altered cathepsin B abundance was a direct effect of the inhibition of V-ATPase, the target of archazolid, the V_0c subunit, was silenced by RNAi.

Analyzing V_0c mRNA expression 24 and 48 hours after transfection, a clear knockdown of subunit V_0c was detectable (Figure 3-24 A). Similar to archazolid treatment, silencing of subunit V_0c induced cathepsin B mRNA expression (Figure 3-24 B).

Western blot analysis of supernatants of V_0c silenced cells showed an induced procathepsin B secretion (Figure 3-24 C), while in whole cell lysates intracellular mature cathepsin B was reduced in V_0c -siRNA treated samples. Procathepsin B was slightly elevated in V_0c-siRNA treated cells compared to the noncoding control (Figure 3-24 D).
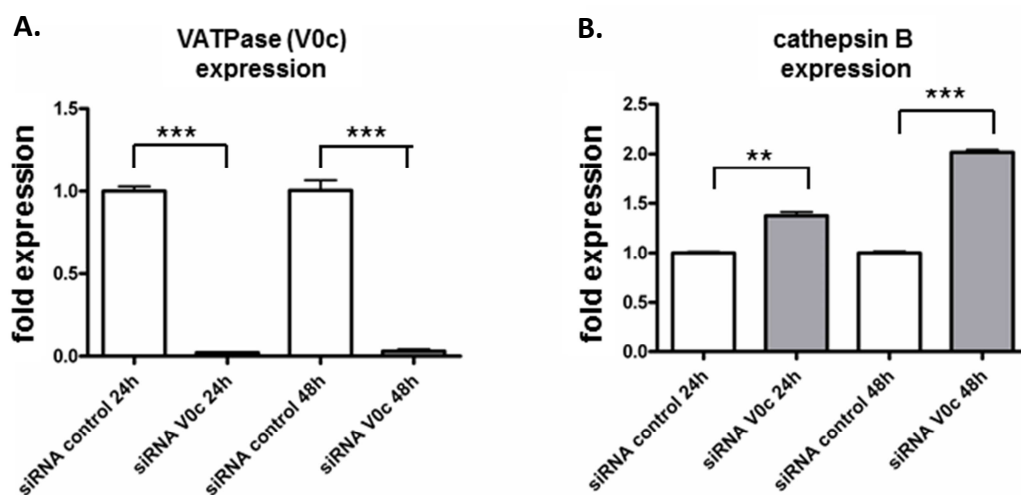
Figure 3-24 continued
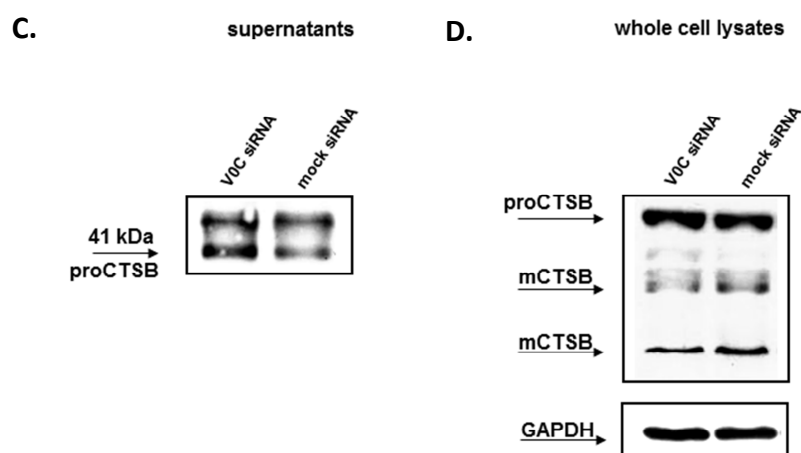
Figure 3-24 Effect of V-ATPase knockdown on mRNA and protein level
T-24 cells were transfected either with siRNA against V_0c or control siRNA. Cells were lysed 24 or 48 hours after transfection. **A.** Sufficient knockdown was monitored by qPCR of V-ATPase subunit V_0c. **B.** Expression of cathepsin B mRNA during V_0c knockdown was analyzed by qPCR. **C.** procathepsin B secretion and **D.** intracellular cathepsin B after 24 hours was analyzed by western blot. **p< 0.005, ***p<0.0005 (t-test)

In summary, the described archazolid effects on cathepsin B expression could be mimicked by silencing of the archazolid target domain (V_0c) of the V-ATPase by RNAi.

3.3.4 Procathepsin B secretion is induced by lysosome neutralization

In the previous chapter it was shown that the archazolid effects on cathepsin B expression arise from V-ATPase inhibition. Therefore it was analyzed if other V-ATPase inhibitors exhibit similar effects on procathepsin B secretion. Thus, T-24 cells were treated with the following V-ATPase inhibitors: 1) bafilomycin A1 and 2) concanamycin A.

Analyzing the supernatants of bafilomycin and concanamycin T-24 cells for cathepsin B abundance by western blot analysis, an elevated procathepsin B secretion was detected in bafilomycin and concanamycin treated samples but not in supernatants of control treated cells. As a second control T-24 cells were treated with DNA-intercalator doxorubicin (Figure 3-25). Neither 5 nM nor 10 nM doxorubicin did induce procathepsin B secretion after 24 hours. Similar results were obtained for cathepsin D.

supernatants
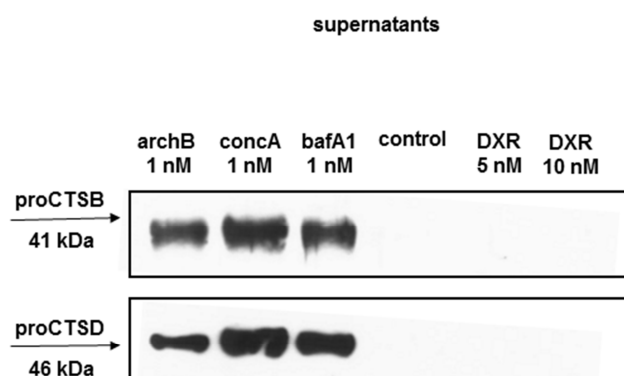
Figure 3-25 Induction of procathepsin B secretion by different V-ATPase inhibitors
T-24 cells were treated with 1 nM archazolid = archB, 1 nM concanamycin A = concA, 1 nM bafilomycin A1 =bafA1, 0.01% DMSO = control or 5 and 10 nM doxorubicin = DXR for 24 hours. Supernatants were collected, concentrated and western blot was performed.

These results indicate that archazolid induced reduction of mature cathepsin B and induced procathepsin B secretion is caused by hampered lysosome function. Due to the fact that V-ATPase inhibition leads to the neutralization of the lysosome [29], it was evaluated whether the detected secretion of procathepsin B in T-24 cells by archazolid was a result of lysosome neutralization. For this purpose, cells were treated with lysosomotrophic agents: chloroquine and NH_4Cl. In both cases procathepsin B secretion was detected in the supernatants (Figure 3-26).
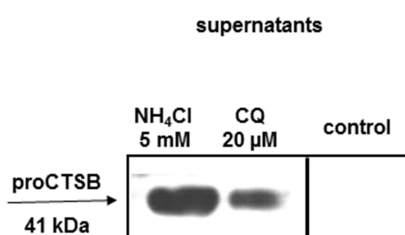
supernatants

Figure 3-26 Induction of procathepsin B secretion by lysosomotropic agents
T-24 cells were treated with lysosome disruption agents NH_4Cl (5 mM) and chloroquine = CQ (20 µM) for 24 h. Supernatants were collected, concentrated and western blot was performed.

3.3.5 M6PR-dependent transport of procathepsin B to the lysosome

In the previous chapters it could be shown that archazolid induced procathepsin B secretion and intracellular mature cathepsin B reduction is a result of lysosome neutralization by V-ATPase inhibition. To analyze in detail how archazolid action interferes with the cathepsin B maturation process further experiments were performed.

It is known from literature that procathepsin B transport to pre-lysosomal compartments is mediated through the mannose-6-phosphate receptor (M6PR) [57]. After glycosylation in the Golgi apparatus, procathepsin B is bound to M6PR in the trans-Golgi network (TGN). M6PR containing vesicles are then fusing with prelysosomal compartments (PLC). After acidification of the PLC, M6PR can release its cargo and recycles to the TGN. M6PR cannot release its cargo if the pH of the compartment is too high [72]. As archazolid strongly raises the lysosomal pH by inhibiting V_0c of the V-ATPase it was hypothesized based on the literature that bound procathepsin B cannot be released by the M6PR, when the lysosomal pH is elevated by archazolid action. As a result, no new mature cathepsin B can be generated and existing mature cathepsin B loses its activity in a non-acidic environment. The lack of cathepsin B might lead to an increased transcription of cathepsin B mRNA resulting in a procathepsin B overload, as new translated preprocathepsin B can be converted into glycosylated procathepsin B but cannot be subjected to M6PR mediated transport, which leads to the secretion of procathepsin B (schematically summarized in Figure 3-27 A.

In order to prove this hypothesis, T-24 cells were treated with tunicamycin, an inhibitor of N--acetylglucosamine transferase which is part of the glycosylation process of lysosome targeted proteases [73]. As shown in Figure 3-27 B tunicamycin induces the secretion of a slightly smaller version of procathepsin B, indicating that blocking of the glycosylation process also impairs the M6PR mediated transport, resulting in secretion of procathepsin B in an unglycosylated form. Unglycosylated procathepsin B will not be bound to the M6PR as it lacks the tagging-sequence.

Additionally, the transport from the endoplasmatic reticulum to the Golgi app. was inhibited by brefeldin. As shown in Figure 3-27 B treatment of T-24 cells using brefeldin fully blocked the archazolid induced procathepsin B secretion, as procathepsin B could not be transported to the Golgi app..

A. mRNA
preprocathepsin B
procathepsin B
glycol. procathepsin B
one chain mature cathepsin B
two chain mature cathepsin B

ER
brefeldin
Golgi app.
tunicamycin
M6PR recycling
archazolid induced secretion
PLC
archazolid
lysosome
cytoplasm
extracellular space

B.

supernatants

41 kDa
proCTSB
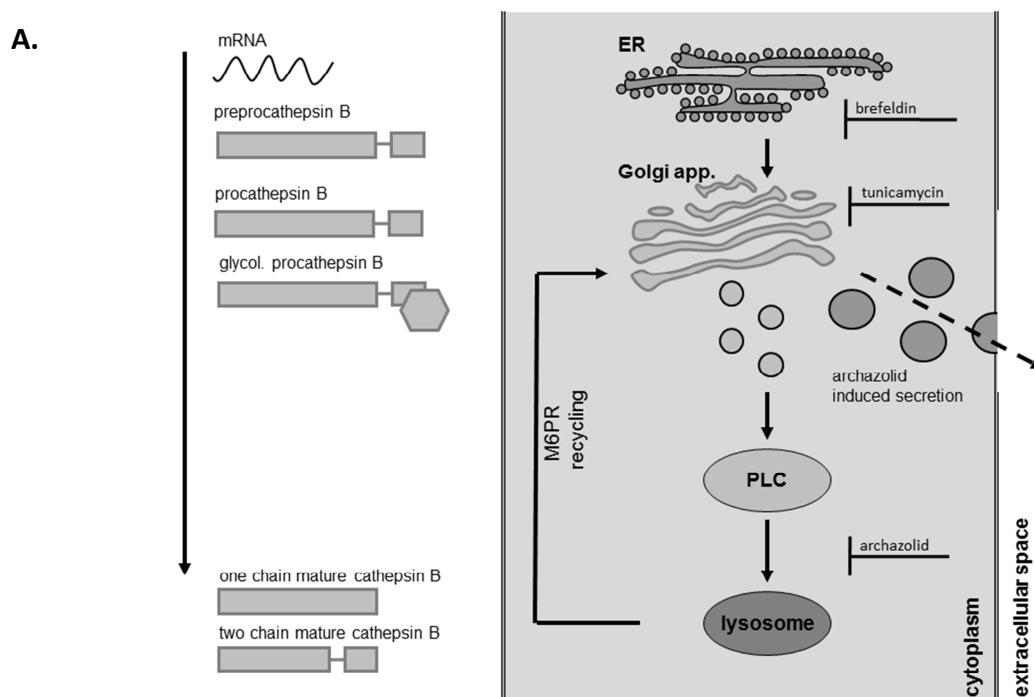
tunm 5 µg/ml   contr.   archB 5 nM   bref 5 µg/ml   bref + archB
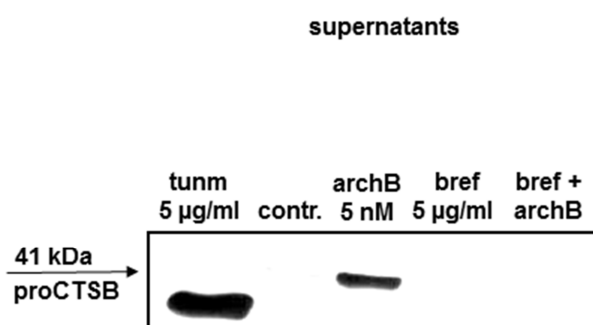
Figure 3-27 Effect of tunicamycin and brefeldin on procathepsin B secretion
A. schematically overview of the cathepsin B maturation process **B.** T-24 cells were treated either with tunicamycin = tunm (5 µg/ml), archazolid = archB (5 nM), brefeldin = bref or a combination of brefeldin = bref+archB (5 µg/ml) and archazolid (5 nM) for 24 hours.

To visualize the archazolid induced impaired M6PR-trafficking immuno-fluorescence staining of M6PR was carried out (Figure 3-28). Archazolid treatment strongly altered the M6PR distribution in the cell, indicating an impaired recycling process. In untreated T-24 cells M6PR signals were distributed all over cell, concentrating in a nucleus associated region. In contrast, in archazolid treated cells M6PR signals were detected in vesicular compartments evenly distributed all over the cell (Figure 3-28).

control
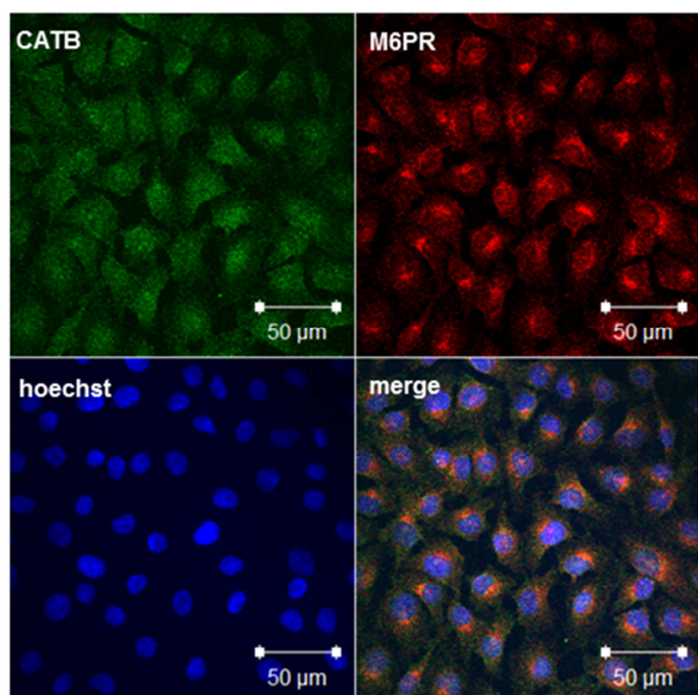
1 nM archazolid B
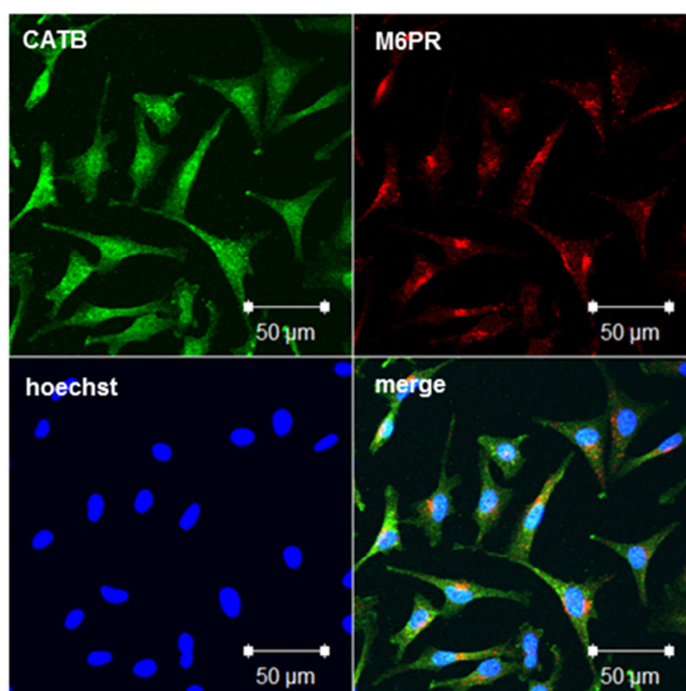
Figure 3-28 continued
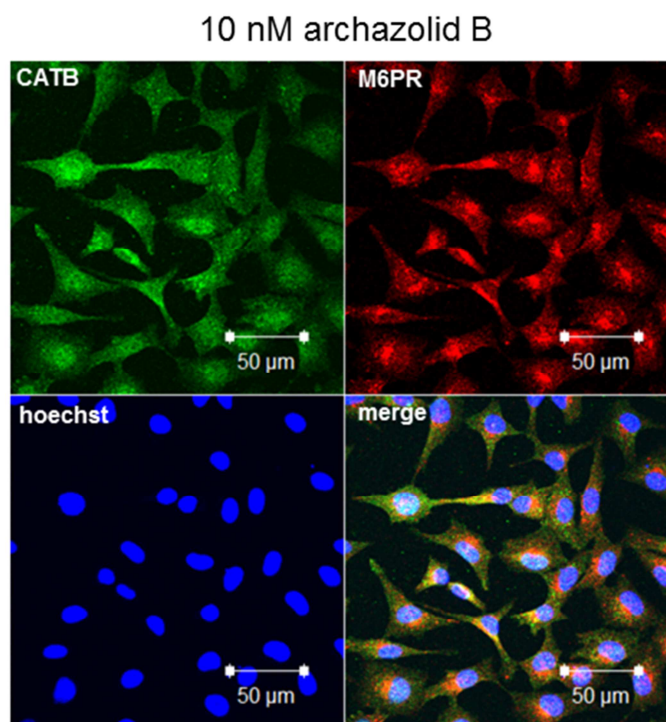
Figure 3-28 Immuno-fluorescence imaging of M6PR and cathepsin B
T-24 cells were seeded on cover slips and treated with 1 nM and 10 nM archazolid for 24 hours. Cells were fixed and immuno-fluorescence was performed using antibodies against cathepsin B (green) and M6PR (red). Nuclei were stained using Hoechst dye (blue).

In summary these results show that V-ATPase inhibition by archazolid impairs M6PR mediated trafficking from the TGN to prelysosomal compartments, resulting in a decrease of active lysosomal proteases like cathepsin B.

3.4 Action of archazolid and other myxobacterial compounds *in vivo*

To evaluate if the detected archazolid action on cathepsin B maturation was also present *in vivo*, tumor bearing mice were treated with archazolid. These experiments were performed in cooperation with Laura Schreiner (PhD thesis 2013, LMU). In a first experiment two other myxobacterial compounds 1) pretubulysin and 2) chondramid B were included.

An syngenic mouse model using mouse mammary gland tumor cells (4T1*luc*) stably expressing luciferase as a reporter gene was applied to analyze archazolid, pretubulysin and chondramid B action on tumor growth *in vivo*. 4T1*luc* cells were injected into the flank of BALB/c mice. Starting at day 3 after tumor injection, mice were treated 3 times per week *i.v.* with 3 mg/kg archazolid, 0.1 mg/kg pretubulysin, 0.5 mg/kg chondramid B or vehicle control (5% DMSO in PBS). None of the 3 substances reduced the growth of the main tumor significantly (Figure 3-29 A). Except that archazolid injection induced local cutaneous inflammation at the tail injection site, when not been totally injected intravenously, no acute toxicity of archazolid, pretubulysin or chondramid B was noticed during the treatment. Mice were euthanized on day 18 subsequently to tumor injection (after a total of 7 treatments).
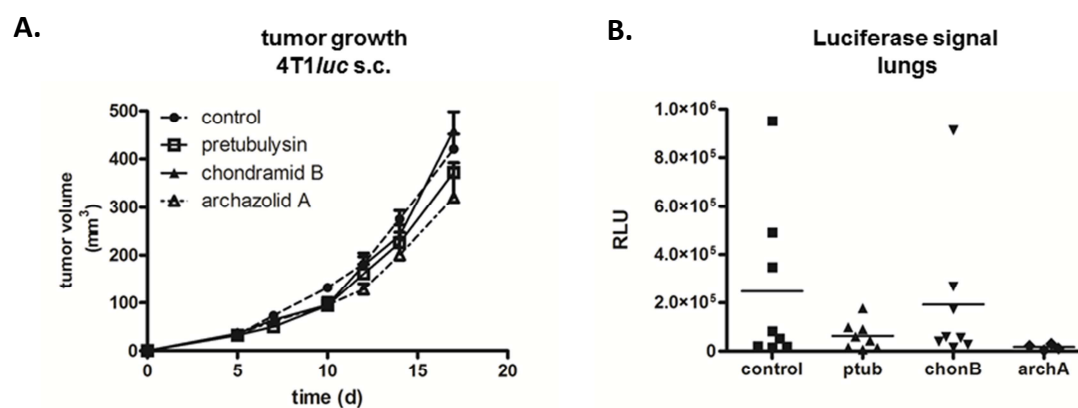
Figure 3-29 *In vivo* effect of myxobacterial compounds
4T1*luc* cells were injected into the flanks of BALB/c mice. Starting on day 3, mice were treated 3 times per week *i.v.* with 3 mg/kg archazolid, 0.1 mg/kg pretubulysin, 0.5 mg/kg chondramid B or vehicle control (5% DMSO in PBS). On day 18 mice were euthanized. **A.** tumor growth **B.** *ex vivo* luciferase signal of the lungs on day 18

None of the three substances exhibited a direct effect on tumor growth in this model. As it was known from literature, that 4T1 cells form metastases [74], distant metastases in the lungs were detected by the measurement of the luciferase signal. Although obtained results

were statistically not significant, lungs of mice which were treated with pretubulysin or archazolid showed less metastatic burden (Figure 3-29 B).

A second experiment was focused on archazolid action on cathepsin B maturation. Again 4T1*luc* cells were injected into the flanks of BALB/c mice. Starting at day 3 after tumor injection, mice were treated 3 times per week *i.v.* with 3 mg/kg archazolid. On day 16 mice were euthanized, tumors, and organs (lung, heart, kidney, spleen and liver) were harvested. Again archazolid treatment did not reduce tumor growth of 4T1*luc* cells (Figure 3-30 A). Furthermore, tumors showed no significant differences in morphology (Figure 3-30 B).
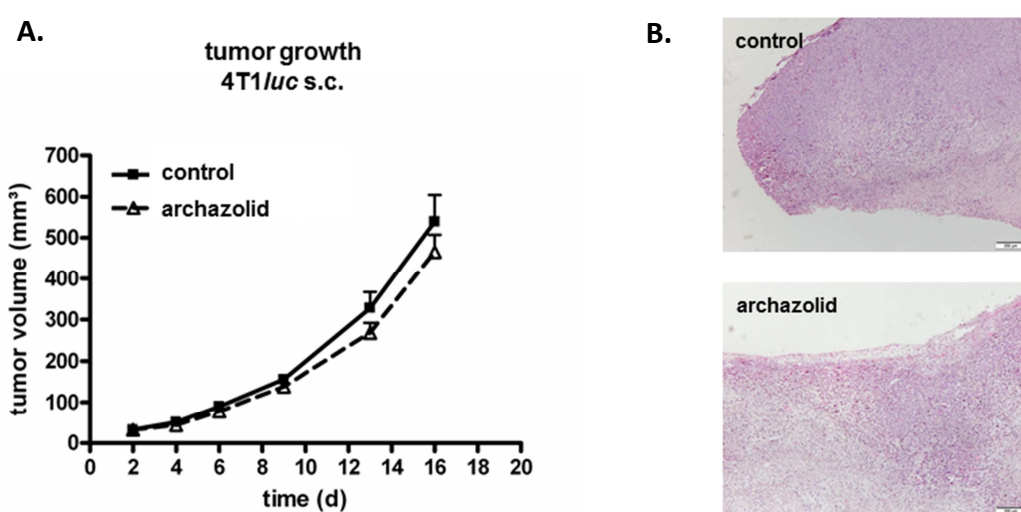
Figure 3-30 Archazolid treatment of *s.c.* 4T1*luc* tumors *in vivo*
4T1*luc* cells were injected into the flanks of BALB/c mice. At day 2, 3, 4 , 5, 9, 13 and 17 mice were treated with 3 mg/kg archazolid or vehicle control (5% DMSO in PBS). On day 18 mice were euthanized. **A.** tumor growth and **B.** H&E stain of the tumor tissue

To determine systemic archazolid action cathepsin B activity in livers of archazolid treated *versus* mock treated mice was analyzed. As shown Figure 3-31 A cathepsin B activity in the liver was strongly reduced by archazolid. To further evaluate if archazolid impaired also tumor cathepsin B, its activity in tumor lysates was determined. As shown in Figure 3-31 B, cathepsin B activity was reduced in tumors of archazolid treated mice. In accordance mature cathepsin B protein was reduced in the treatment group (Figure 3-31 C). Also in this experiment metastatic burden of the lungs was slightly but not significantly reduced in the archazolid treated group (Figure 3-31 D).

In correspondence with *in vitro* results of 4T1*luc* cells cathepsin B mRNA expression was slightly, however not significantly induced (Figure 3-32).
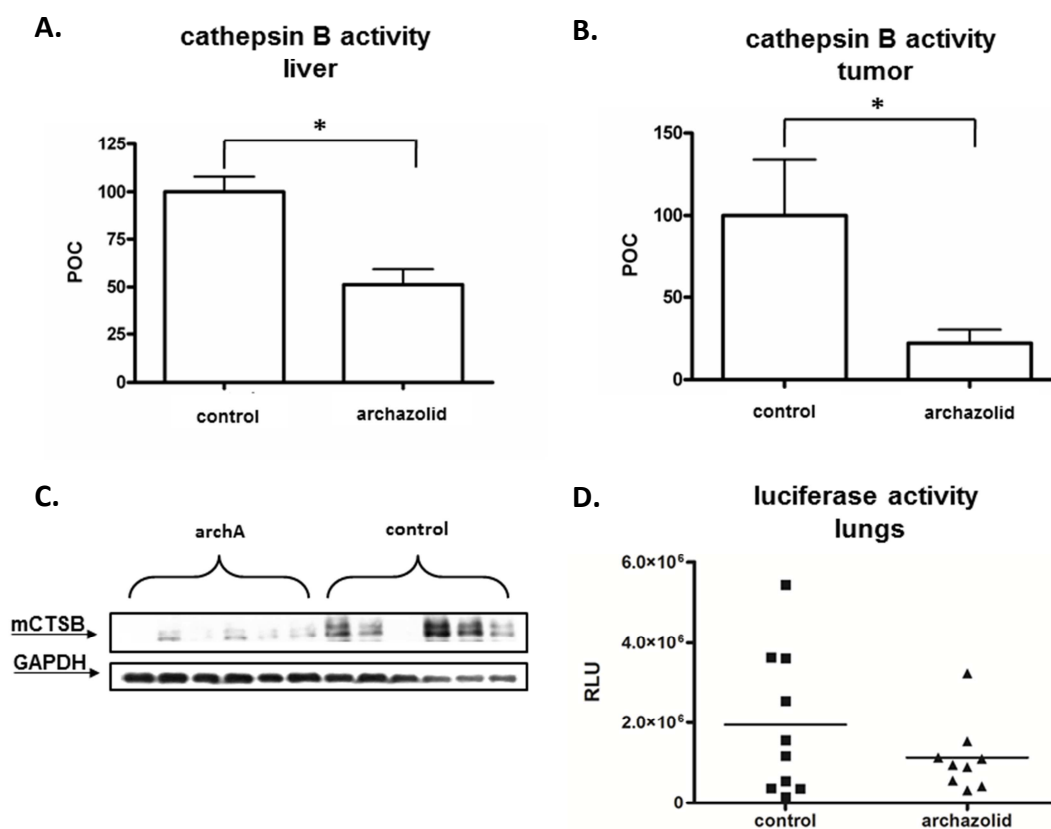
Figure 3-31 Archazolid action on cathepsin B activity *in vivo*
A. relative cathepsin B activity of the liver **B.** relative cathepsin B activity of the tumor *$p < 0.05$ (t-test) **C.** western blot analysis of tumor samples **D**. *ex vivo* luciferase activity measurement of the lungs (n=10). Whole lungs were homogenized and luciferase activity of metastasized 4T1*luc* cells of each sample was determined. Significant outlier were removed using Grubbs' test (alpha = 0.05).
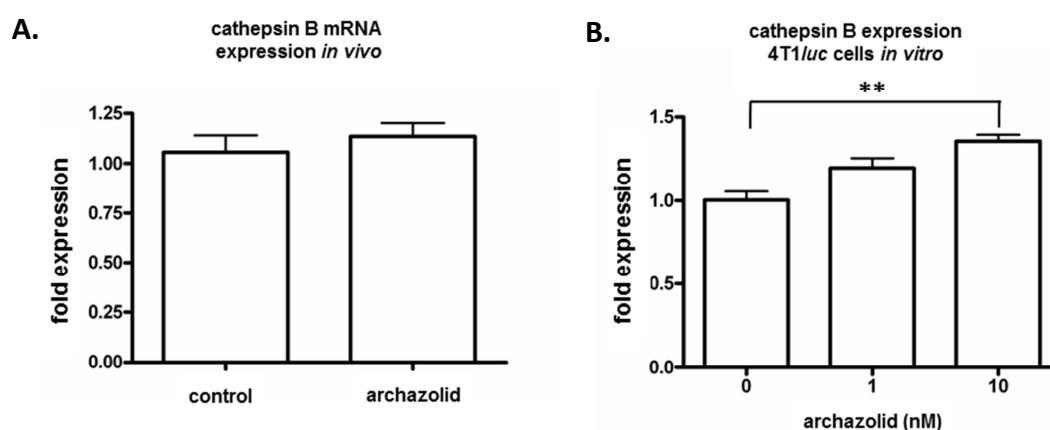
Figure 3-32 Cathepsin B mRNA expression of 4T1*luc* cells
A. RNA of 30 μg of 5 tumors per group was isolated and cDNA was transcribed. qPCR was performed analyzing cathepsin B mRNA expression. **B.** Archazolid treatment of 4T1*luc* cells using 1 and 10 nM was performed for 24 hours. RNA was isolated and cDNA was transcribed. qPCR was performed analyzing cathepsin B mRNA expression.

In summary, *in vitro* results were confirmed *in vivo*, as archazolid treated mice showed a reduced amount of cathepsin B protein in tumor tissue as well as a decreased proteolytic cathepsin B activity. Furthermore, a functional effect of archazolid on the formation of distant metastasis was detected. In two experiments archazolid treated mice exhibited a lesser metastatic burden in the lungs as control treated mice.

4   Discussion

4.1   Resistance formation upon metronomic cyclophosphamide therapy

Cells developing resistance to metronomic cyclophosphamide (CPA) therapy undergo a complex molecular evolution. Changes in many different factors and pathways contribute to the formation of a resistant phenotype. Metronomically administered CPA acts anti-angiogenically on tumor vessels, whereas CPA given in standard dose is mainly acting on the tumor itself [11-13, 75]. Most of the classical resistance mechanisms can be ruled out in the present study (Figure 1-2). Neither increased MDR-transporter activity, nor neo angiogenesis, vascular mimicry or impaired CPA activation was observed (Figure 1-2 and [13]). Additionally a pharmacodynamic study of metronomically administered CPA suggests that it is unlikely that resistance to this kind of regimen is caused by impaired CPA activation [75]. The mechanisms of resistance formation to anti-angiogenic therapy are classified into four major groups: 1) *evasive resistance*, 2) *vascular cooption*, 3*) reduced vascular dependence* and 4) *vascular remodeling* [12]. In the present study the resistant tumor grows under conditions of hypoxia and restricted nutrients without the formation of additional tumor vessels [13] thus, the underlying mechanism leading to chemoresistance was assigned to the group of "reduced vascular dependence".

Previously to this work, a genome wide microarray was performed in a prostate cancer (PC3) xenograft model to investigate the molecular basis of *in vivo* resistance mechanisms to anti-angiogenic CPA therapy.

First the importance of appropriate *in vivo* controls was shown, as already the comparison of the gene expression profile of the *in vivo* passaged and standard PC3 tumors displayed a dramatic difference [14]. The gene expression profile of the standard, not *in vivo* passaged PC3 samples were clearly distinct from all other *in vivo* passaged tumor sublines (Figure 1-3). Moreover, gene expression of resistant tumors namely PC3 D3 and PC3 D4 clearly differed from the passaged not resistant PC3 A3 tumors. Within the group of resistant tumors an acute CPA treatment of the respective tumors for 24 hours only influenced gene expression marginally (Figure 1-3). All PC3 D3 samples from four mice clustered in one group, distinct from the PC3 D4 group. This indicates that resistant tumors of PC3 D3 and PC3 D4 share certain properties but originate from different cell clones.

The differentially expressed genes of untreated PC3 D3 and PC3 D4 *versus* PC3 A3 (*in vivo* passaged control) were regarded as more important and short term CPA effects were taken as lesser important. Approximately 50% of the differentially expressed genes in PC3 D3 and PC3 D4 *versus* PC3 A3 were shared by both resistant sub lines (Figure 1-4).

For microarray validation the most differentially regulated genes dehydrogenase/reductase member 2 (DHRS2), PAS domain containing protein 1 (PASD1) and Neurotensin (NTS) as well as resistance related genes like special AT-rich sequence-binding protein-1 (SATB1) and bone morphogenetic protein receptor type I B (BMPR1B) were chosen (3.1.1).

Dehydrogenase/reductase SDR family member 2 (DHRS2) is a less studied enzyme with the alternative name HEP27. It is described as a nuclear protein found in growth-arrested human hepatoblastoma cells. It is a member of the short-chain alcohol dehydrogenase family. Furthermore, its expression in fibroblasts is reported [76-78].

PAS domain containing protein 1 (PASD1) is also less studied. It is reported to be a leukaemia-associated antigen [79, 80].

Neurotensin (NTS) is an enzyme prominent in various kind of tissue. It was first isolated from extracts of the bovine hypothalamus [81]. Beside its function in endocrine cells of the small intestine, where it leads to secretion and smooth muscle contraction, it was also described to induce proliferation of colorectal cancer cells [82, 83].

Special AT-rich sequence-binding protein-1 (SATB1) is a transcription factor. It displays a key factor for integration of higher-order chromatin architecture with gene regulation [84-87]. Moreover, SATB1 expression is associated with a number of different kinds of cancer [88-92]. Additionally, it has been reported to be involved in multidrug resistance of breast and colorectal cancer [93, 94] as well as in cisplatin resistance in hepatocellular carcinoma [64].

Bone morphogenetic protein receptor type I B (BMPR1B) is a member of the bone morphogenetic protein (BMP) receptor family, which members are transmembrane serine/threonine kinases. Their ligands are the BMPs (bone morphogenetic proteins) which are involved in endochondral bone formation and embryogenesis (reviewed by [95]). BMPs are also involved in cancer, exhibiting both oncogene and tumor suppressor gene functions [96].

A qPCR analysis of these genes proofed the microarray results as valid. Furthermore, the expression of the named genes under cell culture conditions strongly differed between *in vivo* and *in vitro*. This finding agreed with the fact that resistant cell lines showed no resistance *in vitro*.

To test the ability to induce resistance *in vitro* two genes were chosen: 1) SATB1, was strongly upregulated (5-fold) in resistant tumors *in vivo* but showed only a slight upregulation in PC3 D4 cells *in vitro.* 2) ANXA3, a protein previously found in a proteomic study to be more abundant in resistant PC3 clones on protein level [13], was upregulated *in vivo* but not *in vitro*. ANXA3 is a member of the Ca^{2+} binding-lipocortin family which are also known as annexins [97, 98].

The generation of SATB1 and ANXA3 overexpressing PC3 clones was performed by Mark Laible (DKFZ, Heidelberg). The induction of the target gene expression by doxycycline was feasible and led to the expression of the proper protein as shown by qPCR, western blot and immuno-fluorescence staining (3.1.2). Neither SATB1 nor ANXA3 overexpression led to resistance formation *in vitro* against the alkylating drug melphalan. However, SATB1 overexpression induced resistance to cisplatin treatment. This finding confirms the work of Kuo *et al.* [64], who have described a role of SATB1 in cisplatin resistance in hepatocellular carcinoma by SATB1-mediated induction of survivin (Figure 4-1). An *in vivo* resistance of the transgenic PC3 clones was not tested for practical reasons and therefore cannot be excluded.
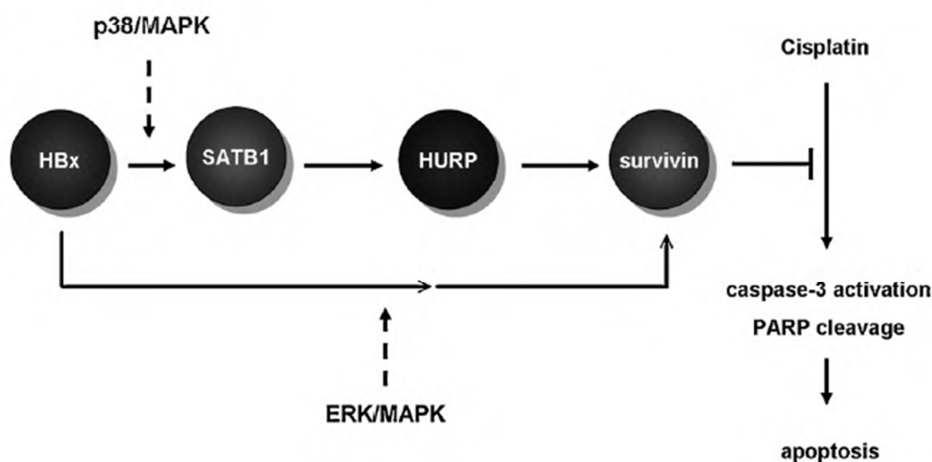
Figure 4-1 Proposed model to explain the link between the viral protein HBx and the p38/MAPK pathway [64]

Due to the complex molecular evolution, leading to the ability to survive the restrictive conditions of anti-angiogenic therapy it is unlikely that a single main mechanism acts as a main factor for resistance acquisition. In the present study the expression of resistance related genes *in vivo* strongly differs from gene expression *in vitro*, indicating an involvement of microenvironmental factors leading to the observed *in vivo* resistance. Indeed, three pathways could be identified which potentially contribute to the described resistant phenotype (3.1.3): 1) *axon guidance*, 2) *steroid biosynthesis* and 3) *complement and coagulation cascades*. Prostate cancer cells are able to gain neuronal properties [99, 100], thus neuroendocrine-like differentiation might take place as a side effect of resistance formation. Steroid synthesis might be altered leading to hormone promoted increased proliferation. The most interesting functional group is "*complement and coagulation cascades*". This group consists of six differentially expressed genes which are associated with the coagulation cascade. During anti-angiogenic treatment, blood vessels are destroyed and coagulation takes place. It was hypothesized that resistant tumor cells hamper the coagulation process in order to overcome the reduced oxygen and nutrient supply. This hypothesis is strengthened by the fact that it has been described for flavone acetic acid, also an anti-angiogenic drug, that the coagulation time in mice is strongly reduced [101]. Anti coagulation associated genes 1) PLAT (reviewed in [102]) and 2) ANXA3 [67] showed increased expression in resistant tumors, whereas expression of 3 members of the serine protease inhibitor family (SERPINs), which act potentially pro-coagulative [66] was decreased in resistant tumor tissue. Increased diffusion of oxygen and nutrients is facilitated by impaired thrombosis and fibrosis.

In contrast to the finding that the expression of anti-coagulation genes is increased and of pro-coagulation genes is decreased, PROS a potential anti-coagulation factor [103] was downregulated and tissue factor (F3), the main mediator of the extrinsic pathway of blood coagulation [104, 105] was highly expressed in PC3 D4 tumor tissue. Interestingly, F3 shows an altered exon expression profile in PC3 D4 tumor samples. Comparing the expression level of PC3 D4 to PC3 A3, exons 3 to 6 are highly expressed in resistant PC3 D4 tumor tissue, whereas no differential expression of exon 1 and 2 can be seen. A version of F3, missing exon 1 and 2, has not yet been described, whereas an alternatively spliced variant of F3, missing exon 5, has been reported [106]. Exon 1 and 2 of F3 are coding for the first 70 amino

acids of the protein. In this area according to *uniprot.org* [107] a signal peptide and parts of a topological domain are located, leading to the hypothesis that the expression of an altered F3 protein might result in an impaired activation of blood coagulation by resistant tumor tissue or even in facilitating blood flow.

Based on the microarray results, resistance to metronomic CPA therapy was sought to be induced by the application of anti-coagulation therapy to CPA treated PC3 A3 tumors *in vivo* (3.1.4). For anti-coagulation Warfarin was chosen. Warfarin is a 4-hydroxycoumarin, which inhibits the vitamin K-dependent step in clotting factor synthesis [108].

First Warfarin was administered through the drinking water as mice stopped drinking it was further administered *i.p..* In this treatment regimen no enhanced resistance formation could be provoked by anti-coagulative therapy. The co-treatment using another anti-coagulative drug may be one opportunity to proof the involvement of coagulation in resistance formation. Another approach would be *vice versa* to inhibit resistance formation by induction of coagulation.

In conclusion, resistance formation to metronomic CPA therapy can be seen as a molecular evolutionary process. Anti-coagulation properties of the cells (increased PLAT and ANXA3, increased exon deletion variant of F3, decreased SERPIND1, SERPINA1 and SERPINB7) could be part of a complex resistance mechanism, but the functional relevance remains to be confirmed by subsequent studies.

4.2 Myxobacterial compounds in cancer treatment

Archazolid is a novel myxobacterial V-ATPase inhibitor. V-ATPases are conserved proton pumps involved in pH regulation of the cell. They recently came into focus as a novel target in cancer therapy because they are overexpressed in many tumor types. Their abundance at the plasma membrane in breast and pancreatic cancer cells was shown to correlate with an invasive phenotype [34, 109]. When inhibiting V-ATPase for therapeutic reasons, membrane bound V-ATPase was regarded as the primary target [110]. Their inhibition was proposed to elevate the extracellular pH, as tumors often have and an acidic microenvironment, which is correlated with an elevated invasive potential [36]. Moreover, an acidic microenvironment is related to an increased ability to express an elevated amount of growth and angiogenic factors [111, 112]. Moreover a raised intracellular pH is correlated with serum- and substrate independent growth and cell cycle progression [113-116].

However, the data presented here draw attention to another intriguing aspect of V-ATPase in cancer therapy: the inhibition of intracellular V-ATPase. In this study it could be shown that intracellular V-ATPases control the processing and secretion of lysosomal proteases, which are involved in tumor progression and metastasis [42-45, 57, 117].

Lysosomal proteases were found in the supernatants of archazolid treated urinary bladder carcinoma as well as of breast cancer cells. Further analysis revealed that predominantly the proforms of lysosomal proteases were secreted upon archazolid treatment. In particular V-ATPase inhibition by archazolid strongly induced the secretion of procathepsin B (3.2.2). Most importantly, the intracellular proteolytic activity of cathepsin B was strongly reduced after archazolid treatment, indicating an altered maturation process of cathepsin B (3.3.2). Furthermore, the impact of archazolid treatment on immune cells was evaluated. Archazolid induced reduction of intracellular cathepsin B was also detected in human macrophages (3.2.1). In monocytes no detectable amounts of cathepsin B were found and thus no archazolid action on cathepsin B maturation was present. But furthermore, the secretion profile of archazolid treated monocytes was analyzed and quantified (3.2.1). The secretion of thrombospondin (TSP1) was reduced in all three samples and thus displays a potential candidate for further evaluation. In one of the three samples interleukin 6 (IL-6) and 8 (IL-8) were less abundant. This is in accordance with unpublished results of the group of Prof. Dr.

Oliver Werz, Jena University. Using ELISA (Enzyme-linked immuno sorbent assay) they found that archazolid treated LPS-activated monocytes display a decreased secretion of IL-6 and IL-8. Nevertheless, additional studies are necessary to evaluate a distinct action of archazolid on these cells.

Focussing on archazolid action on cathepsin B maturation, it could be shown that the secretion of procathepsin B is a consequence of lysosome malfunction. Procathepsin B secretion was proven to be induced by other V-ATPase inhibitors bafilomycin and concanamycin as well as lysosomotropic agents chloroquine and NH_4Cl (3.3.4, 3.3.5). Furthermore, RNAi experiments revealed that the archazolid effect on cathepsin B is a direct result from V-ATPase inhibition. Knockdown of the archazolid target domain V_0c exhibited similar effects on cathepsin B maturation as archazolid treatment (3.3.3).

Transport and activation of lysosomal proteases are carefully controlled processes [56]. Missorted, active proteases can lead to uncontrolled proteolysis and apoptosis. Many of those proteases are thus translated as inactive proforms. After glycosylation in the Golgi apparatus lysosomal proteases are bound to the mannose-6-phosphate-receptor (M6PR) (Figure 4-2 Schematic overview archazolid action on M6PR mediated trafficking). Subsequently, M6PR containing vesicles are fusing with prelysosomal compartments (PLC), followed by acidification of the vesicle by V-ATPase action. Receptor bound proteases can only be released if the pH is decreased, followed by a relocalization of M6PR to the trans-Golgi network (TGN) [56, 57].

In contrast, if the pH cannot decrease in these PLC, e.g. caused by V-ATPase inhibition, the release of the cargo from M6PR is impaired and M6PR does not recycle to the TGN [72]. As a consequence newly glycosylated lysosomal proenzymes are accumulating and are thus transported out of the cell as there is no free M6PR they can be bound to (Figure 4-2).

In accordance to the present study, also macrophages treated with V-ATPase inhibitor bafilomycin are reported to secreted elevated amounts of lysosomal proteases [118]. Likewise, the lysosomotropic, anti-malaria drug chloroquine was reported to strongly induce lysosomal enzyme secretion [119]. Moreover constitutive procathepsin D secretion by breast cancer cells (MCF-7) and colorectal cancer (CaCo-2) cells was found to be promoted by lysosome neutralizing reagent NH_4Cl [120].
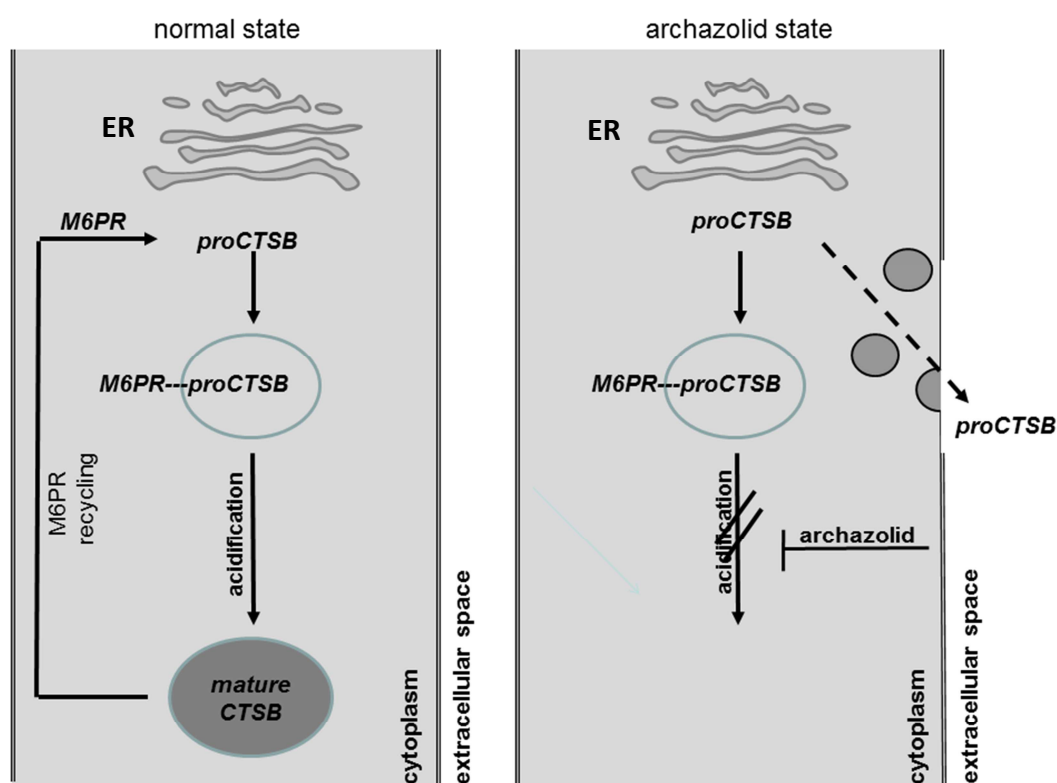
Figure 4-2 Schematic overview archazolid action on M6PR mediated trafficking

The *in vitro* results presented in the current study showed that archazolid blocks the maturation process of cathepsin B. Resulting in strongly decreased intracellular cathepsin B levels and a reduced cathepsin B activity. In cancer research lysosomal proteases like the cathepsins became more and more important as tumor markers [42-45]. Cathepsin B is upregulated in many types of cancer but its distinct role in tumor progression is not fully understood and controversially discussed. Nevertheless, cathepsin B genetic down regulation or inhibition by specific inhibitors has been shown to reduce invasive properties of cancer cells *in vitro* and *in vivo* [49, 51]. Earlier, a reduced activity of the pro-invasion protease matrix metalloproteinase 9 (MMP9) upon V-ATPase inhibition in pancreatic cancer was shown [109]. As it has been reported that inhibition of cathepsin B expression is linked to a decreased MMP9 activity in glioblastoma cells [121] the here presented results may be a link between these two publications. But most importantly, cathepsin B inhibition by the small molecule inhibitor CA-074 has been very recently shown to reduce bone metastasis of breast cancer cells *in vivo* [74]. The *in vivo* results of the present study showed that archazolid reduces the intracellular level of mature cathepsin B of tumor cells (3.4). In

particular, in a syngenic mouse model sub cutaneous tumors of mouse mammary gland tumor cells 4T1*luc* showed reduced cathepsin B protein amounts and had a reduced proteolytic cathepsin B activity. Furthermore, a functional correlation of reduced cathepsin B activity may be drawn to the fact that treated animals exhibited a reduced metastatic burden in the lungs, indicating that the reduction of cathepsin B by archazolid in tumors lead to a reduced metastatic potential of these cells.

In summary, it could be shown that the V-ATPase inhibitor archazolid reduces the intracellular activity of pro-invasion cathepsin B. Furthermore the present study provides additional information how inhibition of the V-ATPase can lead to the reduction of the invasive potential of cancer cells by blockage of mannose-6-phosphate mediated maturation of lysosomal proteases. Moreover, in a pharmaceutical point of view, archazolid displays various advantages compared to an anti-metastatic therapy using specific cathepsin B inhibitors which are no V-ATPase inhibitors: Archazolid reduces 1) the invasive potential by inhibition of membrane bound V-ATPase 2) the migratory potential [29] and 3) the activity of pro-metastatic proteases. Furthermore it has been shown that archazolid specifically induces apoptosis in cancer cells [30].

Taken together archazolid can be proposed as a promising anti-metastatic drug.

5 Summary

In the present study the mechanisms leading to acquired chemoresistance, as well as new treatment strategies implying the prevention evading of tumor cells were addressed.

Resistance formation is one of the major hurdles in cancer therapy. Metronomic anti-angiogenic treatment of xenografted prostate cancer tumors in mice with cyclophosphamide (CPA) results in the appearance of resistant tumors. To investigate the complex molecular changes occurring during resistance formation, a comprehensive gene expression analysis of the resistant tumors *in vivo* was performed. A multitude of differentially expressed genes, e.g. PAS domain containing protein 1 (PASD1), annexin A3 (ANXA3), neurotensin (NTS) or plasminogen activator tissue (PLAT), were observed, when comparing resistant to *in vivo* passaged tumor samples. Moreover, tumor cells from *in vivo* and *in vitro* conditions showed a significant difference in target gene expression. For clarification of the mechanisms leading to the survival of tumor cells during maintained anti-angiogenic CPA therapy the differentially expressed genes were assigned to functional pathways like: *axon guidance*, *steroid biosynthesis* and *complement and coagulation cascades*. As blood flow might play a crucial role during maintained anti-angiogenic therapy, further analysis was focused on the genes grouped in *complement and coagulation cascades*. Upregulation of anti-coagulatory ANXA3 and PLAT and downregulation of SERPIN A1 and other SERPIN-family members was shown by qPCR analysis. In contrast coagulation factor F3 was upregulated, accompanied by the expression of an altered gene product. Taken together, a potential role of anti-coagulation as a resistance mechanism for anti-angiogenic CPA therapy could be described.

Furthermore, the role of archazolid, a novel myxobacterial V-ATPase inhibitor in cancer treatment and in particular its action on the secreted cellular proteome was evaluated. As extracellular protein secretion may have an impact on invasive properties of tumor cells, the changes of the secretome profile of highly migratory urinary bladder carcinoma cells upon archazolid treatment were analyzed. An induced secretion of prometastatic lysosomal proteins such as the cathepsin family was observed. Interestingly, intracellular cathepsin B activity however strongly decreases and mature cathepsin B protein diminishes. It could be shown that archazolid inhibits the mannose-6-phosphate receptor mediated trafficking of procathepsin B from the trans-Golgi network to prelysosomal compartments, leading to an impaired cathepsin B maturation process. This results in an unnatural secretion of the

inactive proenzyme and a dramatic decrease in intracellular cathepsin B activity. Importantly, also *in vivo* an archazolid induced reduction of cathepsin B activity was proven and archazolid treatment resulted in a reduced formation of distant metastases in the lungs. In summary these results indicate that archazolid in addition to its known anti-migratory properties might exert an anti-metastatic effect by reducing the activity of pro metastatic proteases like cathepsin B.

6 Abbreviations

DNA	deoxyribonucleic acid
LC-MS/MS	liqud chromatography tandem mass spectormetry
µM	micro molar (10-6)
4-HOO-CPA	4-hydroxy cyclophosphamide
APS	ammonium persulfate
arch	archazolid
ATP	adenosin-5`-triphosphat
bafA	bafilomycin A1
BALB/c	*mus musculus* laboratory inbred strain
BCA	bicinchoninic acid
bref	brefeldin
cDNA	complementary DNA
concA	concanamycin A
CP	chlorpromazine
CPA	cyclophosphamide
CQ	chloroquine
DAPI	4',6-diamidino-2-phenylindole
DMEM	Dulbecco`s Modified Essential Medium
DMSO	dimethyl sulfoxid
dox	doxycycline
DTT	dithiothreitol
e.g.	exempli gratia (for example)
EDTA	ethylenediamine tetraacetic acid

FCS	fetal calf serum
i.p.	intraperitoneal(ly)
i.v.	intravenous(ly)
kDa	kilo dalton
LSM	laser scanning microscope
mM	milli molar (10^{-3})
mRNA	messenger ribobucleic acid
nM	nano molar (10^{-9})
PBS	phosphate buffered saline
PVDF	polyvinylidene fluoride
qPCR	quantitative polymerase chain reaction
RMA	robust multichip analysis
RNA	ribonucleic acid
RT	room temperature
s.c.	sub cutaneous(ly)
S.E.M.	standard error of the mean
SCID	severe combined immuno deficiency
SDS	sodium dodecyl sulfate -polyacrylamide gel electrophoresis
SDS-PAGE	sodium dodecyl sulfate
siRNA	small interfering ribonucleic acid
TEMED	Tetramethylene ethane diamine
TGN	trans-Golgi network
Tris	trishydroxymethylaminomethane
tunm	tunicamycin

7 Publications and associated bachelor theses

7.1 Original papers

<u>Kubisch R</u>, Fröhlich T, Arnold GJ, Schreiner L, Herrmann A, von Schwarzenberg K, Roidl A, Vollmar AM, Wagner E (2013). V-ATPase *inhibition by archazolid leads to lysosomal dysfunction resulting in impaired cathepsin B activation in vivo.* (in preparation)

<u>Kubisch R</u>, Meissner L, Krebs S, Blum H, Günther M, Roidl A, Wagner E (2013). *A comprehensive gene expression analysis of resistance 1 formation upon 2 metronomic cyclophosphamide therapy.* Translational Oncology **6**, 1-9

Wiedmann RM, von Schwarzenberg K, Palamidessi A, Schreiner L, <u>Kubisch R</u>, Liebl J, Schempp C*, Trauner, D., Vereb, G.. Zahler, S.. Wagner E, Muller R, Scita G,Vollmar A M (2012). The V-ATPase -inhibitor Archazolid abrogates tumor metastasis via inhibition of endocytic activation of the Rho-GTPase Rac1*. Cancer Research **72**, 5976-5987

<u>Kubisch R</u>, Bohrn U, Fleischer M, Stütz E (2012). *Cell-Based Sensor System Using L6 Cells for Broad Band Continuous Pollutant Monitoring in Aquatic Environments.* Sensors (Basel). 2012;12(3):3370-93.

7.2 Abstracts and poster presentations

<u>Kubisch R</u>, Fröhlich T, Ardelt M, Arnold GJ, Vollmar AM, Wagner E (2012) *The antitumoral V-ATPase inhibitor Archazolid induces extracellular accumulation of proCathepsin B.* Natural Anticancer Drugs, Olomouc, Czech Republic

<u>Kubisch R</u>, Thoenes L, Hoehn M, Fröhlich T, Ogris M, Arnold GJ, Wagner E, Guenther M (2012). *In vivo Chemoresistance of Prostate Cancer in Metronomic Cyclophosphamide (CPA) Therapy*, Mildred Scheel Cancer Conference, Königswinter, Germany

7.3 Associated bachelor theses

Maximilian Ardelt, May 2012:
Characterization of Cathepsin B Secreted by Archazolid B Treated Breast Cancer Cells

Aicha Jeridi, September, 2011:
Evaluation of Annexin A3 and SATB1 as a potential keyplayers in chemoresistance to metronomic Cyclophosphomide therapy in prostate cancer

Janek Kibat, February 2011*:*
Evaluation of STAT1 as a potential keyplayer in prostate cancer chemoresistance

Manuel Gregoritza, July 2010:
Evaluation of candidates derived from whole genome analysis potentially involved in prostate cancer chemoresistance

Katharina Huber, July 2009:
Transfection of PC-3 cells in a matrix-based 3D culture model

8 Acknowledgments

I want to deeply thank Prof. Dr. Ernst Wagner for giving me the opportunity to perform my PhD-thesis under his supervision. I will always appreciate his trust and scientific support throughout the past years. Furthermore I want to thank Prof. Dr. Angelika Vollmar for the great support and for her help in scientific problems at any time point.

Special thanks to Dr. Andreas Roidl for having his door always open for any kind of scientific questions, daily business problems or discussion of results. Thanks for teaching me how to write a paper and how to respond to reviewers comments. Also thanks to the "Friday seminar group" for the inspiring scientific discussions and effective suggestions.

Thanks to Dr. Georg J. Arnold and Dr. Thomas Fröhlich for being good collaboration partners from LAFUGA: Dr. Georg Arnold and Dr. Thomas Fröhlich from the proteomics facility as well as Dr. Helmut Blum and Dr. Stefan Krebs at the genomics facility. All of them made great contributions to this work. Thanks to the group of Prof. Dr. Oliver Werz especially Dr. Carlo Pergola and Olga Scherer for hosting me during my 3 weeks internship.

Thanks to all lab members for all their help. Especially to Laura Schreiner who did an unbelievable good job at the animal facility. Furthermore, I want to thank Florian Kopp ad Dr. Karin von Schwarzenberg for their help by discussion of results and in technical questions.Special thanks to Dr. Dorit Nägler who helped a lot in all cathepsin topics. Thanks to the technical assistants Ursula Biebl, Anna Kulinyak, Markus Kovac and Wolfgang Rödl for keeping the lab running. Furthermore, thanks to all the students working with me on the projects. All of you did a great job.

Special thanks to my dear friends Dr. Myriam Demant for reading and correction of the manuscript. Thanks to Dr. Christian Dohmen for always being at my side. Thanks to my whole family Mama, Papa, Simon, Gregor and Oma Sophia. You all made me what I am today and gave me all the encouragement, trust and love to get easily through all what people call challenging.

Last but not least: special thanks to the DFG and the NIM for funding.

9 Literature

[1]   Hajdu SI (2011). A note from history: landmarks in history of cancer, part 1. *Cancer* **117**, 1097-1102.

[2]   Hanahan D, and Weinberg RA (2000). The hallmarks of cancer. *Cell* **100**, 57-70.

[3]   Hanahan D, and Weinberg RA (2011). Hallmarks of cancer: the next generation. *Cell* **144**, 646-674.

[4]   Kerbel RS (2011). Reappraising antiangiogenic therapy for breast cancer. *Breast* **20 Suppl 3**, S56-60.

[5]   Kerbel RS (1991). Inhibition of tumor angiogenesis as a strategy to circumvent acquired resistance to anti-cancer therapeutic agents. *BioEssays : news and reviews in molecular, cellular and developmental biology* **13**, 31-36.

[6]   Oudard S, Banu E, Beuzeboc P, Voog E, Dourthe LM, Hardy-Bessard AC, Linassier C, Scotte F, Banu A, Coscas Y*, et al.* (2005). Multicenter randomized phase II study of two schedules of docetaxel, estramustine, and prednisone versus mitoxantrone plus prednisone in patients with metastatic hormone-refractory prostate cancer. *J Clin Oncol* **23**, 3343-3351.

[7]   Petrylak DP, Tangen CM, Hussain MH, Lara PN, Jr., Jones JA, Taplin ME, Burch PA, Berry D, Moinpour C, Kohli M*, et al.* (2004). Docetaxel and estramustine compared with mitoxantrone and prednisone for advanced refractory prostate cancer. *N Engl J Med* **351**, 1513-1520.

[8]   Emmenegger U, Francia G, Shaked Y, and Kerbel RS (2010). Metronomic chemotherapy: principles and lessons learned from applications in the treatment of metastatic prostate cancer. *Recent Results Cancer Res* **180**, 165-183.

[9]   Kerbel RS, and Kamen BA (2004). The anti-angiogenic basis of metronomic chemotherapy. *Nature reviews. Cancer* **4**, 423-436.

[10]   Hanahan D, Bergers G, and Bergsland E (2000). Less is more, regularly: metronomic dosing of cytotoxic drugs can target tumor angiogenesis in mice. *J Clin Invest* **105**, 1045-1047.

[11]   Browder T, Butterfield CE, Kraling BM, Shi B, Marshall B, O'Reilly MS, and Folkman J (2000). Antiangiogenic scheduling of chemotherapy improves efficacy against experimental drug-resistant cancer. *Cancer research* **60**, 1878-1886.

[12]   Emmenegger U, Francia G, Chow A, Shaked Y, Kouri A, Man S, and Kerbel RS (2011). Tumors that acquire resistance to low-dose metronomic cyclophosphamide retain sensitivity to maximum tolerated dose cyclophosphamide. *Neoplasia* **13**, 40-48.

[13]   Thoenes L, Hoehn M, Kashirin R, Ogris M, Arnold GJ, Wagner E, and Guenther M (2010). In vivo chemoresistance of prostate cancer in metronomic cyclophosphamide therapy. *J Proteomics* **73**, 1342-1354.

[14]   Kubisch R, Meissner L, Krebs S, Blum H, Gunther M, Roidl A, and Wagner E (2013). A Comprehensive Gene Expression Analysis of Resistance Formation upon Metronomic Cyclophosphamide Therapy. *Translational oncology* **6**, 1-9.

[15]   Bode HB, and Muller R (2006). Analysis of myxobacterial secondary metabolism goes molecular. *Journal of industrial microbiology & biotechnology* **33**, 577-588.

[16]   Vahdat LT (2008). Clinical studies with epothilones for the treatment of metastatic breast cancer. *Seminars in oncology* **35**, S22-30; quiz S40.

[17]   Elnakady YA, Sasse F, Lunsdorf H, and Reichenbach H (2004). Disorazol A1, a highly effective antimitotic agent acting on tubulin polymerization and inducing apoptosis in mammalian cells. *Biochemical pharmacology* **67**, 927-935.

[18]   Sasse F, Steinmetz H, Heil J, Hofle G, and Reichenbach H (2000). Tubulysins, new cytostatic peptides from myxobacteria acting on microtubuli. Production, isolation, physico-chemical and biological properties. *The Journal of antibiotics* **53**, 879-885.

[19]   Gronewold TM, Sasse F, Lunsdorf H, and Reichenbach H (1999). Effects of rhizopodin and latrunculin B on the morphology and on the actin cytoskeleton of mammalian cells. *Cell and tissue research* **295**, 121-129.

[20]   Sasse F, Steinmetz H, Hofle G, and Reichenbach H (1993). Rhizopodin, a new compound from Myxococcus stipitatus (myxobacteria) causes formation of rhizopodia-like structures in animal cell cultures. Production, isolation, physico-chemical and biological properties. *The Journal of antibiotics* **46**, 741-748.

[21]   Sasse F, Kunze B, Gronewold TM, and Reichenbach H (1998). The chondramides: cytostatic agents from myxobacteria acting on the actin cytoskeleton. *Journal of the National Cancer Institute* **90**, 1559-1563.

[22]   Sasse F, Steinmetz H, Hofle G, and Reichenbach H (2003). Archazolids, new cytotoxic macrolactones from Archangium gephyra (Myxobacteria). Production, isolation, physico-chemical and biological properties. *The Journal of antibiotics* **56**, 520-525.

[23]   Bockelmann S, Menche D, Rudolph S, Bender T, Grond S, von Zezschwitz P, Muench SP, Wieczorek H, and Huss M (2010). Archazolid A binds to the equatorial region of the c-ring of the vacuolar H+-ATPase. *The Journal of biological chemistry* **285**, 38304-38314.

[24]   Rath S, Liebl J, Furst R, Ullrich A, Burkhart JL, Kazmaier U, Herrmann J, Muller R, Gunther M, Schreiner L*, et al.* (2012). Anti-angiogenic effects of the tubulysin precursor pretubulysin and of simplified pretubulysin derivatives. *British journal of pharmacology* **167**, 1048-1061.

[25]   Huss M, Sasse F, Kunze B, Jansen R, Steinmetz H, Ingenhorst G, Zeeck A, and Wieczorek H (2005). Archazolid and apicularen: novel specific V-ATPase inhibitors. *BMC biochemistry* **6**, 13.

[26]   Osteresch C, Bender T, Grond S, von Zezschwitz P, Kunze B, Jansen R, Huss M, and Wieczorek H (2012). The binding site of the V-ATPase inhibitor apicularen is in the vicinity of those for bafilomycin and archazolid. *The Journal of biological chemistry* **287**, 31866-31876.

[27]   Persch E, Basile T, Bockelmann S, Huss M, Wieczorek H, Carlomagno T, and Menche D (2012). Synthesis and biological evaluation of a water-soluble derivative of the potent V-ATPase inhibitor archazolid. *Bioorganic & medicinal chemistry letters*.

[28]   Roethle PA, Chen IT, and Trauner D (2007). Total synthesis of (-)-archazolid B. *Journal of the American Chemical Society* **129**, 8960-8961.

[29]   Wiedmann RM, von Schwarzenberg K, Palamidessi A, Schreiner L, Kubisch R, Liebl J, Schempp C, Trauner D, Vereb G, Zahler S*, et al.* (2012). The V-ATPase-inhibitor Archazolid abrogates tumor metastasis via inhibition of endocytic activation of the Rho-GTPase Rac1. *Cancer research*.

[30]   von Schwarzenberg K, Wiedmann RM, Oak P, Schulz S, Zischka H, Wanner G, Efferth T, Trauner D, and Vollmar AM (2012). Mode of cell death induction by pharmacological vacuolar H+-ATPase (V-ATPase) inhibition. *The Journal of biological chemistry*.

[31]   Nishi T, and Forgac M (2002). The vacuolar (H+)-ATPases--nature's most versatile proton pumps. *Nature reviews. Molecular cell biology* **3**, 94-103.

[32]   Forgac M (2007). Vacuolar ATPases: rotary proton pumps in physiology and pathophysiology. *Nature reviews. Molecular cell biology* **8**, 917-929.

[33]   Vaupel P, Kallinowski F, and Okunieff P (1989). Blood flow, oxygen and nutrient supply, and metabolic microenvironment of human tumors: a review. *Cancer research* **49**, 6449-6465.

[34]   Sennoune SR, Bakunts K, Martinez GM, Chua-Tuan JL, Kebir Y, Attaya MN, and Martinez-Zaguilan R (2004). Vacuolar H+-ATPase in human breast cancer cells with distinct metastatic potential: distribution and functional activity. *American journal of physiology. Cell physiology* **286**, C1443-1452.

[35]   Lu X, Qin W, Li J, Tan N, Pan D, Zhang H, Xie L, Yao G, Shu H, Yao M*, et al.* (2005). The growth and metastasis of human hepatocellular carcinoma xenografts are inhibited by small interfering RNA targeting to the subunit ATP6L of proton pump. *Cancer research* **65**, 6843-6849.

[36]   Fais S, De Milito A, You H, and Qin W (2007). Targeting vacuolar H+-ATPases as a new strategy against cancer. *Cancer research* **67**, 10627-10630.

[37]   Huss M, Ingenhorst G, Konig S, Gassel M, Drose S, Zeeck A, Altendorf K, and Wieczorek H (2002). Concanamycin A, the specific inhibitor of V-ATPases, binds to the V(o) subunit c. *The Journal of biological chemistry* **277**, 40544-40548.

[38]   Rautiala TJ, Koskinen AM, and Vaananen HK (1993). Purification of vacuolar ATPase with bafilomycin C1 affinity chromatography. *Biochemical and biophysical research communications* **194**, 50-56.

[39]   Bowman BJ, and Bowman EJ (2002). Mutations in subunit C of the vacuolar ATPase confer resistance to bafilomycin and identify a conserved antibiotic binding site. *The Journal of biological chemistry* **277**, 3965-3972.

[40]   Kinashi H, Someno K, and Sakaguchi K (1984). Isolation and characterization of concanamycins A, B and C. *The Journal of antibiotics* **37**, 1333-1343.

[41]   Werner G, Hagenmaier H, Drautz H, Baumgartner A, and Zahner H (1984). Metabolic products of microorganisms. 224. Bafilomycins, a new group of macrolide antibiotics.

Production, isolation, chemical structure and biological activity. *The Journal of antibiotics* **37**, 110-117.

[42]   Yan S, Sameni M, and Sloane BF (1998). Cathepsin B and human tumor progression. *Biological chemistry* **379**, 113-123.

[43]   Fernandez PL, Farre X, Nadal A, Fernandez E, Peiro N, Sloane BF, Shi GP, Chapman HA, Campo E, and Cardesa A (2001). Expression of cathepsins B and S in the progression of prostate carcinoma. *International journal of cancer. Journal international du cancer* **95**, 51-55.

[44]   Campo E, Munoz J, Miquel R, Palacin A, Cardesa A, Sloane BF, and Emmert-Buck MR (1994). Cathepsin B expression in colorectal carcinomas correlates with tumor progression and shortened patient survival. *The American journal of pathology* **145**, 301-309.

[45]   Lah TT, Cercek M, Blejec A, Kos J, Gorodetsky E, Somers R, and Daskal I (2000). Cathepsin B, a prognostic indicator in lymph node-negative breast carcinoma patients: comparison with cathepsin D, cathepsin L, and other clinical indicators. *Clinical cancer research : an official journal of the American Association for Cancer Research* **6**, 578-584.

[46]   Chambers AF, Groom AC, and MacDonald IC (2002). Dissemination and growth of cancer cells in metastatic sites. *Nature reviews. Cancer* **2**, 563-572.

[47]   Joyce JA, and Pollard JW (2009). Microenvironmental regulation of metastasis. *Nature reviews. Cancer* **9**, 239-252.

[48]   Weigelt B, Peterse JL, and van 't Veer LJ (2005). Breast cancer metastasis: markers and models. *Nature reviews. Cancer* **5**, 591-602.

[49]   Leto G, Pizzolanti G, Tumminello FM, and Gebbia N (1994). Effects of E-64 (cysteine-proteinase inhibitor) and pepstatin (aspartyl-proteinase inhibitor) on metastasis formation in mice with mammary and ovarian tumors. *In Vivo* **8**, 231-236.

[50]   Van Noorden CJ, Jonges TG, Van Marle J, Bissell ER, Griffini P, Jans M, Snel J, and Smith RE (1998). Heterogeneous suppression of experimentally induced colon cancer metastasis in rat liver lobes by inhibition of extracellular cathepsin B. *Clinical & experimental metastasis* **16**, 159-167.

[51]   Coulibaly S, Schwihla H, Abrahamson M, Albini A, Cerni C, Clark JL, Ng KM, Katunuma N, Schlappack O, Glossl J, *et al.* (1999). Modulation of invasive properties of murine squamous carcinoma cells by heterologous expression of cathepsin B and cystatin C. *International journal of cancer. Journal international du cancer* **83**, 526-531.

[52]   Buck MR, Karustis DG, Day NA, Honn KV, and Sloane BF (1992). Degradation of extracellular-matrix proteins by human cathepsin B from normal and tumour tissues. *The Biochemical journal* **282 (Pt 1)**, 273-278.

[53]   Tu C, Ortega-Cava CF, Chen G, Fernandes ND, Cavallo-Medved D, Sloane BF, Band V, and Band H (2008). Lysosomal cathepsin B participates in the podosome-mediated extracellular matrix degradation and invasion via secreted lysosomes in v-Src fibroblasts. *Cancer research* **68**, 9147-9156.

[54] Szpaderska AM, and Frankfater A (2001). An intracellular form of cathepsin B contributes to invasiveness in cancer. *Cancer research* **61**, 3493-3500.

[55] Kobayashi H, Moniwa N, Sugimura M, Shinohara H, Ohi H, and Terao T (1993). Effects of membrane-associated cathepsin B on the activation of receptor-bound prourokinase and subsequent invasion of reconstituted basement membranes. *Biochimica et biophysica acta* **1178**, 55-62.

[56] Brix K, Dunkhorst A, Mayer K, and Jordans S (2008). Cysteine cathepsins: cellular roadmap to different functions. *Biochimie* **90**, 194-207.

[57] Mort JS, and Buttle DJ (1997). Cathepsin B. *The International Journal of Biochemistry & Cell Biology* **29**, 715-720.

[58] Ishidoh K, and Kominami E (2002). Processing and activation of lysosomal proteinases. *Biological chemistry* **383**, 1827-1831.

[59] Barrett AJ (1980). Fluorimetric assays for cathepsin B and cathepsin H with methylcoumarylamide substrates. *The Biochemical journal* **187**, 909-912.

[60] Huang DW, Sherman BT, and Lempicki RA (2008). Systematic and integrative analysis of large gene lists using DAVID bioinformatics resources. *Nat. Protocols* **4**, 44-57.

[61] Keller A, Nesvizhskii AI, Kolker E, and Aebersold R (2002). Empirical statistical model to estimate the accuracy of peptide identifications made by MS/MS and database search. *Analytical chemistry* **74**, 5383-5392.

[62] Fleige S, Walf V, Huch S, Prgomet C, Sehm J, and Pfaffl MW (2006). Comparison of relative mRNA quantification models and the impact of RNA integrity in quantitative real-time RT-PCR. *Biotechnol Lett* **28**, 1601-1613.

[63] Laemmli UK (1970). Cleavage of structural proteins during the assembly of the head of bacteriophage T4. *Nature* **227**, 680-685.

[64] Kuo TC, and Chao CC (2010). Hepatitis B virus X protein prevents apoptosis of hepatocellular carcinoma cells by upregulating SATB1 and HURP expression. *Biochemical pharmacology* **80**, 1093-1102.

[65] Fenselau C (1976). Review of the metabolism and mode of action of cyclophosphamide. *Journal - Association of Official Analytical Chemists* **59**, 1028-1036.

[66] Law RH, Zhang Q, McGowan S, Buckle AM, Silverman GA, Wong W, Rosado CJ, Langendorf CG, Pike RN, Bird PI*, et al.* (2006). An overview of the serpin superfamily. *Genome Biol* **7**, 216.

[67] Tait JF, Sakata M, McMullen BA, Miao CH, Funakoshi T, Hendrickson LE, and Fujikawa K (1988). Placental anticoagulant proteins: isolation and comparative characterization four members of the lipocortin family. *Biochemistry* **27**, 6268-6276.

[68] Sobota JA, Back N, Eipper BA, and Mains RE (2009). Inhibitors of the V0 subunit of the vacuolar H+-ATPase prevent segregation of lysosomal- and secretory-pathway proteins. *Journal of cell science* **122**, 3542-3553.

[69]   Dettmer J, Hong-Hermesdorf A, Stierhof YD, and Schumacher K (2006). Vacuolar H+-ATPase activity is required for endocytic and secretory trafficking in Arabidopsis. *The Plant cell* **18**, 715-730.

[70]   Lee SJ, Cho SC, Lee EJ, Kim S, Lee SB, Lim JH, Choi YH, Kim WJ, and Moon SK (2013). Interleukin-20 promotes migration of bladder cancer cells through extracellular signal-regulated kinase (ERK)-mediated MMP-9 protein expression leading to nuclear factor (NF-kappaB) activation by inducing the up-regulation of p21(WAF1) protein expression. *The Journal of biological chemistry* **288**, 5539-5552.

[71]   Zieske LR (2006). A perspective on the use of iTRAQ reagent technology for protein complex and profiling studies. *Journal of experimental botany* **57**, 1501-1508.

[72]   Borden LA, Einstein R, Gabel CA, and Maxfield FR (1990). Acidification-dependent dissociation of endocytosed insulin precedes that of endocytosed proteins bearing the mannose 6-phosphate recognition marker. *The Journal of biological chemistry* **265**, 8497-8504.

[73]   Kuo SC, and Lampen JO (1974). Tunicamycin--an inhibitor of yeast glycoprotein synthesis. *Biochemical and biophysical research communications* **58**, 287-295.

[74]   Withana NP, Blum G, Sameni M, Slaney C, Anbalagan A, Olive MB, Bidwell BN, Edgington L, Wang L, Moin K*, et al.* (2012). Cathepsin B inhibition limits bone metastasis in breast cancer. *Cancer research* **72**, 1199-1209.

[75]   Emmenegger U, Shaked Y, Man S, Bocci G, Spasojevic I, Francia G, Kouri A, Coke R, Cruz-Munoz W, Ludeman SM*, et al.* (2007). Pharmacodynamic and pharmacokinetic study of chronic low-dose metronomic cyclophosphamide therapy in mice. *Molecular cancer therapeutics* **6**, 2280-2289.

[76]   Gabrielli F, Donadel G, Bensi G, Heguy A, and Melli M (1995). A nuclear protein, synthesized in growth-arrested human hepatoblastoma cells, is a novel member of the short-chain alcohol dehydrogenase family. *European journal of biochemistry / FEBS* **232**, 473-477.

[77]   Shafqat N, Shafqat J, Eissner G, Marschall HU, Tryggvason K, Eriksson U, Gabrielli F, Lardy H, Jornvall H, and Oppermann U (2006). Hep27, a member of the short-chain dehydrogenase/reductase family, is an NADPH-dependent dicarbonyl reductase expressed in vascular endothelial tissue. *Cell Mol Life Sci* **63**, 1205-1213.

[78]   Donadel G, Garzelli C, Frank R, and Gabrielli F (1991). Identification of a novel nuclear protein synthesized in growth-arrested human hepatoblastoma HepG2 cells. *European journal of biochemistry / FEBS* **195**, 723-729.

[79]   Guinn BA, Bland EA, Lodi U, Liggins AP, Tobal K, Petters S, Wells JW, Banham AH, and Mufti GJ (2005). Humoral detection of leukaemia-associated antigens in presentation acute myeloid leukaemia. *Biochemical and biophysical research communications* **335**, 1293-1304.

[80]   Liggins AP, Brown PJ, Asker K, Pulford K, and Banham AH (2004). A novel diffuse large B-cell lymphoma-associated cancer testis antigen encoding a PAS domain protein. *Br J Cancer* **91**, 141-149.

[81] Carraway R, and Leeman SE (1973). The isolation of a new hypotensive peptide, neurotensin, from bovine hypothalami. *The Journal of biological chemistry* **248**, 6854-6861.

[82] Maoret JJ, Anini Y, Rouyer-Fessard C, Gully D, and Laburthe M (1999). Neurotensin and a non-peptide neurotensin receptor antagonist control human colon cancer cell growth in cell culture and in cells xenografted into nude mice. *International journal of cancer. Journal international du cancer* **80**, 448-454.

[83] Friry C, Feliciangeli S, Richard F, Kitabgi P, and Rovere C (2002). Production of recombinant large proneurotensin/neuromedin N-derived peptides and characterization of their binding and biological activity. *Biochemical and biophysical research communications* **290**, 1161-1168.

[84] Gong H, Wang Z, Zhao GW, Lv X, Wei GH, Wang L, Liu DP, and Liang CC (2009). SATB1 regulates beta-like globin genes through matrix related nuclear relocation of the cluster. *Biochemical and biophysical research communications* **383**, 11-15.

[85] Kumar PP, Bischof O, Purbey PK, Notani D, Urlaub H, Dejean A, and Galande S (2007). Functional interaction between PML and SATB1 regulates chromatin-loop architecture and transcription of the MHC class I locus. *Nat Cell Biol* **9**, 45-56.

[86] Pavan Kumar P, Purbey PK, Sinha CK, Notani D, Limaye A, Jayani RS, and Galande S (2006). Phosphorylation of SATB1, a global gene regulator, acts as a molecular switch regulating its transcriptional activity in vivo. *Molecular cell* **22**, 231-243.

[87] Nechanitzky R, Davila A, Savarese F, Fietze S, and Grosschedl R (2012). Satb1 and Satb2 are dispensable for X chromosome inactivation in mice. *Developmental cell* **23**, 866-871.

[88] Chu SH, Ma YB, Feng DF, Li ZQ, and Jiang PC (2012). Correlation between SATB1 and Bcl-2 expression in human glioblastoma multiforme. *Molecular medicine reports*.

[89] Endo K, Shackelford J, Aga M, Yoshizaki T, and Pagano JS (2012). Up-regulation of SATB1 by EBV LMP1 in human nasopharyngeal cells and nasopharyngeal cancer. *The Journal of general virology*.

[90] Nodin B, Hedner C, Uhlen M, and Jirstrom K (2012). Expression of the global regulator SATB1 is an independent factor of poor prognosis in high grade epithelial ovarian cancer. *Journal of ovarian research* **5**, 24.

[91] Shukla S, Sharma H, Abbas A, Maclennan GT, Fu P, Danielpour D, and Gupta S (2013). Upregulation of SATB1 Is Associated with Prostate Cancer Aggressiveness and Disease Progression. *PloS one* **8**, e53527.

[92] Zhang J, Zhang B, Zhang X, Sun Y, Wei X, McNutt MA, Lu S, Liu Y, Zhang D, Wang M*, et al.* (2013). SATB1 Expression Is Associated with Biologic Behavior in Colorectal Carcinoma In Vitro and In Vivo. *PloS one* **8**, e47902.

[93] Li QQ, Chen ZQ, Xu JD, Cao XX, Chen Q, Liu XP, and Xu ZD (2010). Overexpression and involvement of special AT-rich sequence binding protein 1 in multidrug resistance in human breast carcinoma cells. *Cancer science* **101**, 80-86.

[94]   Sun F, Lu X, Li H, Peng Z, Wu K, Wang G, and Tong Q (2012). Special AT-rich sequence binding protein 1 regulates the multidrug resistance and invasion of human gastric cancer cells. *Oncology letters* **4**, 156-162.

[95]   Ruschke K, Hiepen C, Becker J, and Knaus P (2012). BMPs are mediators in tissue crosstalk of the regenerating musculoskeletal system. *Cell and tissue research* **347**, 521-544.

[96]   Alarmo EL, and Kallioniemi A (2010). Bone morphogenetic proteins in breast cancer: dual role in tumourigenesis? *Endocrine-related cancer* **17**, R123-139.

[97]   Ernst JD, Hoye E, Blackwood RA, and Jaye D (1990). Purification and characterization of an abundant cytosolic protein from human neutrophils that promotes Ca2(+)-dependent aggregation of isolated specific granules. *J Clin Invest* **85**, 1065-1071.

[98]   Gerke V, Creutz CE, and Moss SE (2005). Annexins: linking Ca2+ signalling to membrane dynamics. *Nature reviews. Molecular cell biology* **6**, 449-461.

[99]   Uysal-Onganer P, Kawano Y, Caro M, Walker MM, Diez S, Darrington RS, Waxman J, and Kypta RM (2010). Wnt-11 promotes neuroendocrine-like differentiation, survival and migration of prostate cancer cells. *Mol Cancer* **9**, 55.

[100]   Marchiani S, Tamburrino L, Nesi G, Paglierani M, Gelmini S, Orlando C, Maggi M, Forti G, and Baldi E (2010). Androgen-responsive and -unresponsive prostate cancer cell lines respond differently to stimuli inducing neuroendocrine differentiation. *Int J Androl* **33**, 784-793.

[101]   Murray JC, Smith KA, and Thurston G (1989). Flavone acetic acid induces a coagulopathy in mice. *British journal of cancer* **60**, 729-733.

[102]   Ny T, Elgh F, and Lund B (1984). The structure of the human tissue-type plasminogen activator gene: correlation of intron and exon structures to functional and structural domains. *Proceedings of the National Academy of Sciences of the United States of America* **81**, 5355-5359.

[103]   Castoldi E, and Hackeng TM (2008). Regulation of coagulation by protein S. *Curr Opin Hematol* **15**, 529-536.

[104]   McVey JH (1999). Tissue factor pathway. *Baillieres Best Pract Res Clin Haematol* **12**, 361-372.

[105]   Gouault-Helimann M, and Josso F (1979). Initiation in vivo of blood coagulation. The role of white blood cells and tissue factor *Nouv Presse Med* **8**, 3249-3253.

[106]   Bogdanov VY, Balasubramanian V, Hathcock J, Vele O, Lieb M, and Nemerson Y (2003). Alternatively spliced human tissue factor: a circulating, soluble, thrombogenic protein. *Nat Med* **9**, 458-462.

[107]   UniProtConsortium (2012). Reorganizing the protein space at the Universal Protein Resource (UniProt). *Nucleic acids research* **40**, D71-75.

[108]   Park BK (1988). Warfarin: metabolism and mode of action. *Biochemical pharmacology* **37**, 19-27.

[109]   Chung C, Mader CC, Schmitz JC, Atladottir J, Fitchev P, Cornwell ML, Koleske AJ, Crawford SE, and Gorelick F (2011). The vacuolar-ATPase modulates matrix metalloproteinase isoforms in

human pancreatic cancer. *Laboratory investigation; a journal of technical methods and pathology* **91**, 732-743.

[110]   Perez-Sayans M, Garcia-Garcia A, Reboiras-Lopez MD, and Gandara-Vila P (2009). Role of V-ATPases in solid tumors: importance of the subunit C (Review). *International journal of oncology* **34**, 1513-1520.

[111]   Xu L, Fukumura D, and Jain RK (2002). Acidic extracellular pH induces vascular endothelial growth factor (VEGF) in human glioblastoma cells via ERK1/2 MAPK signaling pathway: mechanism of low pH-induced VEGF. *The Journal of biological chemistry* **277**, 11368-11374.

[112]   Martinez-Zaguilan R, Seftor EA, Seftor RE, Chu YW, Gillies RJ, and Hendrix MJ (1996). Acidic pH enhances the invasive behavior of human melanoma cells. *Clinical & experimental metastasis* **14**, 176-186.

[113]   Reshkin SJ, Bellizzi A, Caldeira S, Albarani V, Malanchi I, Poignee M, Alunni-Fabbroni M, Casavola V, and Tommasino M (2000). Na+/H+ exchanger-dependent intracellular alkalinization is an early event in malignant transformation and plays an essential role in the development of subsequent transformation-associated phenotypes. *FASEB journal : official publication of the Federation of American Societies for Experimental Biology* **14**, 2185-2197.

[114]   Hagag N, Lacal JC, Graber M, Aaronson S, and Viola MV (1987). Microinjection of ras p21 induces a rapid rise in intracellular pH. *Molecular and cellular biology* **7**, 1984-1988.

[115]   Ober SS, and Pardee AB (1987). Intracellular pH is increased after transformation of Chinese hamster embryo fibroblasts. *Proceedings of the National Academy of Sciences of the United States of America* **84**, 2766-2770.

[116]   Gerweck LE, and Seetharaman K (1996). Cellular pH gradient in tumor versus normal tissue: potential exploitation for the treatment of cancer. *Cancer research* **56**, 1194-1198.

[117]   Hughes SJ, Glover TW, Zhu XX, Kuick R, Thoraval D, Orringer MB, Beer DG, and Hanash S (1998). A novel amplicon at 8p22-23 results in overexpression of cathepsin B in esophageal adenocarcinoma. *Proceedings of the National Academy of Sciences of the United States of America* **95**, 12410-12415.

[118]   Tapper H, and Sundler R (1995). Bafilomycin A1 inhibits lysosomal, phagosomal, and plasma membrane H(+)-ATPase and induces lysosomal enzyme secretion in macrophages. *Journal of cellular physiology* **163**, 137-144.

[119]   Gonzalez-Noriega A, Grubb JH, Talkad V, and Sly WS (1980). Chloroquine inhibits lysosomal enzyme pinocytosis and enhances lysosomal enzyme secretion by impairing receptor recycling. *The Journal of cell biology* **85**, 839-852.

[120]   Kokkonen N, Rivinoja A, Kauppila A, Suokas M, Kellokumpu I, and Kellokumpu S (2004). Defective acidification of intracellular organelles results in aberrant secretion of cathepsin D in cancer cells. *The Journal of biological chemistry* **279**, 39982-39988.

[121]   Yanamandra N, Gumidyala KV, Waldron KG, Gujrati M, Olivero WC, Dinh DH, Rao JS, and Mohanam S (2004). Blockade of cathepsin B expression in human glioblastoma cells is associated with suppression of angiogenesis. *Oncogene* **23**, 2224-2230.

10 Appendix

Table 10-1 List of identified proteins in supernatants of archazolid treated T-24 cells
Numbers on the right indicate the quantity of different identified peptides in each replicate (1-5).

#	Identified Proteins (375)	Accession	r1	r2	r3	r4	r5
1	Fibronectin OS=Homo sapiens GN=FN1 PE=1 SV=4	FINC_HUMAN	63	55	51	70	72
2	Keratin, type II cytoskeletal 1 OS=Homo sapiens GN=KRT1 PE=1 SV=6	K2C1_HUMAN	13	21	25	16	16
3	Alpha-enolase OS=Homo sapiens GN=ENO1 PE=1 SV=2	ENOA_HUMAN	18	18	19	21	25
4	Galectin-3-binding protein OS=Homo sapiens GN=LGALS3BP PE=1 SV=1	LG3BP_HUMAN	16	16	18	20	17
5	Keratin, type I cytoskeletal 10 OS=Homo sapiens GN=KRT10 PE=1 SV=6	K1C10_HUMAN	14	20	23	12	14
6	Serum albumin OS=Homo sapiens GN=ALB PE=1 SV=2	ALBU_HUMAN	5	5	7	8	7
7	Actin, cytoplasmic 1 OS=Homo sapiens GN=ACTB PE=1 SV=1	ACTB_HUMAN	13	14	15	18	19
8	Pentraxin-related protein PTX3 OS=Homo sapiens GN=PTX3 PE=1 SV=3	PTX3_HUMAN	14	10	9	13	10
9	EGF-containing fibulin-like extracellular matrix protein 1 OS=Homo sapiens GN=EFEMP1 PE=1 SV=2	FBLN3_HUMAN	13	13	10	14	12
10	Triosephosphate isomerase OS=Homo sapiens GN=TPI1 PE=1 SV=3	TPIS_HUMAN	16	14	14	16	19
11	Collagen alpha-1(VI) chain OS=Homo sapiens GN=COL6A1 PE=1 SV=3	CO6A1_HUMAN	17	14	13	21	24
12	Pyruvate kinase isozymes M1/M2 OS=Homo sapiens GN=PKM PE=1 SV=4	KPYM_HUMAN	11	12	8	20	26
13	Insulin-like growth factor-binding protein 7 OS=Homo sapiens GN=IGFBP7 PE=1 SV=1	IBP7_HUMAN	14	13	14	9	6
14	Heat shock cognate 71 kDa protein OS=Homo sapiens GN=HSPA8 PE=1 SV=1	HSP7C_HUMAN	16	10	11	22	23
15	Laminin subunit alpha-5 OS=Homo sapiens GN=LAMA5 PE=1 SV=8	LAMA5_HUMAN	35	28	20	39	23
16	Alpha-actinin-4 OS=Homo sapiens GN=ACTN4 PE=1 SV=2	ACTN4_HUMAN	5	12	23	31	33
17	Filamin-A OS=Homo sapiens GN=FLNA PE=1 SV=4	FLNA_HUMAN	15	7	17	30	37
18	Sulfhydryl oxidase 1 OS=Homo sapiens GN=QSOX1 PE=1 SV=3	QSOX1_HUMAN	16	9	15	19	16
19	Keratin, type I cytoskeletal 9 OS=Homo sapiens GN=KRT9 PE=1 SV=3	K1C9_HUMAN	10	15	16	5	7
20	Keratin, type II cytoskeletal 2 epidermal OS=Homo sapiens GN=KRT2 PE=1 SV=2	K22E_HUMAN	4	18	16	6	8
21	Phosphoglycerate kinase 1 OS=Homo sapiens GN=PGK1 PE=1 SV=3	PGK1_HUMAN	12	14	12	15	19
22	Profilin-1 OS=Homo sapiens GN=PFN1 PE=1 SV=2	PROF1_HUMAN	13	4	7	11	13
23	Peptidyl-prolyl cis-trans isomerase A OS=Homo sapiens GN=PPIA PE=1 SV=2	PPIA_HUMAN	12	3	6	13	15
24	Calsyntenin-1 OS=Homo sapiens GN=CLSTN1 PE=1 SV=1	CSTN1_HUMAN	15	7	6	17	20
25	Ubiquitin-40S ribosomal protein S27a OS=Homo sapiens GN=RPS27A PE=1 SV=2	RS27A_HUMAN	3	4	4	7	8
26	Fructose-bisphosphate aldolase A OS=Homo sapiens GN=ALDOA PE=1 SV=2	ALDOA_HUMAN	15	16	12	14	12
27	Heat shock protein HSP 90-alpha OS=Homo sapiens GN=HSP90AA1 PE=1 SV=5	HS90A_HUMAN	0	9	11	21	23
28	Glyceraldehyde-3-phosphate dehydrogenase OS=Homo sapiens GN=GAPDH PE=1 SV=3	G3P_HUMAN	7	5	6	8	13
29	L-lactate dehydrogenase A chain OS=Homo sapiens GN=LDHA PE=1 SV=2	LDHA_HUMAN	4	5	5	13	14
30	Metalloproteinase inhibitor 1 OS=Homo sapiens GN=TIMP1 PE=1 SV=1	TIMP1_HUMAN	4	4	6	8	5

31	14-3-3 protein zeta/delta OS=Homo sapiens GN=YWHAZ PE=1 SV=1	1433Z_HUMAN	14	7	8	14	16
32	Laminin subunit gamma-2 OS=Homo sapiens GN=LAMC2 PE=1 SV=2	LAMC2_HUMAN	12	0	0	24	15
33	Moesin OS=Homo sapiens GN=MSN PE=1 SV=3	MOES_HUMAN	1	7	5	21	22
34	Beta-2-microglobulin OS=Homo sapiens GN=B2M PE=1 SV=1	B2MG_HUMAN	6	3	5	5	4
35	Vinculin OS=Homo sapiens GN=VCL PE=1 SV=4	VINC_HUMAN	6	8	15	13	22
36	Filamin-B OS=Homo sapiens GN=FLNB PE=1 SV=2	FLNB_HUMAN	2	8	14	21	30
37	Cofilin-1 OS=Homo sapiens GN=CFL1 PE=1 SV=3	COF1_HUMAN	7	4	4	7	9
38	Phosphoglycerate mutase 1 OS=Homo sapiens GN=PGAM1 PE=1 SV=2	PGAM1_HUMAN	9	4	11	9	8
39	Elongation factor 2 OS=Homo sapiens GN=EEF2 PE=1 SV=4	EF2_HUMAN	1	2	2	15	23
40	Insulin-like growth factor-binding protein 4 OS=Homo sapiens GN=IGFBP4 PE=1 SV=2	IBP4_HUMAN	5	3	6	9	4
41	Tubulin alpha-1B chain OS=Homo sapiens GN=TUBA1B PE=1 SV=1	TBA1B_HUMAN	7	3	4	10	12
42	Laminin subunit gamma-1 OS=Homo sapiens GN=LAMC1 PE=1 SV=3	LAMC1_HUMAN	12	12	8	19	14
43	Transketolase OS=Homo sapiens GN=TKT PE=1 SV=3	TKT_HUMAN	3	6	4	8	18
44	Follistatin-related protein 1 OS=Homo sapiens GN=FSTL1 PE=1 SV=1	FSTL1_HUMAN	9	9	5	11	8
45	Alpha-2-HS-glycoprotein OS=Homo sapiens GN=AHSG PE=1 SV=1	FETUA_HUMAN	3	3	2	3	3
46	Alpha-actinin-1 OS=Homo sapiens GN=ACTN1 PE=1 SV=2	ACTN1_HUMAN	3	5	7	13	14
47	Elongation factor 1-alpha 1 OS=Homo sapiens GN=EEF1A1 PE=1 SV=1	EF1A1_HUMAN	6	3	2	6	10
48	Annexin A2 OS=Homo sapiens GN=ANXA2 PE=1 SV=2	ANXA2_HUMAN	3	5	6	15	11
49	Plasminogen activator inhibitor 1 OS=Homo sapiens GN=SERPINE1 PE=1 SV=1	PAI1_HUMAN	5	5	4	7	6
50	Laminin subunit beta-1 OS=Homo sapiens GN=LAMB1 PE=1 SV=2	LAMB1_HUMAN	11	4	2	14	14
51	Insulin-like growth factor-binding protein 6 OS=Homo sapiens GN=IGFBP6 PE=1 SV=1	IBP6_HUMAN	4	5	6	7	4
52	Tubulointerstitial nephritis antigen-like OS=Homo sapiens GN=TINAGL1 PE=1 SV=1	TINAL_HUMAN	10	6	7	7	7
53	Lactotransferrin OS=Homo sapiens GN=LTF PE=1 SV=6	TRFL_HUMAN	4	3	2	3	2
54	Heat shock protein HSP 90-beta OS=Homo sapiens GN=HSP90AB1 PE=1 SV=4	HS90B_HUMAN	0	3	4	13	13
55	Heat shock 70 kDa protein 1A/1B OS=Homo sapiens GN=HSPA1A PE=1 SV=5	HSP71_HUMAN	3	2	0	4	12
56	Alpha-2-macroglobulin OS=Homo sapiens GN=A2M PE=1 SV=3	A2MG_HUMAN	4	3	4	3	3
57	Fascin OS=Homo sapiens GN=FSCN1 PE=1 SV=3	FSCN1_HUMAN	4	5	4	8	13
58	Clusterin OS=Homo sapiens GN=CLU PE=1 SV=1	CLUS_HUMAN	7	3	4	10	8
59	Ubiquitin-like modifier-activating enzyme 1 OS=Homo sapiens GN=UBA1 PE=1 SV=3	UBA1_HUMAN	1	2	4	4	18
60	Gelsolin OS=Homo sapiens GN=GSN PE=1 SV=1	GELS_HUMAN	7	2	3	12	8
61	Proactivator polypeptide OS=Homo sapiens GN=PSAP PE=1 SV=2	SAP_HUMAN	11	2	0	5	5
62	Serglycin OS=Homo sapiens GN=SRGN PE=1 SV=3	SRGN_HUMAN	3	3	3	6	5
63	Transitional endoplasmic reticulum ATPase OS=Homo sapiens GN=VCP PE=1 SV=4	TERA_HUMAN	0	6	8	6	14
64	SPARC OS=Homo sapiens GN=SPARC PE=1 SV=1	SPRC_HUMAN	5	4	2	6	6
65	14-3-3 protein beta/alpha OS=Homo sapiens GN=YWHAB PE=1 SV=3	1433B_HUMAN	6	2	3	6	9
66	Tissue-type plasminogen activator OS=Homo sapiens GN=PLAT PE=1 SV=1	TPA_HUMAN	5	1	0	9	10

67	Peroxiredoxin-1 OS=Homo sapiens GN=PRDX1 PE=1 SV=1	PRDX1_HUMAN	7	2	4	7	5
68	Lysyl oxidase homolog 2 OS=Homo sapiens GN=LOXL2 PE=1 SV=1	LOXL2_HUMAN	7	1	0	10	5
69	Connective tissue growth factor OS=Homo sapiens GN=CTGF PE=1 SV=2	CTGF_HUMAN	9	3	3	6	4
70	L-lactate dehydrogenase B chain OS=Homo sapiens GN=LDHB PE=1 SV=2	LDHB_HUMAN	2	5	3	9	9
71	Collagen alpha-1(I) chain OS=Homo sapiens GN=COL1A1 PE=1 SV=5	CO1A1_HUMAN	0	2	2	0	1
72	Cadherin-2 OS=Homo sapiens GN=CDH2 PE=1 SV=4	CADH2_HUMAN	10	3	4	6	6
73	Plectin OS=Homo sapiens GN=PLEC PE=1 SV=3	PLEC_HUMAN	0	3	5	15	5
74	Adenosylhomocysteinase OS=Homo sapiens GN=AHCY PE=1 SV=4	SAHH_HUMAN	4	5	7	7	11
75	Amyloid beta A4 protein OS=Homo sapiens GN=APP PE=1 SV=3	A4_HUMAN	2	3	1	12	4
76	Glucose-6-phosphate isomerase OS=Homo sapiens GN=GPI PE=1 SV=4	G6PI_HUMAN	4	5	4	3	9
77	Gamma-glutamyl hydrolase OS=Homo sapiens GN=GGH PE=1 SV=2	GGH_HUMAN	5	2	3	4	3
78	Tubulin beta chain OS=Homo sapiens GN=TUBB PE=1 SV=2	TBB5_HUMAN	2	0	5	9	11
79	Galectin-1 OS=Homo sapiens GN=LGALS1 PE=1 SV=2	LEG1_HUMAN	6	0	4	5	6
80	Glutathione S-transferase P OS=Homo sapiens GN=GSTP1 PE=1 SV=2	GSTP1_HUMAN	5	5	4	6	6
81	CD166 antigen OS=Homo sapiens GN=ALCAM PE=1 SV=2	CD166_HUMAN	7	6	5	4	4
82	Fibulin-1 OS=Homo sapiens GN=FBLN1 PE=1 SV=4	FBLN1_HUMAN	3	3	4	7	7
83	78 kDa glucose-regulated protein OS=Homo sapiens GN=HSPA5 PE=1 SV=2	GRP78_HUMAN	0	4	8	13	4
84	Nidogen-1 OS=Homo sapiens GN=NID1 PE=1 SV=3	NID1_HUMAN	2	1	0	14	12
85	Chloride intracellular channel protein 1 OS=Homo sapiens GN=CLIC1 PE=1 SV=4	CLIC1_HUMAN	1	2	5	6	10
86	Thrombospondin-1 OS=Homo sapiens GN=THBS1 PE=1 SV=2	TSP1_HUMAN	0	1	0	11	10
87	Latent-transforming growth factor beta-binding protein 2 OS=Homo sapiens GN=LTBP2 PE=1 SV=3	LTBP2_HUMAN	8	2	0	6	4
88	Cystatin-C OS=Homo sapiens GN=CST3 PE=1 SV=1	CYTC_HUMAN	3	0	1	3	3
89	Nucleoside diphosphate kinase B OS=Homo sapiens GN=NME2 PE=1 SV=1	NDKB_HUMAN	5	0	0	7	5
90	Heat shock 70 kDa protein 4 OS=Homo sapiens GN=HSPA4 PE=1 SV=4	HSP74_HUMAN	3	1	2	7	7
91	Dickkopf-related protein 3 OS=Homo sapiens GN=DKK3 PE=1 SV=2	DKK3_HUMAN	2	3	2	5	7
92	Metalloproteinase inhibitor 2 OS=Homo sapiens GN=TIMP2 PE=1 SV=2	TIMP2_HUMAN	3	2	0	4	3
93	Protein disulfide-isomerase OS=Homo sapiens GN=P4HB PE=1 SV=3	PDIA1_HUMAN	0	3	2	8	7
94	Peptidyl-prolyl cis-trans isomerase B OS=Homo sapiens GN=PPIB PE=1 SV=2	PPIB_HUMAN	4	4	3	5	3
95	Ezrin OS=Homo sapiens GN=EZR PE=1 SV=4	EZRI_HUMAN	0	1	0	7	9
96	Carboxypeptidase A4 OS=Homo sapiens GN=CPA4 PE=1 SV=2	CBPA4_HUMAN	6	5	3	6	3
97	14-3-3 protein epsilon OS=Homo sapiens GN=YWHAE PE=1 SV=1	1433E_HUMAN	2	4	4	5	5
98	Tyrosine-protein kinase receptor UFO OS=Homo sapiens GN=AXL PE=1 SV=3	UFO_HUMAN	4	2	3	5	4
99	Histone H4 OS=Homo sapiens GN=HIST1H4A PE=1 SV=2	H4_HUMAN	2	0	3	4	4
100	Peroxiredoxin-2 OS=Homo sapiens GN=PRDX2 PE=1 SV=5	PRDX2_HUMAN	2	0	0	4	7
101	Keratin, type I cytoskeletal 18 OS=Homo sapiens GN=KRT18 PE=1 SV=2	K1C18_HUMAN	2	0	2	6	5
102	Collagen alpha-2(VI) chain OS=Homo sapiens GN=COL6A2 PE=1	CO6A2_HUMAN	3	1	1	9	6

	SV=4						
103	Elongation factor 1-gamma OS=Homo sapiens GN=EEF1G PE=1 SV=3	EF1G_HUMAN	5	3	0	5	7
104	Fatty acid-binding protein, epidermal OS=Homo sapiens GN=FABP5 PE=1 SV=3	FABP5_HUMAN	5	0	0	4	6
105	Keratin, type II cytoskeletal 8 OS=Homo sapiens GN=KRT8 PE=1 SV=7	K2C8_HUMAN	2	0	1	9	7
106	Histone H2B type 1-C/E/F/G/I OS=Homo sapiens GN=HIST1H2BC PE=1 SV=4	H2B1C_HUMAN	2	1	0	6	2
107	Alpha-fetoprotein OS=Homo sapiens GN=AFP PE=1 SV=1	FETA_HUMAN	2	2	2	2	0
108	CD44 antigen OS=Homo sapiens GN=CD44 PE=1 SV=3	CD44_HUMAN	2	3	1	3	5
109	Collagen alpha-2(V) chain OS=Homo sapiens GN=COL5A2 PE=1 SV=3	CO5A2_HUMAN	3	4	5	2	0
110	Collagen alpha-2(I) chain OS=Homo sapiens GN=COL1A2 PE=1 SV=7	CO1A2_HUMAN	0	2	2	3	3
111	Protein DJ-1 OS=Homo sapiens GN=PARK7 PE=1 SV=2	PARK7_HUMAN	5	0	1	6	6
112	Fibrillin-1 OS=Homo sapiens GN=FBN1 PE=1 SV=3	FBN1_HUMAN	2	0	0	13	5
113	Syndecan-4 OS=Homo sapiens GN=SDC4 PE=1 SV=2	SDC4_HUMAN	5	3	2	2	3
114	Coactosin-like protein OS=Homo sapiens GN=COTL1 PE=1 SV=3	COTL1_HUMAN	3	0	2	1	5
115	Protein CYR61 OS=Homo sapiens GN=CYR61 PE=1 SV=1	CYR61_HUMAN	4	4	2	1	3
116	Rab GDP dissociation inhibitor beta OS=Homo sapiens GN=GDI2 PE=1 SV=2	GDIB_HUMAN	1	2	3	3	8
117	Fatty acid synthase OS=Homo sapiens GN=FASN PE=1 SV=3	FAS_HUMAN	1	0	0	2	18
118	Eukaryotic initiation factor 4A-I OS=Homo sapiens GN=EIF4A1 PE=1 SV=1	IF4A1_HUMAN	0	0	0	5	11
119	Myosin-9 OS=Homo sapiens GN=MYH9 PE=1 SV=4	MYH9_HUMAN	0	1	5	3	7
120	Transaldolase OS=Homo sapiens GN=TALDO1 PE=1 SV=2	TALDO_HUMAN	1	3	3	6	2
121	Thioredoxin OS=Homo sapiens GN=TXN PE=1 SV=3	THIO_HUMAN	3	0	1	4	5
122	Clathrin heavy chain 1 OS=Homo sapiens GN=CLTC PE=1 SV=5	CLH1_HUMAN	0	1	3	3	7
123	MAM domain-containing protein 2 OS=Homo sapiens GN=MAMDC2 PE=2 SV=3	MAMC2_HUMAN	4	0	0	6	3
124	Cathepsin Z OS=Homo sapiens GN=CTSZ PE=1 SV=1	CATZ_HUMAN	3	2	3	4	2
125	Proliferating cell nuclear antigen OS=Homo sapiens GN=PCNA PE=1 SV=1	PCNA_HUMAN	4	0	1	8	2
126	Phosphatidylethanolamine-binding protein 1 OS=Homo sapiens GN=PEBP1 PE=1 SV=3	PEBP1_HUMAN	2	2	4	3	5
127	Heterogeneous nuclear ribonucleoproteins A2/B1 OS=Homo sapiens GN=HNRNPA2B1 PE=1 SV=2	ROA2_HUMAN	2	2	1	6	3
128	Metallothionein-1G OS=Homo sapiens GN=MT1G PE=1 SV=2	MT1G_HUMAN	1	1	2	1	3
129	Plastin-3 OS=Homo sapiens GN=PLS3 PE=1 SV=4	PLST_HUMAN	0	0	0	2	16
130	Dickkopf-related protein 1 OS=Homo sapiens GN=DKK1 PE=1 SV=1	DKK1_HUMAN	1	3	1	5	2
131	Macrophage migration inhibitory factor OS=Homo sapiens GN=MIF PE=1 SV=4	MIF_HUMAN	2	1	1	2	2
132	Transgelin-2 OS=Homo sapiens GN=TAGLN2 PE=1 SV=3	TAGL2_HUMAN	3	0	0	5	9
133	Hemoglobin subunit alpha OS=Homo sapiens GN=HBA1 PE=1 SV=2	HBA_HUMAN	3	0	0	2	3
134	Protein disulfide-isomerase A3 OS=Homo sapiens GN=PDIA3 PE=1 SV=4	PDIA3_HUMAN	0	3	2	8	2
135	Testican-1 OS=Homo sapiens GN=SPOCK1 PE=1 SV=1	TICN1_HUMAN	2	0	0	5	6
136	Neural cell adhesion molecule L1 OS=Homo sapiens GN=L1CAM PE=1 SV=2	L1CAM_HUMAN	2	4	3	1	2
137	Exportin-2 OS=Homo sapiens GN=CSE1L PE=1 SV=3	XPO2_HUMAN	0	0	0	1	6
138	Semaphorin-4B OS=Homo sapiens GN=SEMA4B PE=1 SV=3	SEM4B_HUMAN	3	2	1	4	1

139	Importin subunit beta-1 OS=Homo sapiens GN=KPNB1 PE=1 SV=2	IMB1_HUMAN	0	0	0	4	10
140	GTP-binding nuclear protein Ran OS=Homo sapiens GN=RAN PE=1 SV=3	RAN_HUMAN	1	1	3	1	4
141	Keratin, type II cytoskeletal 6A OS=Homo sapiens GN=KRT6A PE=1 SV=3	K2C6A_HUMAN	0	4	2	1	1
142	Glycogen phosphorylase, brain form OS=Homo sapiens GN=PYGB PE=1 SV=5	PYGB_HUMAN	0	0	1	3	10
143	Cathepsin D OS=Homo sapiens GN=CTSD PE=1 SV=1	CATD_HUMAN	6	5	0	0	0
144	WD repeat-containing protein 1 OS=Homo sapiens GN=WDR1 PE=1 SV=4	WDR1_HUMAN	3	1	0	1	5
145	Amyloid-like protein 2 OS=Homo sapiens GN=APLP2 PE=1 SV=2	APLP2_HUMAN	0	0	1	4	3
146	Puromycin-sensitive aminopeptidase OS=Homo sapiens GN=NPEPPS PE=1 SV=2	PSA_HUMAN	0	0	2	3	9
147	Histone H2A type 1-D OS=Homo sapiens GN=HIST1H2AD PE=1 SV=2	H2A1D_HUMAN	1	2	3	2	2
148	Histone H3.1t OS=Homo sapiens GN=HIST3H3 PE=1 SV=3	H31T_HUMAN	1	0	0	3	2
149	Neutral alpha-glucosidase AB OS=Homo sapiens GN=GANAB PE=1 SV=3	GANAB_HUMAN	3	1	1	1	0
150	Exostosin-1 OS=Homo sapiens GN=EXT1 PE=1 SV=2	EXT1_HUMAN	2	2	2	2	2
151	Attractin OS=Homo sapiens GN=ATRN PE=1 SV=2	ATRN_HUMAN	4	2	3	2	1
152	Inter-alpha-trypsin inhibitor heavy chain H2 OS=Homo sapiens GN=ITIH2 PE=1 SV=2	ITIH2_HUMAN	3	2	3	1	0
153	Serotransferrin OS=Homo sapiens GN=TF PE=1 SV=3	TRFE_HUMAN	1	0	2	2	0
154	40S ribosomal protein S12 OS=Homo sapiens GN=RPS12 PE=1 SV=3	RS12_HUMAN	2	0	0	3	4
155	Dystroglycan OS=Homo sapiens GN=DAG1 PE=1 SV=2	DAG1_HUMAN	2	1	3	3	1
156	60S ribosomal protein L12 OS=Homo sapiens GN=RPL12 PE=1 SV=1	RL12_HUMAN	2	1	1	3	3
157	Annexin A3 OS=Homo sapiens GN=ANXA3 PE=1 SV=3	ANXA3_HUMAN	0	3	7	0	0
158	Malate dehydrogenase, cytoplasmic OS=Homo sapiens GN=MDH1 PE=1 SV=4	MDHC_HUMAN	3	1	0	3	3
159	Exostosin-2 OS=Homo sapiens GN=EXT2 PE=1 SV=1	EXT2_HUMAN	0	1	1	5	3
160	Cathepsin B OS=Homo sapiens GN=CTSB PE=1 SV=3	CATB_HUMAN	3	2	0	1	0
161	Procollagen-lysine,2-oxoglutarate 5-dioxygenase 1 OS=Homo sapiens GN=PLOD1 PE=1 SV=2	PLOD1_HUMAN	0	1	1	5	4
162	Rho GDP-dissociation inhibitor 1 OS=Homo sapiens GN=ARHGDIA PE=1 SV=3	GDIR1_HUMAN	1	0	0	3	3
163	Heterogeneous nuclear ribonucleoprotein A1 OS=Homo sapiens GN=HNRNPA1 PE=1 SV=5	ROA1_HUMAN	1	0	0	5	3
164	Aspartate aminotransferase, mitochondrial OS=Homo sapiens GN=GOT2 PE=1 SV=3	AATM_HUMAN	1	4	4	0	0
165	Agrin OS=Homo sapiens GN=AGRN PE=1 SV=4	AGRIN_HUMAN	6	0	0	0	0
166	Fructose-bisphosphate aldolase C OS=Homo sapiens GN=ALDOC PE=1 SV=2	ALDOC_HUMAN	2	1	2	2	2
167	Epididymal secretory protein E1 OS=Homo sapiens GN=NPC2 PE=1 SV=1	NPC2_HUMAN	3	1	1	1	2
168	Malate dehydrogenase, mitochondrial OS=Homo sapiens GN=MDH2 PE=1 SV=3	MDHM_HUMAN	2	6	4	1	0
169	Non-histone chromosomal protein HMG-17 OS=Homo sapiens GN=HMGN2 PE=1 SV=3	HMGN2_HUMAN	1	0	1	1	2
170	Alpha-1-antitrypsin OS=Homo sapiens GN=SERPINA1 PE=1 SV=3	A1AT_HUMAN	2	1	0	2	0
171	Laminin subunit beta-3 OS=Homo sapiens GN=LAMB3 PE=1 SV=1	LAMB3_HUMAN	3	0	0	3	4
172	Actin-related protein 2/3 complex subunit 4 OS=Homo sapiens GN=ARPC4 PE=1 SV=3	ARPC4_HUMAN	0	0	1	5	4

173	Prelamin-A/C OS=Homo sapiens GN=LMNA PE=1 SV=1	LMNA_HUMAN	0	0	0	8	1
174	Hornerin OS=Homo sapiens GN=HRNR PE=1 SV=2	HORN_HUMAN	0	3	3	0	0
175	Peptidyl-prolyl cis-trans isomerase FKBP1A OS=Homo sapiens GN=FKBP1A PE=1 SV=2	FKB1A_HUMAN	2	1	1	1	2
176	Thioredoxin domain-containing protein 17 OS=Homo sapiens GN=TXNDC17 PE=1 SV=1	TXD17_HUMAN	2	0	2	2	4
177	Protein-glutamine gamma-glutamyltransferase 2 OS=Homo sapiens GN=TGM2 PE=1 SV=2	TGM2_HUMAN	0	0	2	5	3
178	Keratin, type II cytoskeletal 5 OS=Homo sapiens GN=KRT5 PE=1 SV=3	K2C5_HUMAN	0	3	2	0	0
179	Stathmin OS=Homo sapiens GN=STMN1 PE=1 SV=3	STMN1_HUMAN	2	0	0	2	4
180	Granulins OS=Homo sapiens GN=GRN PE=1 SV=2	GRN_HUMAN	5	1	0	1	1
181	Ribonuclease inhibitor OS=Homo sapiens GN=RNH1 PE=1 SV=2	RINI_HUMAN	0	1	1	3	3
182	4F2 cell-surface antigen heavy chain OS=Homo sapiens GN=SLC3A2 PE=1 SV=3	4F2_HUMAN	6	0	1	1	0
183	Importin-5 OS=Homo sapiens GN=IPO5 PE=1 SV=4	IPO5_HUMAN	0	0	2	3	2
184	Proteasome subunit alpha type-6 OS=Homo sapiens GN=PSMA6 PE=1 SV=1	PSA6_HUMAN	2	1	1	4	3
185	Proteasome subunit alpha type-7 OS=Homo sapiens GN=PSMA7 PE=1 SV=1	PSA7_HUMAN	2	0	2	3	2
186	Procollagen-lysine,2-oxoglutarate 5-dioxygenase 2 OS=Homo sapiens GN=PLOD2 PE=1 SV=2	PLOD2_HUMAN	3	1	0	3	2
187	Endoplasmin OS=Homo sapiens GN=HSP90B1 PE=1 SV=1	ENPL_HUMAN	0	1	2	5	0
188	Stress-induced-phosphoprotein 1 OS=Homo sapiens GN=STIP1 PE=1 SV=1	STIP1_HUMAN	1	0	0	1	5
189	Ubiquitin-like protein ISG15 OS=Homo sapiens GN=ISG15 PE=1 SV=5	ISG15_HUMAN	1	0	0	1	3
190	Biotinidase OS=Homo sapiens GN=BTD PE=1 SV=2	BTD_HUMAN	1	3	1	1	2
191	Lactoylglutathione lyase OS=Homo sapiens GN=GLO1 PE=1 SV=4	LGUL_HUMAN	1	0	1	1	3
192	Inactive tyrosine-protein kinase 7 OS=Homo sapiens GN=PTK7 PE=1 SV=2	PTK7_HUMAN	4	2	1	1	0
193	Ras GTPase-activating-like protein IQGAP1 OS=Homo sapiens GN=IQGAP1 PE=1 SV=1	IQGA1_HUMAN	1	1	0	1	4
194	Eukaryotic translation initiation factor 5A-1 OS=Homo sapiens GN=EIF5A PE=1 SV=2	IF5A1_HUMAN	1	0	0	2	4
195	Eukaryotic translation initiation factor 6 OS=Homo sapiens GN=EIF6 PE=1 SV=1	IF6_HUMAN	2	0	0	4	2
196	Keratin, type I cytoskeletal 14 OS=Homo sapiens GN=KRT14 PE=1 SV=4	K1C14_HUMAN	0	3	2	1	0
197	Translationally-controlled tumor protein OS=Homo sapiens GN=TPT1 PE=1 SV=1	TCTP_HUMAN	2	0	0	1	0
198	Poliovirus receptor OS=Homo sapiens GN=PVR PE=1 SV=2	PVR_HUMAN	1	1	2	2	2
199	Proteasome subunit alpha type-2 OS=Homo sapiens GN=PSMA2 PE=1 SV=2	PSA2_HUMAN	2	0	0	1	1
200	Deoxyuridine 5'-triphosphate nucleotidohydrolase, mitochondrial OS=Homo sapiens GN=DUT PE=1 SV=4	DUT_HUMAN	2	0	1	2	3
201	SH3 domain-binding glutamic acid-rich-like protein 3 OS=Homo sapiens GN=SH3BGRL3 PE=1 SV=1	SH3L3_HUMAN	2	0	1	1	3
202	60S ribosomal protein L10a OS=Homo sapiens GN=RPL10A PE=1 SV=2	RL10A_HUMAN	1	0	0	5	2
203	Phosphoribosylformylglycinamidine synthase OS=Homo sapiens GN=PFAS PE=1 SV=4	PUR4_HUMAN	0	0	0	0	7
204	Semaphorin-7A OS=Homo sapiens GN=SEMA7A PE=1 SV=1	SEM7A_HUMAN	3	1	1	2	1
205	Glucosidase 2 subunit beta OS=Homo sapiens GN=PRKCSH PE=1 SV=2	GLU2B_HUMAN	1	2	1	1	2

206	Protein disulfide-isomerase A6 OS=Homo sapiens GN=PDIA6 PE=1 SV=1	PDIA6_HUMAN	0	2	2	3	1
207	Peroxiredoxin-6 OS=Homo sapiens GN=PRDX6 PE=1 SV=3	PRDX6_HUMAN	3	0	0	2	2
208	Superoxide dismutase [Cu-Zn] OS=Homo sapiens GN=SOD1 PE=1 SV=2	SODC_HUMAN	0	1	2	0	1
209	Plasminogen activator inhibitor 1 RNA-binding protein OS=Homo sapiens GN=SERBP1 PE=1 SV=2	PAIRB_HUMAN	2	0	0	1	1
210	Metastasis-suppressor KiSS-1 OS=Homo sapiens GN=KISS1 PE=1 SV=4	KISS1_HUMAN	0	0	0	3	2
211	Signal-regulatory protein beta-1 OS=Homo sapiens GN=SIRPB1 PE=1 SV=5	SIRB1_HUMAN	0	0	2	0	0
212	Beta-hexosaminidase subunit alpha OS=Homo sapiens GN=HEXA PE=1 SV=2	HEXA_HUMAN	5	2	0	0	0
213	Xaa-Pro dipeptidase OS=Homo sapiens GN=PEPD PE=1 SV=3	PEPD_HUMAN	3	2	2	1	2
214	Inter-alpha-trypsin inhibitor heavy chain H4 OS=Homo sapiens GN=ITIH4 PE=1 SV=4	ITIH4_HUMAN	1	1	2	1	0
215	Glutathione synthetase OS=Homo sapiens GN=GSS PE=1 SV=1	GSHB_HUMAN	2	0	0	1	2
216	Collagen alpha-1(XII) chain OS=Homo sapiens GN=COL12A1 PE=1 SV=2	COCA1_HUMAN	3	3	1	0	0
217	Lysosomal Pro-X carboxypeptidase OS=Homo sapiens GN=PRCP PE=1 SV=1	PCP_HUMAN	4	0	0	0	1
218	10 kDa heat shock protein, mitochondrial OS=Homo sapiens GN=HSPE1 PE=1 SV=2	CH10_HUMAN	2	0	0	3	2
219	14-3-3 protein gamma OS=Homo sapiens GN=YWHAG PE=1 SV=2	1433G_HUMAN	3	0	0	3	1
220	Proteasome subunit alpha type-4 OS=Homo sapiens GN=PSMA4 PE=1 SV=1	PSA4_HUMAN	1	1	1	3	1
221	Protein S100-A6 OS=Homo sapiens GN=S100A6 PE=1 SV=1	S10A6_HUMAN	0	1	0	2	1
222	Aspartate aminotransferase, cytoplasmic OS=Homo sapiens GN=GOT1 PE=1 SV=3	AATC_HUMAN	0	3	3	1	1
223	Soluble calcium-activated nucleotidase 1 OS=Homo sapiens GN=CANT1 PE=1 SV=1	CANT1_HUMAN	2	1	1	4	0
224	NKG2D ligand 2 OS=Homo sapiens GN=ULBP2 PE=1 SV=1	N2DL2_HUMAN	2	0	1	1	1
225	Ubiquitin-conjugating enzyme E2 N OS=Homo sapiens GN=UBE2N PE=1 SV=1	UBE2N_HUMAN	2	0	0	3	3
226	Tubulin-specific chaperone A OS=Homo sapiens GN=TBCA PE=1 SV=3	TBCA_HUMAN	1	0	0	3	3
227	Proteasome subunit beta type-6 OS=Homo sapiens GN=PSMB6 PE=1 SV=4	PSB6_HUMAN	2	0	0	2	1
228	Cellular nucleic acid-binding protein OS=Homo sapiens GN=CNBP PE=1 SV=1	CNBP_HUMAN	1	0	0	1	4
229	Threonine--tRNA ligase, cytoplasmic OS=Homo sapiens GN=TARS PE=1 SV=3	SYTC_HUMAN	0	0	1	0	6
230	Proteasome subunit alpha type-1 OS=Homo sapiens GN=PSMA1 PE=1 SV=1	PSA1_HUMAN	0	0	2	4	0
231	6-phosphogluconolactonase OS=Homo sapiens GN=PGLS PE=1 SV=2	6PGL_HUMAN	2	0	1	1	1
232	Beta-enolase OS=Homo sapiens GN=ENO3 PE=1 SV=5	ENOB_HUMAN	1	0	1	1	2
233	Stanniocalcin-2 OS=Homo sapiens GN=STC2 PE=1 SV=1	STC2_HUMAN	0	1	0	4	1
234	Elongation factor 1-delta OS=Homo sapiens GN=EEF1D PE=1 SV=5	EF1D_HUMAN	0	0	0	3	0
235	Thyroxine-binding globulin OS=Homo sapiens GN=SERPINA7 PE=1 SV=2	THBG_HUMAN	0	0	0	2	2
236	Nucleobindin-1 OS=Homo sapiens GN=NUCB1 PE=1 SV=4	NUCB1_HUMAN	0	0	0	0	2
237	Proteasome subunit alpha type-5 OS=Homo sapiens GN=PSMA5 PE=1 SV=3	PSA5_HUMAN	3	0	0	2	1
238	Ubiquitin-conjugating enzyme E2 variant 1 OS=Homo sapiens GN=UBE2V1 PE=1 SV=2	UB2V1_HUMAN	0	0	0	0	2

239	ATP synthase subunit beta, mitochondrial OS=Homo sapiens GN=ATP5B PE=1 SV=3	ATPB_HUMAN	0	2	4	0	0
240	Cysteine-rich protein 1 OS=Homo sapiens GN=CRIP1 PE=1 SV=3	CRIP1_HUMAN	0	0	0	1	2
241	Dipeptidyl peptidase 3 OS=Homo sapiens GN=DPP3 PE=1 SV=2	DPP3_HUMAN	0	1	1	1	2
242	Pigment epithelium-derived factor OS=Homo sapiens GN=SERPINF1 PE=1 SV=4	PEDF_HUMAN	1	3	1	2	0
243	Talin-1 OS=Homo sapiens GN=TLN1 PE=1 SV=3	TLN1_HUMAN	0	1	2	0	3
244	SH3 domain-binding glutamic acid-rich-like protein OS=Homo sapiens GN=SH3BGRL PE=1 SV=1	SH3L1_HUMAN	1	0	1	1	4
245	T-complex protein 1 subunit beta OS=Homo sapiens GN=CCT2 PE=1 SV=4	TCPB_HUMAN	0	0	0	2	1
246	Collagen alpha-2(IV) chain OS=Homo sapiens GN=COL4A2 PE=1 SV=4	CO4A2_HUMAN	0	1	0	3	0
247	Filamin-C OS=Homo sapiens GN=FLNC PE=1 SV=3	FLNC_HUMAN	0	1	2	0	2
248	Annexin A1 OS=Homo sapiens GN=ANXA1 PE=1 SV=2	ANXA1_HUMAN	0	0	0	3	2
249	Lysosomal protective protein OS=Homo sapiens GN=CTSA PE=1 SV=2	PPGB_HUMAN	4	0	1	1	0
250	Tropomyosin alpha-4 chain OS=Homo sapiens GN=TPM4 PE=1 SV=3	TPM4_HUMAN	0	0	0	2	1
251	Vitamin D-binding protein OS=Homo sapiens GN=GC PE=1 SV=1	VTDB_HUMAN	3	0	0	1	0
252	Actin-related protein 3 OS=Homo sapiens GN=ACTR3 PE=1 SV=3	ARP3_HUMAN	0	0	0	2	5
253	Serine/threonine-protein phosphatase 2A 65 kDa regulatory subunit A alpha isoform OS=Homo sapiens GN=PPP2R1A PE=1 SV=4	2AAA_HUMAN	0	0	0	0	6
254	Collagen alpha-1(XVIII) chain OS=Homo sapiens GN=COL18A1 PE=1 SV=5	COIA1_HUMAN	4	0	0	0	0
255	Heterogeneous nuclear ribonucleoprotein D0 OS=Homo sapiens GN=HNRNPD PE=1 SV=1	HNRPD_HUMAN	1	1	1	2	2
256	Small ubiquitin-related modifier 2 OS=Homo sapiens GN=SUMO2 PE=1 SV=3	SUMO2_HUMAN	1	1	1	1	2
257	Hypoxanthine-guanine phosphoribosyltransferase OS=Homo sapiens GN=HPRT1 PE=1 SV=2	HPRT_HUMAN	2	0	1	1	1
258	Apolipoprotein E OS=Homo sapiens GN=APOE PE=1 SV=1	APOE_HUMAN	0	1	0	2	1
259	Nucleophosmin OS=Homo sapiens GN=NPM1 PE=1 SV=2	NPM_HUMAN	0	1	0	2	1
260	Cysteine-rich motor neuron 1 protein OS=Homo sapiens GN=CRIM1 PE=1 SV=1	CRIM1_HUMAN	2	0	4	0	0
261	Growth-regulated alpha protein OS=Homo sapiens GN=CXCL1 PE=1 SV=1	GROA_HUMAN	1	0	0	2	2
262	Annexin A5 OS=Homo sapiens GN=ANXA5 PE=1 SV=2	ANXA5_HUMAN	0	0	2	2	1
263	6-phosphogluconate dehydrogenase, decarboxylating OS=Homo sapiens GN=PGD PE=1 SV=3	6PGD_HUMAN	0	1	0	1	4
264	Hepatocyte growth factor receptor OS=Homo sapiens GN=MET PE=1 SV=4	MET_HUMAN	4	1	0	0	0
265	Receptor-type tyrosine-protein phosphatase F OS=Homo sapiens GN=PTPRF PE=1 SV=2	PTPRF_HUMAN	1	0	0	3	0
266	Protein S100-A11 OS=Homo sapiens GN=S100A11 PE=1 SV=2	S10AB_HUMAN	2	0	0	1	1
267	Ras-related protein Rab-7a OS=Homo sapiens GN=RAB7A PE=1 SV=1	RAB7A_HUMAN	1	0	0	1	3
268	Histidine triad nucleotide-binding protein 1 OS=Homo sapiens GN=HINT1 PE=1 SV=2	HINT1_HUMAN	0	0	0	2	3
269	Follistatin OS=Homo sapiens GN=FST PE=1 SV=2	FST_HUMAN	0	0	0	5	0
270	Procollagen-lysine,2-oxoglutarate 5-dioxygenase 3 OS=Homo sapiens GN=PLOD3 PE=1 SV=1	PLOD3_HUMAN	0	1	2	1	0
271	Transferrin receptor protein 1 OS=Homo sapiens GN=TFRC PE=1 SV=2	TFR1_HUMAN	2	0	1	1	1
272	14-3-3 protein theta OS=Homo sapiens GN=YWHAQ PE=1 SV=1	1433T_HUMAN	1	0	1	2	1

273	Calreticulin OS=Homo sapiens GN=CALR PE=1 SV=1	CALR_HUMAN	0	1	0	2	2
274	Endothelial protein C receptor OS=Homo sapiens GN=PROCR PE=1 SV=1	EPCR_HUMAN	3	1	0	1	0
275	Legumain OS=Homo sapiens GN=LGMN PE=1 SV=1	LGMN_HUMAN	1	0	0	2	2
276	Desmocollin-3 OS=Homo sapiens GN=DSC3 PE=1 SV=3	DSC3_HUMAN	3	0	1	1	0
277	Heat shock protein 105 kDa OS=Homo sapiens GN=HSPH1 PE=1 SV=1	HS105_HUMAN	0	0	0	3	2
278	Histone-binding protein RBBP4 OS=Homo sapiens GN=RBBP4 PE=1 SV=3	RBBP4_HUMAN	0	0	0	1	2
279	Adenylyl cyclase-associated protein 1 OS=Homo sapiens GN=CAP1 PE=1 SV=5	CAP1_HUMAN	0	0	0	1	4
280	Fibroblast growth factor-binding protein 1 OS=Homo sapiens GN=FGFBP1 PE=1 SV=1	FGFP1_HUMAN	3	0	0	1	0
281	Heat shock protein beta-1 OS=Homo sapiens GN=HSPB1 PE=1 SV=2	HSPB1_HUMAN	2	0	0	3	0
282	Basement membrane-specific heparan sulfate proteoglycan core protein OS=Homo sapiens GN=HSPG2 PE=1 SV=4	PGBM_HUMAN	4	0	0	0	0
283	Collagen alpha-1(IV) chain OS=Homo sapiens GN=COL4A1 PE=1 SV=3	CO4A1_HUMAN	0	1	1	2	1
284	Inositol monophosphatase 1 OS=Homo sapiens GN=IMPA1 PE=1 SV=1	IMPA1_HUMAN	1	0	2	1	1
285	Macrophage-capping protein OS=Homo sapiens GN=CAPG PE=1 SV=2	CAPG_HUMAN	1	0	0	1	2
286	Insulin-like growth factor II OS=Homo sapiens GN=IGF2 PE=1 SV=1	IGF2_HUMAN	1	0	0	1	2
287	Tubulin beta-4B chain OS=Homo sapiens GN=TUBB4B PE=1 SV=1	TBB4B_HUMAN	1	0	0	3	2
288	Ras-related protein Rab-1A OS=Homo sapiens GN=RAB1A PE=1 SV=3	RAB1A_HUMAN	1	0	1	0	3
289	40S ribosomal protein S5 OS=Homo sapiens GN=RPS5 PE=1 SV=4	RS5_HUMAN	1	0	0	1	2
290	Proprotein convertase subtilisin/kexin type 9 OS=Homo sapiens GN=PCSK9 PE=1 SV=3	PCSK9_HUMAN	0	0	0	1	3
291	Dipeptidyl peptidase 1 OS=Homo sapiens GN=CTSC PE=1 SV=2	CATC_HUMAN	2	1	0	0	0
292	Proteasome subunit alpha type-3 OS=Homo sapiens GN=PSMA3 PE=1 SV=2	PSA3_HUMAN	0	0	0	2	2
293	Actin-related protein 2/3 complex subunit 3 OS=Homo sapiens GN=ARPC3 PE=1 SV=3	ARPC3_HUMAN	0	0	0	1	2
294	Serpin H1 OS=Homo sapiens GN=SERPINH1 PE=1 SV=2	SERPH_HUMAN	0	0	0	3	1
295	Carbonyl reductase [NADPH] 1 OS=Homo sapiens GN=CBR1 PE=1 SV=3	CBR1_HUMAN	0	0	1	2	1
296	F-actin-capping protein subunit alpha-1 OS=Homo sapiens GN=CAPZA1 PE=1 SV=3	CAZA1_HUMAN	0	0	1	2	1
297	DNA-(apurinic or apyrimidinic site) lyase OS=Homo sapiens GN=APEX1 PE=1 SV=2	APEX1_HUMAN	0	0	1	2	2
298	Multiple inositol polyphosphate phosphatase 1 OS=Homo sapiens GN=MINPP1 PE=1 SV=1	MINP1_HUMAN	2	1	1	0	0
299	Guanine nucleotide-binding protein subunit beta-2-like 1 OS=Homo sapiens GN=GNB2L1 PE=1 SV=3	GBLP_HUMAN	1	0	1	2	0
300	Endoplasmic reticulum aminopeptidase 1 OS=Homo sapiens GN=ERAP1 PE=1 SV=3	ERAP1_HUMAN	0	0	0	2	0
301	40S ribosomal protein S28 OS=Homo sapiens GN=RPS28 PE=1 SV=1	RS28_HUMAN	1	0	0	1	2
302	Glypican-1 OS=Homo sapiens GN=GPC1 PE=1 SV=2	GPC1_HUMAN	3	0	0	1	0
303	Keratin, type II cytoskeletal 1b OS=Homo sapiens GN=KRT77 PE=1 SV=3	K2C1B_HUMAN	0	1	2	0	0
304	Vascular endothelial growth factor C OS=Homo sapiens GN=VEGFC PE=1 SV=1	VEGFC_HUMAN	3	0	0	0	0
305	Renin receptor OS=Homo sapiens GN=ATP6AP2 PE=1 SV=2	RENR_HUMAN	3	0	0	2	0

306	Tumor necrosis factor receptor superfamily member 6B OS=Homo sapiens GN=TNFRSF6B PE=1 SV=1	TNF6B_HUMAN	2	0	0	3	0
307	Glutamate dehydrogenase 1, mitochondrial OS=Homo sapiens GN=GLUD1 PE=1 SV=2	DHE3_HUMAN	0	0	3	0	0
308	Endoplasmic reticulum resident protein 29 OS=Homo sapiens GN=ERP29 PE=1 SV=4	ERP29_HUMAN	0	0	1	2	0
309	40S ribosomal protein S3 OS=Homo sapiens GN=RPS3 PE=1 SV=2	RS3_HUMAN	4	0	0	0	0
310	Integrin beta-1 OS=Homo sapiens GN=ITGB1 PE=1 SV=2	ITB1_HUMAN	0	1	1	0	2
311	Beta-hexosaminidase subunit beta OS=Homo sapiens GN=HEXB PE=1 SV=3	HEXB_HUMAN	2	1	0	0	2
312	Destrin OS=Homo sapiens GN=DSTN PE=1 SV=3	DEST_HUMAN	1	0	0	1	2
313	Thioredoxin domain-containing protein 5 OS=Homo sapiens GN=TXNDC5 PE=1 SV=2	TXND5_HUMAN	0	0	1	2	0
314	Protein disulfide-isomerase A4 OS=Homo sapiens GN=PDIA4 PE=1 SV=2	PDIA4_HUMAN	0	1	0	2	0
315	C-1-tetrahydrofolate synthase, cytoplasmic OS=Homo sapiens GN=MTHFD1 PE=1 SV=3	C1TC_HUMAN	0	0	0	1	2
316	Glyoxalase domain-containing protein 4 OS=Homo sapiens GN=GLOD4 PE=1 SV=1	GLOD4_HUMAN	0	1	3	0	0
317	ATP-citrate synthase OS=Homo sapiens GN=ACLY PE=1 SV=3	ACLY_HUMAN	0	0	0	0	2
318	D-dopachrome decarboxylase OS=Homo sapiens GN=DDT PE=1 SV=3	DOPD_HUMAN	1	0	0	0	3
319	Transgelin OS=Homo sapiens GN=TAGLN PE=1 SV=4	TAGL_HUMAN	1	0	0	0	2
320	PDZ and LIM domain protein 1 OS=Homo sapiens GN=PDLIM1 PE=1 SV=4	PDLI1_HUMAN	1	0	0	0	2
321	14-3-3 protein sigma OS=Homo sapiens GN=SFN PE=1 SV=1	1433S_HUMAN	0	0	0	2	1
322	Peroxiredoxin-5, mitochondrial OS=Homo sapiens GN=PRDX5 PE=1 SV=4	PRDX5_HUMAN	0	0	0	0	3
323	40S ribosomal protein S18 OS=Homo sapiens GN=RPS18 PE=1 SV=3	RS18_HUMAN	0	0	0	0	3
324	Lysine--tRNA ligase OS=Homo sapiens GN=KARS PE=1 SV=3	SYK_HUMAN	0	0	0	0	2
325	Protein SET OS=Homo sapiens GN=SET PE=1 SV=3	SET_HUMAN	0	0	0	3	0
326	Phosphoserine aminotransferase OS=Homo sapiens GN=PSAT1 PE=1 SV=2	SERC_HUMAN	0	2	1	0	1
327	T-complex protein 1 subunit eta OS=Homo sapiens GN=CCT7 PE=1 SV=2	TCPH_HUMAN	0	1	0	2	1
328	Protein jagged-1 OS=Homo sapiens GN=JAG1 PE=1 SV=3	JAG1_HUMAN	1	0	0	1	2
329	N-acetyllactosaminide beta-1,3-N-acetylglucosaminyltransferase OS=Homo sapiens GN=B3GNT1 PE=1 SV=1	B3GN1_HUMAN	0	0	0	1	2
330	Palmitoyl-protein thioesterase 1 OS=Homo sapiens GN=PPT1 PE=1 SV=1	PPT1_HUMAN	2	0	0	1	0
331	Chloride intracellular channel protein 4 OS=Homo sapiens GN=CLIC4 PE=1 SV=4	CLIC4_HUMAN	0	0	0	2	3
332	Lysosome-associated membrane glycoprotein 1 OS=Homo sapiens GN=LAMP1 PE=1 SV=3	LAMP1_HUMAN	0	2	2	0	0
333	60S ribosomal protein L11 OS=Homo sapiens GN=RPL11 PE=1 SV=2	RL11_HUMAN	0	0	0	1	2
334	UMP-CMP kinase OS=Homo sapiens GN=CMPK1 PE=1 SV=3	KCY_HUMAN	0	0	0	1	2
335	Ubiquitin-conjugating enzyme E2 D3 OS=Homo sapiens GN=UBE2D3 PE=1 SV=1	UB2D3_HUMAN	0	0	0	1	2
336	Importin-7 OS=Homo sapiens GN=IPO7 PE=1 SV=1	IPO7_HUMAN	0	0	0	0	2
337	Beta-galactosidase OS=Homo sapiens GN=GLB1 PE=1 SV=2	BGAL_HUMAN	2	0	0	0	0
338	G-protein coupled receptor 126 OS=Homo sapiens GN=GPR126 PE=1 SV=3	GP126_HUMAN	2	0	0	0	0
339	Calsyntenin-3 OS=Homo sapiens GN=CLSTN3 PE=1 SV=1	CSTN3_HUMAN	3	0	0	0	0

340	Cochlin OS=Homo sapiens GN=COCH PE=1 SV=1	COCH_HUMAN	0	0	0	1	2
341	Ras-related C3 botulinum toxin substrate 1 OS=Homo sapiens GN=RAC1 PE=1 SV=1	RAC1_HUMAN	1	0	0	0	2
342	RNA-binding motif protein, X chromosome OS=Homo sapiens GN=RBMX PE=1 SV=3	RBMX_HUMAN	2	0	0	2	0
343	Serpin B5 OS=Homo sapiens GN=SERPINB5 PE=1 SV=2	SPB5_HUMAN	0	0	0	2	1
344	Signal recognition particle 9 kDa protein OS=Homo sapiens GN=SRP9 PE=1 SV=2	SRP09_HUMAN	1	0	0	0	2
345	Low molecular weight phosphotyrosine protein phosphatase OS=Homo sapiens GN=ACP1 PE=1 SV=3	PPAC_HUMAN	0	0	0	1	2
346	40S ribosomal protein S8 OS=Homo sapiens GN=RPS8 PE=1 SV=2	RS8_HUMAN	2	0	0	1	0
347	CD109 antigen OS=Homo sapiens GN=CD109 PE=1 SV=2	CD109_HUMAN	0	0	0	2	1
348	40S ribosomal protein S11 OS=Homo sapiens GN=RPS11 PE=1 SV=3	RS11_HUMAN	0	0	0	0	4
349	40S ribosomal protein S19 OS=Homo sapiens GN=RPS19 PE=1 SV=2	RS19_HUMAN	0	0	0	0	3
350	ATP-dependent RNA helicase DDX39A OS=Homo sapiens GN=DDX39A PE=1 SV=2	DX39A_HUMAN	0	0	0	0	2
351	Proliferation-associated protein 2G4 OS=Homo sapiens GN=PA2G4 PE=1 SV=3	PA2G4_HUMAN	0	0	0	2	0
352	Bifunctional purine biosynthesis protein PURH OS=Homo sapiens GN=ATIC PE=1 SV=3	PUR9_HUMAN	0	0	0	0	2
353	NEDD8 OS=Homo sapiens GN=NEDD8 PE=1 SV=1	NEDD8_HUMAN	0	0	0	0	2
354	ATP-binding cassette sub-family E member 1 OS=Homo sapiens GN=ABCE1 PE=1 SV=1	ABCE1_HUMAN	0	0	0	0	2
355	Alpha-galactosidase A OS=Homo sapiens GN=GLA PE=1 SV=1	AGAL_HUMAN	1	0	0	3	0
356	Purine nucleoside phosphorylase OS=Homo sapiens GN=PNP PE=1 SV=2	PNPH_HUMAN	1	0	0	2	0
357	Ras-related protein R-Ras2 OS=Homo sapiens GN=RRAS2 PE=1 SV=1	RRAS2_HUMAN	1	0	0	0	2
358	Alcohol dehydrogenase [NADP(+)] OS=Homo sapiens GN=AKR1A1 PE=1 SV=3	AK1A1_HUMAN	0	0	0	2	1
359	Inorganic pyrophosphatase OS=Homo sapiens GN=PPA1 PE=1 SV=2	IPYR_HUMAN	0	0	0	2	0
360	Cysteine-rich protein 2 OS=Homo sapiens GN=CRIP2 PE=1 SV=1	CRIP2_HUMAN	0	0	0	0	2
361	Glycogen phosphorylase, liver form OS=Homo sapiens GN=PYGL PE=1 SV=4	PYGL_HUMAN	0	0	0	0	3
362	Chromobox protein homolog 3 OS=Homo sapiens GN=CBX3 PE=1 SV=4	CBX3_HUMAN	0	0	0	2	0
363	MUC5A_HUMAN-R	MUC5A_HUMAN-R	0	0	0	0	2
364	Pterin-4-alpha-carbinolamine dehydratase OS=Homo sapiens GN=PCBD1 PE=1 SV=2	PHS_HUMAN	0	0	0	0	2
365	60S ribosomal protein L22 OS=Homo sapiens GN=RPL22 PE=1 SV=2	RL22_HUMAN	0	0	0	0	2
366	40S ribosomal protein S20 OS=Homo sapiens GN=RPS20 PE=1 SV=1	RS20_HUMAN	0	0	0	0	2
367	Acylamino-acid-releasing enzyme OS=Homo sapiens GN=APEH PE=1 SV=4	ACPH_HUMAN	0	0	0	2	0
368	CD70 antigen OS=Homo sapiens GN=CD70 PE=1 SV=2	CD70_HUMAN	0	0	0	2	0
369	Protein canopy homolog 2 OS=Homo sapiens GN=CNPY2 PE=1 SV=1	CNPY2_HUMAN	0	0	0	2	0
370	Calcyclin-binding protein OS=Homo sapiens GN=CACYBP PE=1 SV=2	CYBP_HUMAN	0	0	0	2	0
371	Follistatin-related protein 3 OS=Homo sapiens GN=FSTL3 PE=1 SV=1	FSTL3_HUMAN	0	0	0	2	0
372	Platelet-activating factor acetylhydrolase IB subunit gamma OS=Homo sapiens GN=PAFAH1B3 PE=1 SV=1	PA1B3_HUMAN	0	0	0	2	0

373	Staphylococcal nuclease domain-containing protein 1 OS=Homo sapiens GN=SND1 PE=1 SV=1	SND1_HUMAN	0	0	0	2	0
374	T-complex protein 1 subunit alpha OS=Homo sapiens GN=TCP1 PE=1 SV=1	TCPA_HUMAN	0	0	0	2	0
375	T-complex protein 1 subunit theta OS=Homo sapiens GN=CCT8 PE=1 SV=4	TCPQ_HUMAN	0	0	0	2	0

Table 10-2 List of identified proteins in supernatants of primary monocytes
Numbers on the right indicate the quantity of different identified peptides in each sample. **arch** = supernatants of 10 nM, 24 hours archazolid treated monocytes; **co** = supernatants 24 hours control treated monocytes**; arch LPS** = supernatants of 10 nM, 24 hours archazolid + LPS treated monocytes ; **co LPS** = supernatants 24 hours control + LPS treated monocytes

#	Identified Proteins (154)	Accession Number	arch	co	arch LPS	co LPS
1	Keratin, type II cytoskeletal 1 OS=Homo sapiens GN=KRT1 PE=1 SV=6	K2C1_HUMAN	148	169	68	120
2	Filamin-A OS=Homo sapiens GN=FLNA PE=1 SV=4	FLNA_HUMAN	21	8	67	26
3	Serum albumin OS=Homo sapiens GN=ALB PE=1 SV=2	ALBU_HUMAN	91	57	65	85
4	Thrombospondin-1 OS=Homo sapiens GN=THBS1 PE=1 SV=2	TSP1_HUMAN	96	77	59	75
5	Actin, cytoplasmic 1 OS=Homo sapiens GN=ACTB PE=1 SV=1	ACTB_HUMAN (+1)	67	37	52	53
6	Moesin OS=Homo sapiens GN=MSN PE=1 SV=3	MOES_HUMAN	19	6	48	43
7	Vimentin OS=Homo sapiens GN=VIM PE=1 SV=4	VIME_HUMAN	30	5	42	13
8	Plastin-2 OS=Homo sapiens GN=LCP1 PE=1 SV=6	PLSL_HUMAN	30	9	40	38
9	Keratin, type I cytoskeletal 10 OS=Homo sapiens GN=KRT10 PE=1 SV=6	K1C10_HUMAN	119	134	39	112
10	Keratin, type II cytoskeletal 2 epidermal OS=Homo sapiens GN=KRT2 PE=1 SV=2	K22E_HUMAN	85	88	38	57
11	Alpha-actinin-4 OS=Homo sapiens GN=ACTN4 PE=1 SV=2	ACTN4_HUMAN	19	21	33	13
12	Vinculin OS=Homo sapiens GN=VCL PE=1 SV=4	VINC_HUMAN	17	1	32	17
13	Fructose-bisphosphate aldolase A OS=Homo sapiens GN=ALDOA PE=1 SV=2	ALDOA_HUMAN	14	13	31	18
14	Myosin-9 OS=Homo sapiens GN=MYH9 PE=1 SV=4	MYH9_HUMAN	12		30	12
15	Myeloperoxidase OS=Homo sapiens GN=MPO PE=1 SV=1	PERM_HUMAN	31	11	29	23
16	Transketolase OS=Homo sapiens GN=TKT PE=1 SV=3	TKT_HUMAN	10	13	27	17
17	Alpha-actinin-1 OS=Homo sapiens GN=ACTN1 PE=1 SV=2	ACTN1_HUMAN	18	30	26	13
18	Keratin, type I cytoskeletal 9 OS=Homo sapiens GN=KRT9 PE=1 SV=3	K1C9_HUMAN	63	81	24	55
19	Profilin-1 OS=Homo sapiens GN=PFN1 PE=1 SV=2	PROF1_HUMAN	5	3	23	3
20	L-lactate dehydrogenase B chain OS=Homo sapiens GN=LDHB PE=1 SV=2	LDHB_HUMAN	21	5	22	18
21	Integrin beta-2 OS=Homo sapiens GN=ITGB2 PE=1 SV=2	ITB2_HUMAN	22	25	21	16
22	Talin-1 OS=Homo sapiens GN=TLN1 PE=1 SV=3	TLN1_HUMAN	12		21	11
23	Leukocyte elastase inhibitor OS=Homo sapiens GN=SERPINB1 PE=1 SV=1	ILEU_HUMAN	10	2	20	22
24	Plectin OS=Homo sapiens GN=PLEC PE=1 SV=3	PLEC_HUMAN	5	1	20	3
25	Plasminogen activator inhibitor 2 OS=Homo sapiens GN=SERPINB2 PE=1 SV=2	PAI2_HUMAN	18	14	19	26
26	Triosephosphate isomerase OS=Homo sapiens GN=TPI1 PE=1 SV=3	TPIS_HUMAN	21	10	19	18
27	Annexin A2 OS=Homo sapiens GN=ANXA2 PE=1 SV=2	ANXA2_HUMAN	10	4	18	7
28	L-lactate dehydrogenase A chain OS=Homo sapiens GN=LDHA PE=1 SV=2	LDHA_HUMAN	13		18	14
29	Alpha-enolase OS=Homo sapiens GN=ENO1 PE=1 SV=2	ENOA_HUMAN	30	11	17	30
30	Annexin A1 OS=Homo sapiens GN=ANXA1 PE=1 SV=2	ANXA1_HUMAN	4	4	16	6
31	Peptidyl-prolyl cis-trans isomerase A OS=Homo sapiens GN=PPIA PE=1 SV=2	PPIA_HUMAN	9	2	15	2
32	Transitional endoplasmic reticulum ATPase OS=Homo sapiens GN=VCP PE=1 SV=4	TERA_HUMAN	3	2	15	4
33	Alpha-2-HS-glycoprotein OS=Homo sapiens GN=AHSG PE=1 SV=1	FETUA_HUMAN	21	11	15	21
34	Heat shock 70 kDa protein 1A/1B OS=Homo sapiens GN=HSPA1A PE=1 SV=5	HSP71_HUMAN	3		15	12
35	Lysozyme C OS=Homo sapiens GN=LYZ PE=1 SV=1	LYSC_HUMAN	12	8	14	7
36	14-3-3 protein zeta/delta OS=Homo sapiens GN=YWHAZ PE=1 SV=1	1433Z_HUMAN	14	6	13	17

37	Gelsolin OS=Homo sapiens GN=GSN PE=1 SV=1	GELS_HUMAN	6	7	13	7
38	Heat shock cognate 71 kDa protein OS=Homo sapiens GN=HSPA8 PE=1 SV=1	HSP7C_HUMAN	6		13	12
39	Annexin A5 OS=Homo sapiens GN=ANXA5 PE=1 SV=2	ANXA5_HUMAN	5	3	12	7
40	Ras GTPase-activating-like protein IQGAP1 OS=Homo sapiens GN=IQGAP1 PE=1 SV=1	IQGA1_HUMAN	1	1	12	5
41	Glutathione S-transferase P OS=Homo sapiens GN=GSTP1 PE=1 SV=2	GSTP1_HUMAN	7		12	5
42	Histone H4 OS=Homo sapiens GN=HIST1H4A PE=1 SV=2	H4_HUMAN	8	22	11	8
43	Histone H2B type 1-D OS=Homo sapiens GN=HIST1H2BD PE=1 SV=2	H2B1D_HUMAN	13	7	10	5
44	Lamin-B1 OS=Homo sapiens GN=LMNB1 PE=1 SV=2	LMNB1_HUMAN	4		10	4
45	Interleukin-6 OS=Homo sapiens GN=IL6 PE=1 SV=1	IL6_HUMAN	4	5	10	4
46	Glucose-6-phosphate isomerase OS=Homo sapiens GN=GPI PE=1 SV=4	G6PI_HUMAN	4		10	11
47	Glyceraldehyde-3-phosphate dehydrogenase OS=Homo sapiens GN=GAPDH PE=1 SV=3	G3P_HUMAN	12	4	10	7
48	Transaldolase OS=Homo sapiens GN=TALDO1 PE=1 SV=2	TALDO_HUMAN	11	3	9	11
49	Macrophage-capping protein OS=Homo sapiens GN=CAPG PE=1 SV=2	CAPG_HUMAN	6		9	6
50	Platelet glycoprotein Ib alpha chain OS=Homo sapiens GN=GP1BA PE=1 SV=1	GP1BA_HUMAN	15	10	9	5
51	Integrin alpha-M OS=Homo sapiens GN=ITGAM PE=1 SV=2	ITAM_HUMAN	17	4	9	10
52	Actin-related protein 2/3 complex subunit 4 OS=Homo sapiens GN=ARPC4 PE=1 SV=3	ARPC4_HUMAN	2		9	1
53	Neutrophil elastase OS=Homo sapiens GN=ELANE PE=1 SV=1	ELNE_HUMAN	8		9	5
54	Protein S100-A9 OS=Homo sapiens GN=S100A9 PE=1 SV=1	S10A9_HUMAN	4		8	2
55	Phosphoglycerate kinase 1 OS=Homo sapiens GN=PGK1 PE=1 SV=3	PGK1_HUMAN	21	13	8	30
56	Transgelin-2 OS=Homo sapiens GN=TAGLN2 PE=1 SV=3	TAGL2_HUMAN	5	1	8	4
57	Serpin B6 OS=Homo sapiens GN=SERPINB6 PE=1 SV=3	SPB6_HUMAN			8	2
58	Monocyte differentiation antigen CD14 OS=Homo sapiens GN=CD14 PE=1 SV=2	CD14_HUMAN	10	3	8	8
59	Malate dehydrogenase, cytoplasmic OS=Homo sapiens GN=MDH1 PE=1 SV=4	MDHC_HUMAN	8	2	8	6
60	Histone H2A type 1-D OS=Homo sapiens GN=HIST1H2AD PE=1 SV=2	H2A1D_HUMAN (+4)	1	2	8	7
61	14-3-3 protein beta/alpha OS=Homo sapiens GN=YWHAB PE=1 SV=3	1433B_HUMAN	11	2	8	12
62	Hexokinase-3 OS=Homo sapiens GN=HK3 PE=1 SV=2	HXK3_HUMAN	5	1	7	
63	Integrin alpha-IIb OS=Homo sapiens GN=ITGA2B PE=1 SV=3	ITA2B_HUMAN	6	1	7	5
64	Protein DJ-1 OS=Homo sapiens GN=PARK7 PE=1 SV=2	PARK7_HUMAN	2	1	7	1
65	Receptor-type tyrosine-protein phosphatase C OS=Homo sapiens GN=PTPRC PE=1 SV=2	PTPRC_HUMAN	4		7	1
66	Phosphatidylethanolamine-binding protein 1 OS=Homo sapiens GN=PEBP1 PE=1 SV=3	PEBP1_HUMAN	1	1	7	1
67	Fructose-bisphosphate aldolase C OS=Homo sapiens GN=ALDOC PE=1 SV=2	ALDOC_HUMAN	2		7	
68	Alpha-1-antitrypsin OS=Homo sapiens GN=SERPINA1 PE=1 SV=3	A1AT_HUMAN	14	5	6	3
69	Alpha-2-macroglobulin OS=Homo sapiens GN=A2M PE=1 SV=3	A2MG_HUMAN	18	7	6	8
70	14-3-3 protein gamma OS=Homo sapiens GN=YWHAG PE=1 SV=2	1433G_HUMAN	11	2	6	10
71	Rab GDP dissociation inhibitor beta OS=Homo sapiens GN=GDI2 PE=1 SV=2	GDIB_HUMAN	4	1	6	7
72	Malate dehydrogenase, mitochondrial OS=Homo sapiens GN=MDH2 PE=1 SV=3	MDHM_HUMAN	4	2	6	4
73	Tumor necrosis factor OS=Homo sapiens GN=TNF PE=1 SV=1	TNFA_HUMAN	4		6	2
74	Fructose-1,6-bisphosphatase 1 OS=Homo sapiens GN=FBP1 PE=1 SV=5	F16P1_HUMAN		1	6	1

75	78 kDa glucose-regulated protein OS=Homo sapiens GN=HSPA5 PE=1 SV=2	GRP78_HUMAN	5		6	6
76	Keratin, type II cytoskeletal 6A OS=Homo sapiens GN=KRT6A PE=1 SV=3	K2C6A_HUMAN	21	35	6	19
77	Heat shock 70 kDa protein 4 OS=Homo sapiens GN=HSPA4 PE=1 SV=4	HSP74_HUMAN	1	1	5	1
78	Coactosin-like protein OS=Homo sapiens GN=COTL1 PE=1 SV=3	COTL1_HUMAN	2	1	5	1
79	Lactotransferrin OS=Homo sapiens GN=LTF PE=1 SV=6	TRFL_HUMAN	10	4	5	4
80	6-phosphogluconate dehydrogenase, decarboxylating OS=Homo sapiens GN=PGD PE=1 SV=3	6PGD_HUMAN	7	3	5	7
81	Serpin B9 OS=Homo sapiens GN=SERPINB9 PE=1 SV=1	SPB9_HUMAN	9	1	5	2
82	Fermitin family homolog 3 OS=Homo sapiens GN=FERMT3 PE=1 SV=1	URP2_HUMAN	2	1	5	1
83	Core histone macro-H2A.1 OS=Homo sapiens GN=H2AFY PE=1 SV=4	H2AY_HUMAN	2		5	1
84	Nucleoside diphosphate kinase B OS=Homo sapiens GN=NME2 PE=1 SV=1	NDKB_HUMAN	1		5	1
85	Peroxiredoxin-1 OS=Homo sapiens GN=PRDX1 PE=1 SV=1	PRDX1_HUMAN	4		5	3
86	Rho GDP-dissociation inhibitor 2 OS=Homo sapiens GN=ARHGDIB PE=1 SV=3	GDIR2_HUMAN	4	1	5	5
87	Tropomyosin alpha-4 chain OS=Homo sapiens GN=TPM4 PE=1 SV=3	TPM4_HUMAN	1		5	2
88	Intercellular adhesion molecule 3 OS=Homo sapiens GN=ICAM3 PE=1 SV=2	ICAM3_HUMAN	2	1	5	5
89	Actin-related protein 2/3 complex subunit 1B OS=Homo sapiens GN=ARPC1B PE=1 SV=3	ARC1B_HUMAN	6		5	3
90	Endoplasmin OS=Homo sapiens GN=HSP90B1 PE=1 SV=1	ENPL_HUMAN	1		5	
91	Heat shock protein HSP 90-alpha OS=Homo sapiens GN=HSP90AA1 PE=1 SV=5	HS90A_HUMAN	2		4	4
92	Ras-related protein Rab-7a OS=Homo sapiens GN=RAB7A PE=1 SV=1	RAB7A_HUMAN			4	
93	Leukotriene A-4 hydrolase OS=Homo sapiens GN=LTA4H PE=1 SV=2	LKHA4_HUMAN			4	5
94	Cathepsin S OS=Homo sapiens GN=CTSS PE=1 SV=3	CATS_HUMAN	13		4	
95	Phosphoglycerate mutase 1 OS=Homo sapiens GN=PGAM1 PE=1 SV=2	PGAM1_HUMAN	4	1	4	6
96	Alcohol dehydrogenase [NADP(+)] OS=Homo sapiens GN=AKR1A1 PE=1 SV=3	AK1A1_HUMAN	2	1	4	4
97	Histone H3.1t OS=Homo sapiens GN=HIST3H3 PE=1 SV=3	H31T_HUMAN (+3)	5	2	4	1
98	Adenylyl cyclase-associated protein 1 OS=Homo sapiens GN=CAP1 PE=1 SV=5	CAP1_HUMAN	1		4	1
99	Alpha-fetoprotein OS=Homo sapiens GN=AFP PE=1 SV=1	FETA_HUMAN	4	3	4	3
100	Cofilin-1 OS=Homo sapiens GN=CFL1 PE=1 SV=3	COF1_HUMAN	4	2	4	5
101	Lysosome-associated membrane glycoprotein 1 OS=Homo sapiens GN=LAMP1 PE=1 SV=3	LAMP1_HUMAN	3		4	
102	Actin-related protein 2/3 complex subunit 3 OS=Homo sapiens GN=ARPC3 PE=1 SV=3	ARPC3_HUMAN	1		4	1
103	Purine nucleoside phosphorylase OS=Homo sapiens GN=PNP PE=1 SV=2	PNPH_HUMAN	2		4	
104	Glyoxalase domain-containing protein 4 OS=Homo sapiens GN=GLOD4 PE=1 SV=1	GLOD4_HUMAN			4	1
105	F-actin-capping protein subunit beta OS=Homo sapiens GN=CAPZB PE=1 SV=4	CAPZB_HUMAN	3		4	4
106	14-3-3 protein epsilon OS=Homo sapiens GN=YWHAE PE=1 SV=1	1433E_HUMAN	3	1	4	3
107	Poly(rC)-binding protein 1 OS=Homo sapiens GN=PCBP1 PE=1 SV=2	PCBP1_HUMAN		1	3	
108	Acylamino-acid-releasing enzyme OS=Homo sapiens GN=APEH PE=1 SV=4	ACPH_HUMAN		1	3	1
109	N-acetyl-D-glucosamine kinase OS=Homo sapiens GN=NAGK PE=1 SV=4	NAGK_HUMAN	2		3	1

110	Proteasome subunit beta type-9 OS=Homo sapiens GN=PSMB9 PE=1 SV=2	PSB9_HUMAN	2	2	3	2
111	Ferritin light chain OS=Homo sapiens GN=FTL PE=1 SV=2	FRIL_HUMAN	3	2	3	1
112	F-actin-capping protein subunit alpha-1 OS=Homo sapiens GN=CAPZA1 PE=1 SV=3	CAZA1_HUMAN	2		3	2
113	Proteasome subunit alpha type-6 OS=Homo sapiens GN=PSMA6 PE=1 SV=1	PSA6_HUMAN	2		3	3
114	Serotransferrin OS=Homo sapiens GN=TF PE=1 SV=3	TRFE_HUMAN	1		3	2
115	Inter-alpha-trypsin inhibitor heavy chain H2 OS=Homo sapiens GN=ITIH2 PE=1 SV=2	ITIH2_HUMAN	4		3	
116	Ubiquitin-conjugating enzyme E2 N OS=Homo sapiens GN=UBE2N PE=1 SV=1	UBE2N_HUMAN (+1)	1		3	2
117	Phospholipase B-like 1 OS=Homo sapiens GN=PLBD1 PE=1 SV=2	PLBL1_HUMAN	8		2	
118	Epididymal secretory protein E1 OS=Homo sapiens GN=NPC2 PE=1 SV=1	NPC2_HUMAN	3	2	2	1
119	Ferritin heavy chain OS=Homo sapiens GN=FTH1 PE=1 SV=2	FRIH_HUMAN	6	1	2	
120	ATRIP_HUMAN-R	ATRIP_HUMAN-R			2	
121	Coronin-1A OS=Homo sapiens GN=CORO1A PE=1 SV=4	COR1A_HUMAN	6	2	2	9
122	Fibrinogen gamma chain OS=Homo sapiens GN=FGG PE=1 SV=3	FIBG_HUMAN	10	5	2	9
123	Tryptophan--tRNA ligase, cytoplasmic OS=Homo sapiens GN=WARS PE=1 SV=2	SYWC_HUMAN	3		2	6
124	Pyruvate kinase isozymes M1/M2 OS=Homo sapiens GN=PKM PE=1 SV=4	KPYM_HUMAN	4	2	2	1
125	Glutathione reductase, mitochondrial OS=Homo sapiens GN=GSR PE=1 SV=2	GSHR_HUMAN	1	2	2	3
126	Cathepsin Z OS=Homo sapiens GN=CTSZ PE=1 SV=1	CATZ_HUMAN	4		2	2
127	Actin-related protein 2 OS=Homo sapiens GN=ACTR2 PE=1 SV=1	ARP2_HUMAN	1		2	4
128	Elongation factor 2 OS=Homo sapiens GN=EEF2 PE=1 SV=4	EF2_HUMAN	4	1	2	
129	Isocitrate dehydrogenase [NADP] cytoplasmic OS=Homo sapiens GN=IDH1 PE=1 SV=2	IDHC_HUMAN	4		2	1
130	Ras-related C3 botulinum toxin substrate 1 OS=Homo sapiens GN=RAC1 PE=1 SV=1	RAC1_HUMAN (+2)	4	1	2	
131	Fibrinogen alpha chain OS=Homo sapiens GN=FGA PE=1 SV=2	FIBA_HUMAN	6	2	1	2
132	MUC5A_HUMAN-R	MUC5A_HUMAN-R	1	2	1	1
133	Protein disulfide-isomerase A3 OS=Homo sapiens GN=PDIA3 PE=1 SV=4	PDIA3_HUMAN	8	1	1	1
134	Guanine nucleotide-binding protein G(i) subunit alpha-2 OS=Homo sapiens GN=GNAI2 PE=1 SV=3	GNAI2_HUMAN	2		1	3
135	Aminopeptidase N OS=Homo sapiens GN=ANPEP PE=1 SV=4	AMPN_HUMAN	4		1	
136	Alpha-1-antichymotrypsin OS=Homo sapiens GN=SERPINA3 PE=1 SV=2	AACT_HUMAN	2		1	
137	N-acetylglucosamine-6-sulfatase OS=Homo sapiens GN=GNS PE=1 SV=3	GNS_HUMAN	5		1	
138	Chloride intracellular channel protein 1 OS=Homo sapiens GN=CLIC1 PE=1 SV=4	CLIC1_HUMAN	3		1	1
139	Thymidine phosphorylase OS=Homo sapiens GN=TYMP PE=1 SV=2	TYPH_HUMAN	1	2	1	3
140	Proteasome subunit alpha type-7 OS=Homo sapiens GN=PSMA7 PE=1 SV=1	PSA7_HUMAN	2		1	2
141	EMILIN-1 OS=Homo sapiens GN=EMILIN1 PE=1 SV=2	EMIL1_HUMAN	2	1	1	
142	Integrin beta-3 OS=Homo sapiens GN=ITGB3 PE=1 SV=2	ITB3_HUMAN	1	4	1	
143	Catalase OS=Homo sapiens GN=CAT PE=1 SV=3	CATA_HUMAN	1		1	2
144	Keratin, type I cytoskeletal 14 OS=Homo sapiens GN=KRT14 PE=1 SV=4	K1C14_HUMAN	26	37		26
145	Keratin, type II cytoskeletal 5 OS=Homo sapiens GN=KRT5 PE=1 SV=3	K2C5_HUMAN	11	26		12
146	Matrix metalloproteinase-9 OS=Homo sapiens GN=MMP9	MMP9_HUMAN	2	7		

	PE=1 SV=3				
147	Ig gamma-1 chain C region OS=Homo sapiens GN=IGHG1 PE=1 SV=1	IGHG1_HUMAN	3	4	1
148	Erythrocyte band 7 integral membrane protein OS=Homo sapiens GN=STOM PE=1 SV=3	STOM_HUMAN	1	2	4
149	Fibrinogen beta chain OS=Homo sapiens GN=FGB PE=1 SV=2	FIBB_HUMAN	1		3
150	Beta-hexosaminidase subunit beta OS=Homo sapiens GN=HEXB PE=1 SV=3	HEXB_HUMAN	4		
151	Keratin, type I cytoskeletal 16 OS=Homo sapiens GN=KRT16 PE=1 SV=4	K1C16_HUMAN		31	
152	Lysosomal alpha-glucosidase OS=Homo sapiens GN=GAA PE=1 SV=4	LYAG_HUMAN	4		
153	Adenosine deaminase CECR1 OS=Homo sapiens GN=CECR1 PE=1 SV=2	CECR1_HUMAN	2		1
154	Cathepsin B OS=Homo sapiens GN=CTSB PE=1 SV=3	CATB_HUMAN	3		